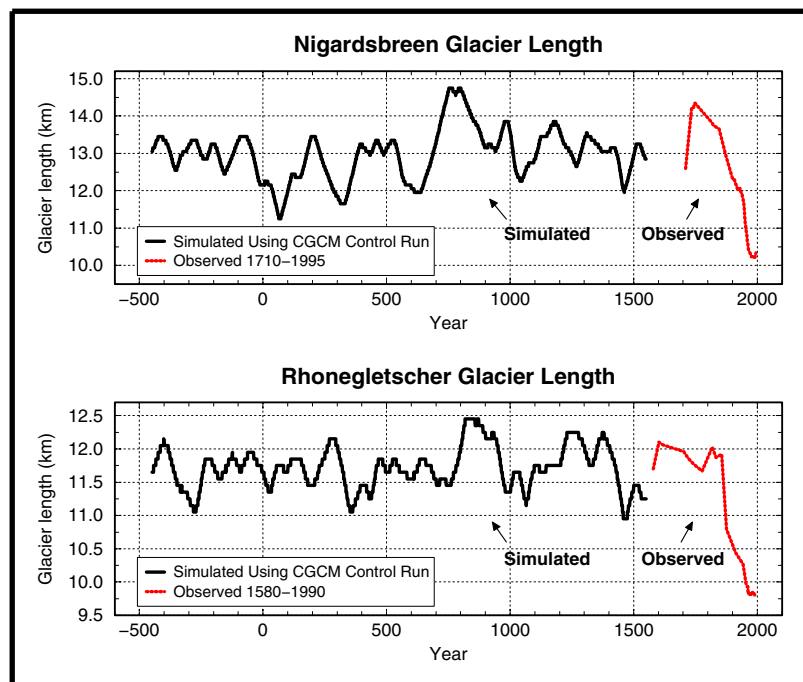




# Max-Planck-Institut für Meteorologie

## EXAMENSARBEIT Nr. 72



### QUANTIFICATION OF NATURAL CLIMATE VARIABILITY IN PALEOCLIMATIC PROXY DATA USING GENERAL CIRCULATION MODELS: APPLICATION TO GLACIER SYSTEMS

von

Bernhard K. Reichert

HAMBURG, Mai 2000

Dissertation zur Erlangung des Doktorgrades

Autor:

Bernhard K. Reichert

Max-Planck-Institut  
für Meteorologie

Universität Hamburg  
Fachbereich:  
Geowissenschaften

MAX-PLANCK-INSTITUT  
FÜR METEOROLOGIE  
BUNDESSTRASSE 55  
D - 20146 HAMBURG  
GERMANY

Tel.: +49-(0)40-4 11 73-0  
Telefax: +49-(0)40-4 11 73-298  
E-Mail: <name> @ dkrz.de

# **Quantification of Natural Climate Variability in Paleoclimatic Proxy Data Using General Circulation Models: Application to Glacier Systems**

(Quantifizierung der natürlichen Klimavariabilität in Paläoklimatischen  
Proxy-Daten mit Hilfe von Modellen der Allgemeinen Zirkulation:  
Anwendung auf Gletschersysteme)

Dissertation  
zur Erlangung des Doktorgrades  
der Naturwissenschaften im Fachbereich  
Geowissenschaften  
der Universität Hamburg

vorgelegt von  
**Bernhard K. Reichert**  
aus Aachen

Hamburg  
2000

ISSN 0938-5177



## Abstract

In this thesis, a methodology using general circulation models (GCMs) for the quantification of natural climate variability as recorded in paleoclimatic proxy data is proposed. A systematic comparison between paleoclimatic proxy data and GCM integrations is made possible by developing a method for a direct and process-based simulation of proxy records using statistically downscaled GCM output. This means that “synthetic” records are generated from GCM experiments for comparison with actual in situ proxy data. The approach is applicable to various paleoclimatic proxy indicators and is demonstrated for the simulation of valley glaciers, using process-oriented models for glacier mass balance and glacier length. Simulated glacier length changes are compared to observed or reconstructed glacier fluctuations, which represent proxy data for low frequency climate variations extending back over several centuries. The role of internal variability in the climate system as a major source of glacier fluctuations is investigated.

A reliable statistical downscaling approach for GCM output is developed based on large-scale predictors obtained from daily reanalyses of the European Centre for Medium-Range Weather Forecasts (ECMWF) and daily operational weather station data in the vicinity of the proxy site to be investigated. The method produces a good simulation of local temperature and precipitation for weather stations in Norway and the Alps. It is successfully applied to European Center/Hamburg (ECHAM4) GCM experiments.

In order to simulate fluctuations of specific valley glaciers using GCM integrations, a method is developed to relate glacier mass balance to meteorological data or to downscaled GCM output. The climate sensitivity of a glacier is quantified by a Seasonal Sensitivity Characteristic (SSC), which represents the dependence of glacier mass balance on monthly anomalies in temperature and precipitation and is calculated from a mass balance model of intermediate complexity. SSCs for a number of valley glaciers located in various parts of the world are calculated. With regard to the climate sensitivity of mass balance to temperature, the SSCs show that for glaciers in dry climates, the effect of temperature is mainly restricted to summer months, whereas for glaciers in wetter climates, spring and Autumn temperatures additionally contribute. The considerable overall sensitivity to precipitation varies significantly between the glaciers, the effect of summer precipitation is also strongly dependant on the altitudinal range of the glaciers. Mass balance simulations using

---

ECMWF reanalyses for the period 1979-1993 are in good agreement with in situ measurements for Nigardsbreen glacier (Norway).

The downscaling methodology and the SSCs described above are used to simulate mass balance fluctuations for Nigardsbreen and Rhonegletscher (Switzerland) using multi-century coupled (ECHAM4/OPYC) and mixed-layer (ECHAM4/MLO) GCM integrations. External forcing is excluded in the GCM experiments. For both glaciers, a high correlation is found between decadal variations in the North Atlantic Oscillation (NAO) and glacier mass balance. The dominant factor for this relationship is the strong impact of winter precipitation associated with the NAO. For Nigardsbreen (Rhonegletscher), a high NAO phase means enhanced (reduced) winter precipitation, typically leading to a higher (lower) than normal annual mass balance. This mechanism, entirely due to internal variations in the climate system, can also explain observed strong positive mass balances for Nigardsbreen and possibly other maritime Norwegian glaciers within the period 1980-1995.

A dynamic ice flow model considering simple shearing flow and sliding is applied, in order to simulate glacier length changes due to internal variations in the climate system using the statistically downscaled GCM integrations described above. 10000 year records of glacier length fluctuations are generated using auto-regressive processes determined by the GCM experiments. Return periods and probabilities of specific glacier length changes, simulated excluding external forcings such as solar irradiation changes, volcanic or anthropogenic effects, are calculated and compared to historical glacier length records.

It is concluded that preindustrial fluctuations of the glaciers as far as observed or reconstructed, including their advance during the “Little Ice Age”, can be explained entirely by internal variations in the climate system as represented by a GCM. External forcing is not required. The probability that these glacier fluctuations occur within a time period of 10000 years is 99.7% for Nigardsbreen and 80.4% for Rhonegletscher. However, fluctuations comparable to the observed present-day retreat of the glaciers (4 km for Nigardsbreen and 2.3 km for Rhonegletscher since the “Little Ice Age” maximum) do not occur in these GCM experiments, it is therefore very unlikely that this retreat is entirely due to internal climate variations. The probability of occurrence for such a retreat is 11.1% for Nigardsbreen and 9.9% for Rhonegletscher within a time period of 10000 years. The results imply that the present-day retreat is in all likelihood due to external forcing, greenhouse gas forcing being the most probable potential candidate.

---

---

# Contents

---

|  |           |
|--|-----------|
| <b>1 INTRODUCTION</b>  | <b>1</b>  |
| 1.1 Background.....  | 1         |
| 1.2 Concept of this Thesis.....  | 5         |
| 1.3 Scientific Objectives .....  | 6         |
| 1.4 Structure of this Thesis .....   | 7         |
| 1.5 Publications.....  | 9         |
| <br>   |           |
| <b>2 MODELING APPROACH FOR THE SIMULATION OF PALEOCLIMATIC PROXY RECORDS</b> | <b>13</b> |
| 2.1 Introduction.....  | 13        |
| 2.2 General Strategy.....  | 15        |
| 2.3 Statistical Model .....  | 17        |
| 2.4 Data Sets: ECMWF Reanalyses and Observed Data.....                       | 18        |
| 2.4.1 ECMWF Reanalyses (Predictors) .....                                    | 18        |
| 2.4.2 Observed Station Data (Predictands) .....                              | 20        |
| 2.5 Results of Statistical Modeling .....                                    | 22        |
| 2.5.1 Role of Near-Surface Predictors.....                                   | 22        |
| 2.5.2 General Model Performance .....  | 23        |
| 2.5.3 Spatial Homogeneity of the Statistical Model.....                      | 27        |
| 2.5.4 Model Runs for Specific Seasons of the Year.....                       | 30        |
| 2.5.5 Model Validation Experiments .....                                     | 32        |
| 2.5.6 Impact of Spatiotemporal Resolution of Predictors .....                | 34        |
| 2.6 Application to ECHAM4 GCM: Control and Preindustrial Run.....            | 35        |
| 2.7 Conclusions.....   | 38        |
| <br>   |           |
| <b>3 RELATING GLACIER MASS BALANCE TO METEOROLOGICAL DATA</b>                | <b>45</b> |
| 3.1 Introduction.....  | 45        |
| 3.2 The Seasonal Sensitivity Characteristic (SSC).....                       | 47        |

---

---

|          |   |           |
|----------|---|-----------|
| 3.3      | Application of the SSC to Reconstruct a Mass Balance Series .....                               | 52        |
| 3.4      | Performance of the Reduced Model .....  | 54        |
| 3.5      | Conclusions .....   | 55        |
| <b>4</b> | <b>MIDLATITUDE FORCING MECHANISMS FOR GLACIER MASS BALANCE</b>                                  | <b>59</b> |
| 4.1      | Introduction .....  | 59        |
| 4.2      | Statistical Downscaling Approach.....   | 61        |
| 4.2.1    | Method.....   | 62        |
| 4.2.2    | Downscaling for Rhonegletscher .....  | 62        |
| 4.2.3    | Downscaling for Nigardsbreen .....  | 65        |
| 4.3      | Sensitivity of Glacier Mass Balance to Meteorological Data.....                                 | 66        |
| 4.3.1    | The Mass Balance Model .....  | 66        |
| 4.3.2    | Seasonal Sensitivity Characteristic (SSC) .....   | 67        |
| 4.3.3    | Sensitivity of Nigardsbreen and Rhonegletscher .....  | 68        |
| 4.4      | Validation of Glacier Mass Balance Using ECMWF Reanalyses.....                                  | 69        |
| 4.5      | Simulation of Glacier Mass Balance Using ECHAM4 GCM Integrations ..                             | 71        |
| 4.5.1    | Coupled GCM Experiment (ECHAM4/OPYC).....   | 71        |
| 4.5.2    | Mixed-Layer GCM Experiment (ECHAM4/MLO).....  | 71        |
| 4.5.3    | Mass Balance Simulations .....  | 72        |
| 4.6      | The Role of the NAO for Glacier Mass Balance.....   | 75        |
| 4.6.1    | NAO Index and Glacier Mass Balance .....  | 75        |
| 4.6.2    | Individual Impact of Temperature and Precipitation on Mass Balance .....                        | 78        |
| 4.6.3    | Seasonal Impact on Mass Balance .....   | 80        |
| 4.6.4    | Seasonal Impact of the NAO .....  | 83        |
| 4.7      | Recently Observed Positive Mass Balances of Norwegian Glaciers .....                            | 86        |
| 4.8      | Conclusions .....   | 88        |
| <b>5</b> | <b>NATURAL CLIMATE VARIABILITY AS INDICATED BY GLACIERS AND IMPLICATIONS FOR CLIMATE CHANGE</b> | <b>95</b> |
| 5.1      | Introduction .....  | 95        |
| 5.2      | Glacier Mass Balance as Simulated Using GCMs .....  | 98        |
| 5.3      | Auto-regressive Processes for the Simulation of Glacier Mass Balance Records Using GCMs.....    | 98        |
| 5.3.1    | General Method .....  | 99        |
| 5.3.2    | AR Processes Applied to Nigardsbreen and Rhonegletscher.....                                    | 99        |
| 5.4      | The Ice Flow Model .....  | 102       |
| 5.5      | Simulation of Glacier Length Fluctuations Using GCMs .....                                      | 103       |
| 5.6      | Comparison with Observed Glacier Fluctuations and Statistical Analysis                          | 105       |
| 5.6.1    | Historical Records of Glacier Length Fluctuations.....  | 105       |

---

---

|          |   |            |
|----------|---|------------|
| 5.6.2    | Statistical Analysis of Simulated Glacier Fluctuations .....  | 106        |
| 5.6.3    | Return Periods of Specific Glacier Length Changes .....   | 109        |
| 5.6.4    | Probability of Simulating Observed Preindustrial Glacier Length Changes and<br>Present-day Glacier Retreat..... | 110        |
| 5.7      | Conclusions.....  | 113        |
| <b>6</b> | <b>CONCLUSIONS AND PERSPECTIVES</b>   | <b>117</b> |
| 6.1      | Conclusions.....  | 117        |
| 6.2      | Perspectives.....   | 120        |

---



# 1 Introduction

---

## 1.1 Background

A major scientific goal of current climate research is the quantification of natural climate variability along with understanding the underlying physical mechanisms. This topic also represents a key element for the investigation of anthropogenic impacts on climate. Global climate change due to anthropogenic activities has to be judged against the full spectrum of natural variability.

The sources responsible for climate variations can be associated with external forcing and internal climate variability. Climate variations on time scales ranging from ten thousands to hundreds of thousands of years can in all likelihood be attributed to external forcing due to variations in the earth's orbital parameters ("Milankovitch forcing", [Milankovitch, 1930; Berger, 1988]). On shorter time scales, potential external forcing mechanisms are volcanic activity [Hansen *et al.*, 1992; Lindzen and Giannitsis, 1998], solar irradiation changes [Lean *et al.*, 1995; Hoyt and Schatten, 1993], and anthropogenic effects [Bengtsson, 1996, 1997; Roeckner *et al.*, 1999; Manabe, 1998; Mitchell *et al.*, 1995]. Internal climate variations are generated within the climate subsystems, consisting of atmosphere, ocean, cryosphere, solid earth, and biosphere, and may explain a major part of climatic variability [e.g. Manabe and Stouffer, 1996]. The stochastic climate model scenario introduced by Hasselmann [1976] can explain internal low frequency fluctuations in the climate system and may be regarded as the null hypothesis for the generation of climate variations on decadal to centennial time scales. The main idea is that the climate system integrates over short-period weather excitation, the dynamics of the physical system turns short-term stochastic forcing into low-frequency variability. Other possible mechanisms inherent to the climate system are internal ocean variability, ENSO variability and other coupled atmosphere-ocean modes [Sarachik *et al.*, 1996; Bengtsson, 1999].

In order to monitor climate variations on a wide range of time scales, long observational records of the past climate are required. However, available records in

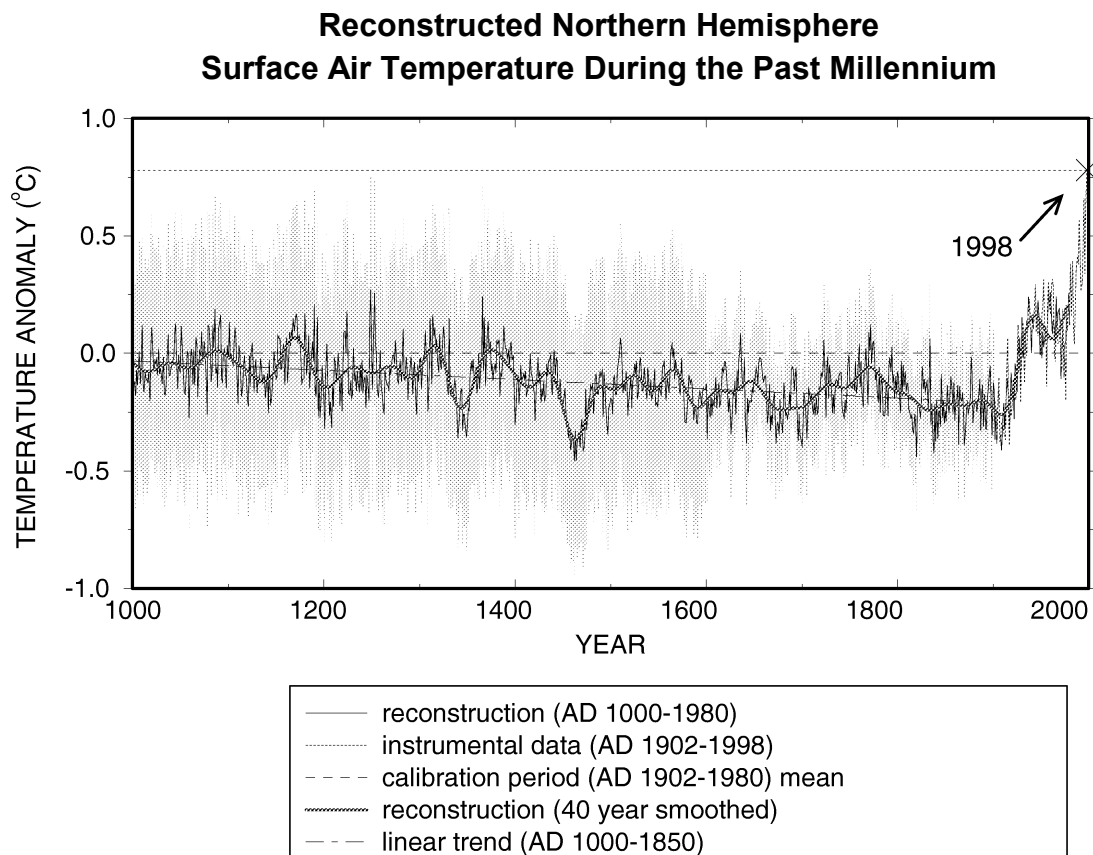
the form of instrumental data or indirect information are spatially and temporally limited. Although routine observations of surface air temperature, precipitation and surface pressure extend back to the late 17<sup>th</sup> and early 18<sup>th</sup> century in western Europe [Jones and Bradley, 1992], the global spatial coverage of these records before the beginning of the 19<sup>th</sup> century is extremely sparse. Therefore, an extension of instrumental records further back in time is required using paleoclimatic proxy data. Proxy data obtained, for example, from tree-rings, ice cores, or corals represent indirect evidence for specific climatic variables, e.g. temperature or precipitation. In this thesis, proxy records over the last millennium are of specific interest. Here, valley glaciers provide important information on low frequency climate variations [Oerlemans, 1996].

In studies of Mann *et al.* [1998, 1999], available instrumental and paleoclimatic proxy data have been combined and a continuous record of the Northern Hemisphere mean annual surface air temperature for the period AD 1000 until present has been produced (Figure 1). The method is based on multivariate, statistical calibration of proxy climate indicators for the present climate involving empirical orthogonal functions (EOFs), paleoclimatic proxy data are then projected onto the obtained modes of variability. Uncertainties in the reconstruction have also been calculated (Figure 1, shaded). The available proxy data before about AD 1600 is spatially very sparsely distributed, consequently, the error in the reconstruction is rather large. The reconstruction suggests a cooling trend of about  $-0.02^{\circ}\text{C}/\text{century}$  before AD 1900. It is concluded that this cooling trend is broadly consistent with Milankovitch forcing which is thought to have affected temperatures at a rate within the range of  $-0.01$  to  $-0.04^{\circ}\text{C}/\text{century}$  since the mid-Holocene [Berger, 1988]. Although considerable temperature fluctuations are found on the annual to multi-decadal scale over the complete time period of the record, the 20<sup>th</sup> century appears anomalous: the 1990s are the warmest decade, and 1998 the warmest year of (at least) the past millennium. Mann *et al.* [1998] suggested explanations for the reconstructed low frequency temperature variations and the steep warming trend during the 20<sup>th</sup> century based on simple correlation with time-series records representing solar variations, volcanic aerosols and a simplified expression for greenhouse gas forcing. However, at this point, general circulation models (GCMs) integrated over a long period of time can further contribute to a more detailed analysis of the role of forcing factors [Bengtsson, 1999; Bengtsson and Reichert, 2000].

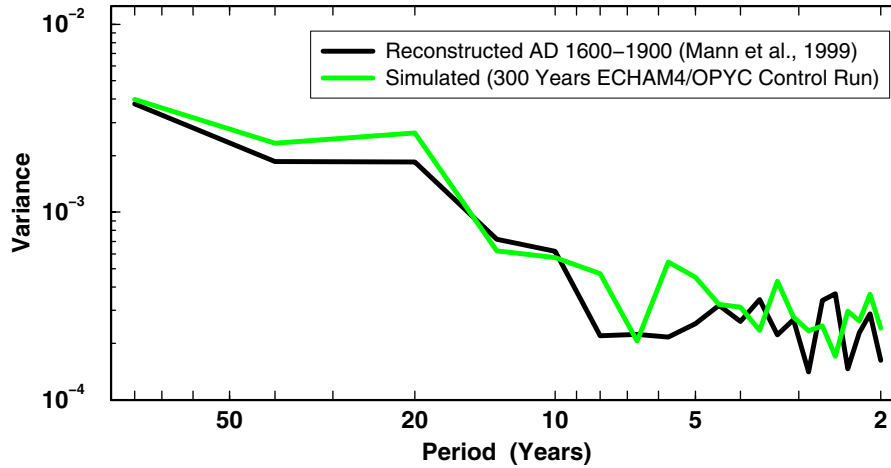
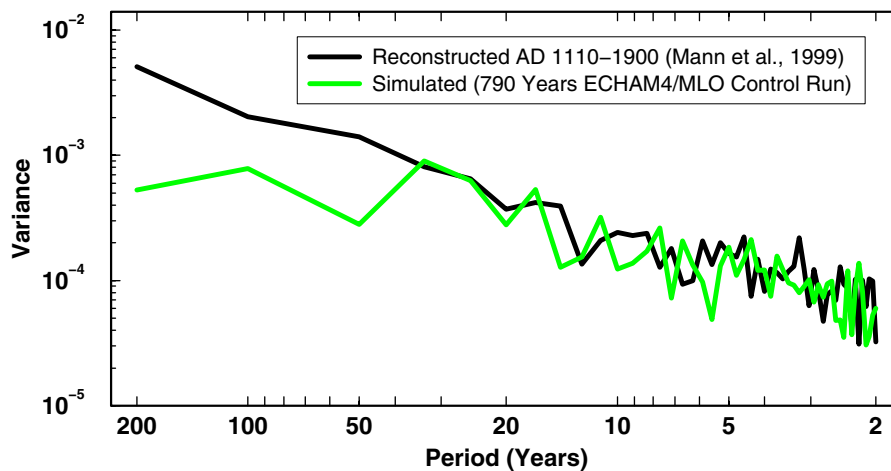
Figure 2 demonstrates the ability of a current state-of-the-art GCM to simulate the spectral content of the reconstructed Northern Hemisphere temperature variations over the past millennium. The model used is the fourth generation of the European Center/Hamburg general circulation model (ECHAM4) developed at the Max-Planck-Institut für Meteorologie and the Deutsches Klimarechenzentrum in Hamburg

---

[Roeckner *et al.*, 1996]. Spectra for a multi-century coupled GCM experiment (ECHAM4/OPYC; Figure 2a) and a mixed-layer GCM integration without an internal ocean (ECHAM4/MLO; Figure 2b) are compared to the reconstructed temperatures for a similar time interval. Temperature variations simulated by the GCM experiments are exclusively due to internal variations in the climate system, external forcing is excluded. Nevertheless, a good agreement is found for the coupled GCM experiment (Figure 2a), indicating that the spectral content of reconstructed temperatures can be well simulated without external forcing. This generally implies that such GCM integrations are valuable tools for the investigation of low frequency variations in the climate system, and they will therefore extensively be used in this thesis. For the mixed-layer GCM (Figure 2b), the spectral analysis suggests that periods of more than about 40 years are underrepresented in comparison with reconstructed temperatures. This may be expected with respect to the lack of an internal ocean which is most likely responsible for the generation of a considerable part of low frequency climate variations.



**Figure 1.** Reconstructed Northern Hemisphere mean annual surface air temperature AD 1000-1980 (thin solid line), 40-year smoothed version (thick line), instrumental data AD 1902-1998 (thin dotted line), linear trend AD 1000-1850 (dot-dashed line), and two standard error limits (shaded). From [Mann *et al.*, 1999].

**Spectral Analysis Northern Hemisphere Temperature****a) Coupled GCM****b) Mixed-Layer GCM**

**Figure 2.** Spectral Analysis of Northern Hemisphere mean annual surface air temperature for reconstructed records [*Mann et al., 1999*] (solid lines) and GCM integrations (shaded lines). Temperature variations simulated by the GCM experiments are exclusively due to internal variations in the climate system, external forcing is excluded. Spectra for (a) 300 years of a coupled GCM integration (ECHAM4/OPYC) in comparison with reconstructed temperatures AD 1600-1900, and (b) 790 years of a mixed-layer GCM (ECHAM4/MLO) in comparison with reconstructed temperatures AD 1110-1900 are shown.

## 1.2 Concept of this Thesis

In this thesis, the problem of a systematic comparison between paleoclimatic proxy data and GCM integrations will be addressed. However, in contrast to many previous studies [e.g., *Landsberg et al.*, 1978; *Bradley and Jones*, 1993; *Barnett et al.*, 1996; *Mann et al.*, 1999], the aim is not the reconstruction of large-scale climatic patterns from (usually inhomogeneous and sparsely distributed) paleoclimatic proxy data using statistical techniques for comparison with GCM output. This approach, generally referred to as “upscaling”, has some general restrictions: firstly, the complex and very often ambiguous relationships between a specific proxy indicator (such as tree-ring width or glacier length) and a climatic parameter (such as temperature or precipitation) are considered in a simplified, statistical sense only, not in a process-oriented way. This means that, for example, main aspects of the biological bases of tree-ring growth or the dynamic behavior of a glacier forced by specific climatic variations are not considered. Secondly, it remains questionable to what extent the very often local climate proxy indicators are representative for the coarse, large-scale, and dynamic grid-point output of GCMs. How representative is, for example, individual annual tree-ring width captured in dendrochronological proxy data for the grid-points of the temperature field simulated by a GCM (typical resolution, for example, 300 x 300 km)?

The problem of model-data intercomparison is therefore, in this thesis, addressed from a different point of view. The output of a GCM is “downscaled” to a specific location where proxy data has been obtained, and individual paleoclimatic proxy records are then directly simulated using a process-based forward modeling approach. This means that “synthetic” proxy records are generated from GCM integrations for comparison with actual in situ proxy data.

The term “downscaling” can generally be defined as the derivation of regional-scale or local-scale information from larger-scale atmospheric circulation dynamics adequately represented by GCMs [*Hewitson and Crane*, 1996]. Two general approaches to downscaling can be distinguished. The first one is *nested model downscaling* in which a regional dynamic model is driven with larger-scale information from a GCM [e.g. *Giorgi and Mearns*, 1991; *Christensen et al.*, 1998; *Giorgi et al.*, 1998]. In such applications, detailed information at spatial scales down to, for example, 10-20 km may be achieved. However, this approach is computationally extremely demanding and therefore, at present time, not adequate for the application to multi-century GCM integrations as used in this thesis. Furthermore, there are other difficulties, concerning, for example, the method of relating the coarse grid cells of the GCM as boundary condition to the finer scale

---

nested models [Hewitson and Crane, 1996]. The alternative approach is *empirical downscaling* [e.g. Kim et al., 1984; Wigley et al., 1990; von Storch et al., 1993; Zorita and von Storch, 1999]. This approach, as applied in this thesis, is based on empirical relations between large-scale circulation patterns and the local climate, established using statistical models fitted to observational data. In comparison with nested modeling, advantages are the computational efficiency allowing the application to long GCM integrations, and the degree of consistency with observations which is enforced by the method [von Storch et al., 1993]. However, the approach is naturally limited to regions with sufficient observational data to train the model, such as, for example, the midlatitude regions investigated in this thesis. The application of downscaling based on the present-day climate is also restricted to climates which are not fundamentally different in their large-scale flow properties, the general coupling between the large-scale circulation and local weather parameters needs to be maintained. Further general information on empirical downscaling is provided in the introduction to Chapter 2.

The method of simulating proxy records using GCM integrations as developed in this thesis is applicable to various paleoclimatic proxy indicators. It will, in this thesis, be demonstrated for the simulation of valley glaciers in Norway and the Swiss Alps using process-oriented models for glacier mass balance (defined as the annual mass gain or loss of a glacier at the surface; see also the introductions to Chapters 3 and 4) and glacier length (which considers the dynamic ice flow of the glacier; see introduction to Chapter 5). Simulated glacier length changes can be compared to observed or reconstructed glacier fluctuations representing paleoclimatic proxy data extending back over several centuries. The aim is to investigate a major source of natural variability in glacier systems: fluctuations due to internal variations in the climate system.

### **1.3 Scientific Objectives**

The following specific questions will be investigated in this thesis:

- 1) Can a statistical downscaling model be established which is appropriate for the simulation of local paleoclimatic proxy records using GCM integrations? In other words, can local output from a GCM be provided which can be used to force a process-based model for a specific proxy indicator? If so, which large-scale predictors from a GCM are most appropriate?
-

- 2) Can fluctuations of specific valley glaciers (which represent proxy indicators for low frequency climate variations over several centuries) be simulated using downscaled GCM integrations? How can individual glacier mass balance be related to meteorological data or to downscaled GCM output?
- 3) A process-based modeling approach for the simulation of glacier fluctuations, as developed in this study, allows the investigation of underlying forcing mechanisms in the climate system. What are the specific forcing mechanisms driving glacier mass balance changes, for example, of Nigardsbreen glacier (Norway, see Figure 3) and Rhonegletscher (Swiss Alps)? Are they connected to fluctuations in the North Atlantic Oscillation (NAO)? What is the individual impact of temperature and precipitation on glacier mass balance?
- 4) Can the response of glacier geometry (including glacier length which is captured in historic records) be simulated for changes in specific mass balance, considering the dynamic ice flow of the glaciers? If so, can glacier length fluctuations be quantified which are exclusively due to internal variations in the climate system as simulated by a GCM?
- 5) What are the forcing mechanisms responsible for preindustrial fluctuations of the glaciers as far as observed or reconstructed, including their advance during the “Little Ice Age” (generally defined as a relatively cold period between AD 1400 and AD 1860, at least in Europe [Grove, 1988])? Can these fluctuations be explained entirely by internal climate variability?
- 6) Is it likely that the observed present-day glacier retreat is entirely due to internal climate variability or is any external forcing required, such as, for example, greenhouse gas forcing?

## 1.4 Structure of this Thesis

In order to address the questions listed above, this thesis is organized as follows:

Chapter 2 contains the general statistical downscaling approach for the simulation of paleoclimatic proxy records as developed in this study. This approach, based on reanalyses of the European Centre for Medium-Range Weather Forecasts (ECMWF) [Gibson *et al.*, 1997] and operational weather station data is generally applicable to a wide range of paleoclimatic proxy indicators.

---

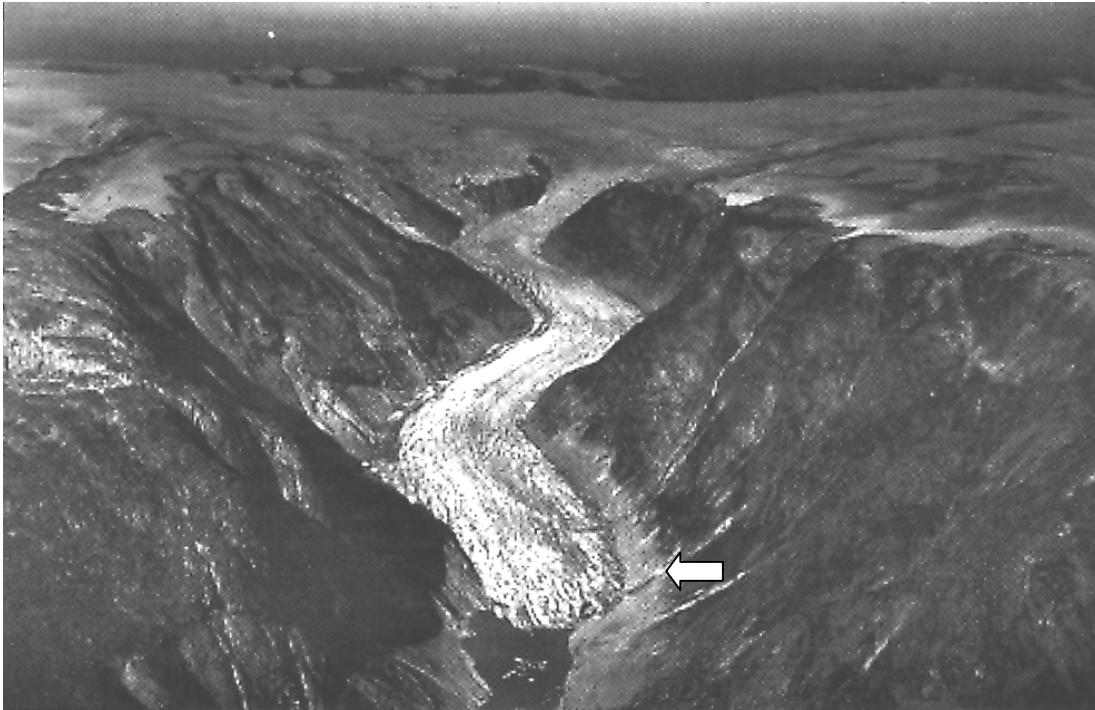


**Figure 3.** Nigardsbreen (Norway), a valley glacier with a long record of observed or reconstructed glacier length changes. Nigardsbreen is one of the glaciers which will be simulated in this study. Trim lines of the AD 1748 maximum stand are visible (arrow). Air photograph taken in 1947 by *Widerøe*, Oslo.

Chapter 3 represents the first step towards applying the established downscaling method for the investigation of proxy information contained in past records of glacier fluctuations. A method to relate glacier mass balance to meteorological data (as well as to downscaled GCM output) is developed. The climate sensitivities of specific valley glaciers are quantified by Seasonal Sensitivity Characteristics (SSCs) representing the dependence of mass balance on monthly anomalies of temperature and precipitation.

In Chapter 4, glacier mass balance is simulated for Nigardsbreen and Rhonegletscher using the above determined SSCs applied to multi-century GCM integrations. Midlatitude forcing mechanisms for glacier mass balance are examined. This leads to the investigation of the impact of seasonal temperature and precipitation anomalies associated with the NAO.

A process-based, dynamic ice flow model is applied to glacier mass balance records in Chapter 5. Glacier length fluctuations over 10000 years are simulated using auto-regressive processes determined by GCM experiments. Return periods and probabilities for specific glacier length changes are analyzed and compared to actual

---

in situ proxy data in the form of historical records of glacier fluctuations. This will lead to the investigation of the question whether preindustrial glacier length changes can be explained entirely by internal variations in the climate system as represented by GCMs. The probability that the observed present-day retreat of the glaciers may be explained by internal climate variability is also calculated.

In addition to the conclusions provided at the end of each chapter, the scientific questions (section 1.3) will finally be answered in the concluding Chapter 6. This chapter also contains perspectives and possible future applications of the modeling approach.

## 1.5 Publications

Chapter 2 to Chapter 5 are based on manuscripts which are either published, in press, or in preparation for publication:

- Chapter 2: A statistical modeling approach for the simulation of local paleoclimatic proxy records using general circulation model output, *Journal of Geophysical Research*, 104, 19071-19083, 1999.
- Chapter 3: Relating glacier mass balance to meteorological data using a Seasonal Sensitivity Characteristic (SSC), *Journal of Glaciology*, 46(152), in press, 2000.
- Chapter 4: Midlatitude forcing mechanisms for glacier mass balance investigated using general circulation models, *Journal of Climate*, in prep., 2000.
- Chapter 5: Natural climate variability as indicated by glaciers and implications for climate change: a modeling study, *Journal of Geophysical Research*, in prep., 2000.
-

## References

- Barnett, T.P., B. D. Santer, P. D. Jones, R. S. Bradley, and K. R. Briffa, Estimates of low frequency natural variability in near-surface air temperature, *Holocene*, 6, 255-263, 1996.
- Bengtsson, L., The climate response to the changing greenhouse gas concentration in the atmosphere, in *Decadal climate variability; dynamics and predictability*, edited by D. L. T. Anderson and J. Willebrand, *NATO ASI series, vol. 44*, Springer, Berlin, 1996.
- Bengtsson, L., A numerical simulation of anthropogenic climate change, *Ambio*, 26, 58-65, 1997.
- Bengtsson, L., Uncertainties of global climate prediction, *Proc. of the Symposium on Global Biogeochemical Cycles in the Climate System, September 22-27, 1998*, Max-Planck-Institut für Biogeochemie, Jena, Germany, in press, 1999.
- Bengtsson, L., and B. K. Reichert, Globaler Klimawandel und natürliche Klimavariabilität - Welche Ursachen haben sie? (Global climate change and natural climate variability - What are their reasons?), in *Energie und Umwelt - Wo liegen optimale Lösungen?*, edited by S. Wittig and J. Wolfrum, Union der deutschen Akademien der Wissenschaften und Heidelberger Akademie der Wissenschaften, Springer Verlag, Heidelberg, Germany, in press, 2000.
- Berger, A., Milankovitch theory and climate, *Rev. of Geophysics*, 26, 624-657, 1988.
- Bradley, R. S., and P. D. Jones, "Little Ice Age" summer temperature variations: Their nature and relevance to recent global warming trends, *Holocene*, 3, 367-376, 1993.
- Christensen, O. B., J. H. Christensen, B. Machenhauer, and M. Botzet, Very high-resolution regional climate simulations over Scandinavia - present climate, *J. Climate*, 11, 3204-3229, 1998.
- Gibson, J. K., P. Kållberg, S. Uppala, A. Nomura, A. Hernandez, and E. Serrano, ERA Description, *ECMWF Re-Anal. Proj. Rep. Ser., Rep. 1*, Eur. Cent. for Medium-Range Weather Forecasts, Reading, England, 1997.
- Giorgi, F., and L. O. Mearns, Approaches to the simulation of regional climate: a review, *Rev. of Geophysics*, 29, 191-216, 1991.
- Giorgi, F., L. O. Mearns, C. Shields, and L. McDaniel, Regional nested model simulations of present-day and 2xCO<sub>2</sub> climate over the Central Plains of the U.S., *Climate Change*, 40, 457-493, 1998.
- Grove, J. M. (Ed.), *The Little Ice Age*, Methuen, London, 1988.
-

- 
- Hansen, J., I. Fung, R. Ruedy, and M. Sato, Potential climate impact of Mount Pinatubo eruption, *Geophys. Res. Lett.*, 19, 215-218, 1992.
- Hasselmann, K., Stochastic Climate Models I: Theory, *Tellus*, 28, 473-485, 1976.
- Hewitson, B. C., and R. G. Crane, Climate downscaling: techniques and application, *Clim. Res.*, 7, 85-95, 1996.
- Hoyt, D. V., and K. H. Schatten, A discussion of plausible solar irradiance variations 1700-1992, *J. Geophys. Res.*, 98, 18895-18906, 1993.
- Jones, P. D., and R. S. Bradley, Climatic variations in the longest instrumental records, in *Climate Since A. D. 1500*, edited by R. S. Bradley and P. D. Jones, pp. 246-268, Routledge, New York, 1992.
- Kim, J.-W., J.-T. Chang, N. L. Baker, D. S. Wilks, and W. L. Gates, The statistical problem of climate inversion: Determination of the relationship between local and large-scale climate, *Mon. Weather Rev.*, 112, 2069-2077, 1984.
- Landsberg, H. E., B. S. Groveman, and I. M. Hakkarinen, A simple method for approximating the annual temperature of the Northern Hemisphere, *Geophys. Res. Lett.*, 5, 505-506, 1978.
- Lean, J., J. Beer, and R. S. Bradley, Reconstruction of solar irradiance since 1610: Implications for climate change, *Geophys. Res. Letters*, 22, 3195-3198, 1995.
- Lindzen, R. S., and C. Giannitsis, On the climatic implications of volcanic cooling, *J. Geophys. Res.*, 103, 5929-5941, 1998.
- Manabe, S., Study of global warming by GFDL climate models, *Ambio*, 27, 182-186, 1998.
- Manabe, S., and R. J. Stouffer, Low-frequency variability of surface air temperature in a 1000-year integration of a coupled atmosphere-ocean-land surface model, *J. Climate*, 9, 376-393, 1996.
- Mann, M. E., R. S. Bradley, and M. K. Hughes, Global-scale temperature patterns and climate forcing over the past six centuries, *Nature*, 392, 779-787, 1998.
- Mann, M. E., R. S. Bradley, and M. K. Hughes, Northern Hemisphere temperatures during the past millennium: inferences, uncertainties, and limitations, *Geophys. Res. Lett.*, 26, 759-762, 1999.
- Milankovitch, M., Mathematische Klimalehre und astronomische Theorie der Klimaschwankungen, in *Handbuch der Klimatologie*, edited by W. Köppen and R. Geiger, Gebrüder Borntraeger, Berlin, 1930.
-

- Mitchell, J. F. B., T. C. Johns, J. M. Gregory, and S. F. B. Tett, Climate response to increasing levels of greenhouse gases and sulphate aerosols, *Nature*, 376, 501-504, 1995.
- Oerlemans, J., Modelling the response of valley glaciers to climatic change, in *Physics and Chemistry of the Atmospheres of the Earth and Other Objects of the Solar System*, edited by C. Boutron, Eur. Res. Course Atmos., vol.2, pp. 91-123, Les Editions de Physique, Les Ulis, France, 1996.
- Roeckner, E., L. Arpe, L. Bengtsson, M. Christoph, M. Claussen, L. Dümenil, M. Esch, M. Giorgetta, U. Schlese, and U. Schulzweida, The atmospheric general circulation model ECHAM-4: Model description and simulation of present-day climate, *Rep. 218*, Max-Planck-Inst. für Meteorol., Hamburg, Germany, 1996.
- Roeckner, E., L. Bengtsson, J. Feichter, J. Lelieveld and H. Rodhe, Transient climate change simulations with a coupled atmosphere-ocean GCM including the tropospheric sulfur cycle, *J. Climate*, 12, 3004-3032, 1999.
- Sarachik, E. S., M. Winton, and F. L. Yin, Mechanisms for decadal-to-centennial climate variability, in *Decadal climate variability*, eds. D. L. T. Anderson and J. Willebrand, *NATO ASI series, vol. 44*, Springer, Berlin, 1996.
- von Storch, H., E. Zorita, and U. Cubasch, Downscaling of global climate change estimates to regional scales: An application to Iberian rainfall in wintertime, *J. Climate*, 6, 1161-1171, 1993.
- Wigley, T. M. L., P. D. Jones, K. R. Briffa, and G. Smith, Obtaining sub-grid-scale information from coarse-resolution general circulation model output, *J. Geophys. Res.*, 95, 1943-1953, 1990.
- Zorita, E., and H. von Storch, The analog method as a simple statistical downscaling technique: comparison with more complicated methods, *J. Climate*, 12, 2474-2489, 1999.
-

## 2 Modeling Approach for the Simulation of Paleoclimatic Proxy Records

---

### ***A Statistical Modeling Approach for the Simulation of Local Paleoclimatic Proxy Records Using General Circulation Model Output<sup>1</sup>***

**Abstract.** A statistical modeling approach is proposed for the simulation of local paleoclimatic proxy records using general circulation model (GCM) output. A method for model-consistent statistical downscaling to local weather conditions is developed which can be used as input for process-based proxy models in order to investigate to what extent climate variability obtained from proxy data can be represented by a GCM, and whether, for example, the response of glaciers to climatic change can be reproduced. Downscaling is based on a multiple linear forward regression model using daily sets of operational weather station data and large-scale predictors at various pressure levels obtained from reanalyses of the European Centre for Medium-Range Weather Forecasts. Composition and relative impact of predictors vary significantly for individual stations within the area of investigation. Owing to a strong dependence on individual synoptic-scale patterns, daily data give the highest performance which can be further increased by developing seasonal-specific relationships. The model is applied to a long integration of a GCM coupled to a mixed layer ocean (ECHAM4/MLO) simulating present-day and preindustrial climate variability. Patterns of variability are realistically simulated compared to observed station data within an area of Norway for the period 1868-1993.

### **2.1 Introduction**

Understanding spatiotemporal patterns and mechanisms of natural climate variability, as well as the anthropogenic impact on climate, requires the extension of instrumental records further back in time by the usage of paleoclimatic proxy data.

---

<sup>1</sup> Reichert, B. K., L. Bengtsson, and O. Åkesson, *Journal of Geophysical Research*, 104, 19071-19083, 1999.

Several attempts to reconstruct reliable temperature patterns over the last few centuries have been made [e.g., *Landsberg et al.*, 1978; *Groverman and Landsberg*, 1979; *Bradley and Jones*, 1993; *Barnett et al.*, 1996; *Bradley*, 1996; *Mann et al.*, 1998, 1999]. Proxy records obtained from ice cores [e.g., *Thompson*, 1982], tree-rings [e.g., *Briffa et al.*, 1992] and corals [e.g., *Dunbar et al.*, 1994], as well as historical data [e.g., *Pfister*, 1992] and long instrumental records [e.g., *Jones and Bradley*, 1992] have been used to reconstruct large-scale or global-scale patterns. Valley glaciers [e.g., *Oerlemans*, 1992, 1997] can also provide important information on the evolution of the regional or local climate.

How can these proxy data best be interpreted and what are the underlying forcing mechanisms? Recent interpretation studies [*Mann et al.*, 1998] have investigated the influence of external forcings, such as solar irradiance variations and explosive volcanism on Northern Hemispheric temperature variations. General circulation models [e.g., *Roeckner et al.*, 1996; *Manabe and Stouffer*, 1996] integrated over a long period of time could contribute as they are an important tool for analyzing mechanisms underlying the climate system behavior and the role of forcing factors. However, a different methodology for a systematic evaluation of paleoclimatic proxy data is then required, as will be proposed in this chapter.

The question we would like to address is whether we are able to simulate “synthetic” paleoclimatic proxy records from GCM output for comparison with actual in situ proxy data. Our strategy is to perform a model-consistent statistical downscaling of the output of a GCM combined with a process-based forward modeling approach to simulate, for example, the behavior of valley glaciers and the growth of trees under specific conditions. Simulated records can be compared to actual in situ proxy records in order to investigate whether, for example, the response of glaciers to climatic change can be reproduced by models, and to what extent climate variability obtained from proxy records (with the main focus on the last millennium) can be interpreted.

The growth of a valley glacier is mainly controlled by local temperature and precipitation [*Paterson*, 1994; *Oerlemans*, 1996]. Such data are very difficult to obtain from grid-point-scale GCM output because of very large deviations due to local orographic conditions. As will be shown in this study, a careful statistical model derived from the present climate can provide reliable local data which can be used to force the growth of such a valley glacier. A similar downscaling approach is required, and can be developed, for the evaluation of dendrochronological data.

One of the initial studies addressing the method of statistical downscaling is the work of *Kim et al.* [1984]. Monthly surface temperature and precipitation for stations in

---

Oregon were analyzed for the purpose of relating their distributions to large-scale monthly anomalies. Downscaling was addressed here as “the statistical problem of climate inversion”. Later, the approach was modified [Wigley *et al.*, 1990] and applied to predict meteorological variables for a number of selected sites in the United States [Karl *et al.*, 1990]. The method was used to predict regional precipitation changes over the Iberian peninsula [von Storch *et al.*, 1993] and to downscale monthly mean North Atlantic air pressure to sea level anomalies in the Baltic Sea [Heyen *et al.*, 1996] using monthly mean predictor data. A comparison of three methods of downscaling [Cubasch *et al.*, 1996] shows that direct interpolation of GCM grid points gives a poor representation of the local climate and that statistical downscaling is an appropriate and inexpensive tool for regions with sufficient observational data to train the model. In a study by Martin *et al.* [1996], GCM output was downscaled to simulate the snow climatology of the French Alps based on an analog procedure which associates a real meteorological situation to model output.

The method of statistical downscaling that is used in this study uses daily operational weather station data and a large set of potential large-scale predictors obtained from daily European Centre for Medium-Range Weather Forecasts (ECMWF) reanalyses [Gibson *et al.*, 1997] in order to develop robust statistical relationships between the large-scale flow and local variables. Specific questions investigated in this study concern the role of near-surface predictors (section 2.5.1) and the spatial homogeneity of the statistical model (section 2.5.3), as well as its performance on single seasons which are most important for a specific proxy indicator (section 2.5.4). Can we, for example, obtain from a GCM reliable local summer temperatures for the growing season of trees, and which predictors do we need in order to do so? Further questions concern the importance of horizontal GCM resolution and the temporal sampling for the determination of suitable predictors (section 2.5.6). It is found, for example, that daily data sets for the development of the statistical model give the closest and most robust relations due to a strong dependence on individual synoptic-scale patterns.

## 2.2 General Strategy

The general strategy proposed in this study is the following (Figure 1). First we develop a statistical model between daily large-scale circulation patterns and corresponding local data observed by operational weather stations located near the proxy site under investigation. Large-scale patterns are represented by daily ECMWF reanalyses (ERA) for the period 1979-1993 which is currently the maximum period

---

available. We use daily data in order to include synoptic timescale variability and to achieve physically robust relations (see section 2.5.6). The obtained statistical relationships are applied to the daily coarse spatial grid point output of a GCM in order to achieve local GCM output (statistical downscaling). A forward modeling approach for a specific proxy, for example, a glacier model [Oerlemans, 1996], can then be used to produce “synthetic” (paleoclimatic) proxy data which finally can be compared to actual in situ proxy data.

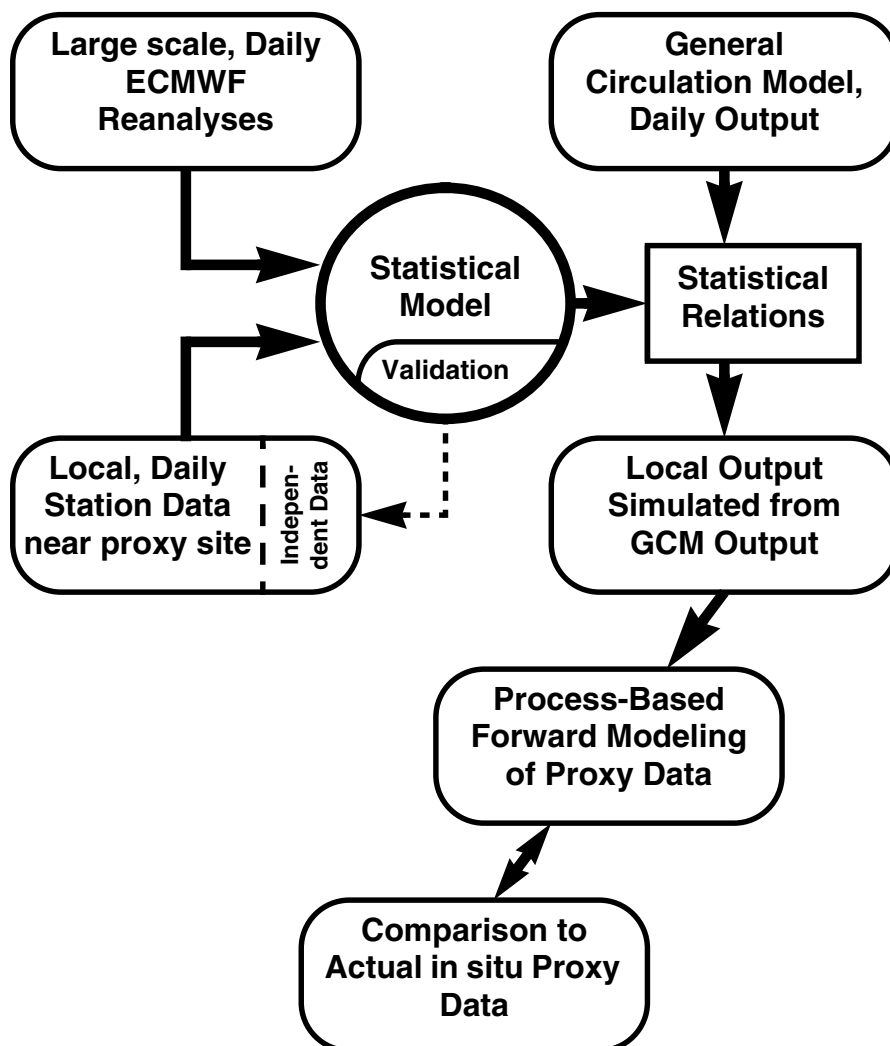


**Figure 1.** General strategy for the interpretation and usage of in situ paleoclimatic proxy data as proposed in this study. See text for further explanations.

## 2.3 Statistical Model

The response of local weather to large-scale flow patterns of the atmosphere has been noted for a very long time, not only by meteorologists, but also by laypersons with an interest in the weather. The most common feature is perhaps the precipitation in mountainous regions which is particularly determined by orographic forcing, generating enhanced precipitation on the windward and reduced precipitation on the leeward side. In most areas, the local conditions (topography and land surface characteristics) have a major effect not only on precipitation but also on wind and temperature as well as on cloudiness and visibility. *Bergeron* [1930] (see also *Bengtsson* [1981]) proposed that a special climatology should be established classifying local climate in terms of the large-scale flow. This approach may be identified as a dynamic climate classification. The significance of this approach became obvious as it became possible to predict the synoptic flow by numerical models. A dynamic climatology can be produced for any particular local weather parameter (predictand), for example, local precipitation, cloud cover, cloud height, visibility, and maximum or minimum temperature, by the use of different large-scale predictors, for example, surface pressure, wind, geopotential thickness, vertical velocity, and large-scale precipitation.

For the purpose of this analysis we use a multiple linear forward regression model in order to establish relations between the large-scale flow and local weather parameters. For the  $i = 1, 2, \dots, n$  values of an observed (dependent) quantity  $y_i$  (predictand) it takes the form of a linear combination

$$y_i = \beta_0 x_{i0} + \beta_1 x_{i1} + \beta_2 x_{i2} + \dots + \beta_p x_{ip} + \varepsilon_i \quad (1)$$

where  $x_{i0} = 1$  and  $x_{i1}, x_{i2}, \dots, x_{ip}$  are the settings of the  $p$  corresponding (independent) quantities (predictors),  $\beta_0, \beta_1, \dots, \beta_p$  are the regression parameters which are to be estimated, and  $\varepsilon_i$  are unknown independent random errors (see, for example, *von Storch and Zwiers* [1999]). We use least squares estimation, which means that best estimates of the unknown regression parameters are calculated by minimizing

$$\sum_{i=1}^n \varepsilon_i^2 \quad (2)$$

for each predictand.

However, it is neither necessary nor desirable to include all potential predictors in the data set for the prediction of a specific observed local variable. The maximum

number of predictors that may be used in the model in order to get a “stable” solution which not only fits the developmental sample but also works on independent data sets is a function of the sample size. Furthermore, some predictors included in the model might be a linear or “near-linear” combination of other predictors (collinearity or “near-collinearity”), which could cause unstable results. In order to address these problems, we choose the following selection procedure for the large daily data set that is used in this study: The model is built up stepwise using an interactive forward selection procedure of independent variables. After having chosen a single predictor with maximum correlation, the next independent variable providing the best fit in conjunction with the first one is added and tested for near-collinearity. In a critical case the user may decide whether this variable should be included or not. Further variables are added in a recursive fashion until a saturation criterion (the correlation does not improve significantly) is reached.

## **2.4 Data Sets: ECMWF Reanalyses and Observed Data**

The development of the statistical model is based on ECMWF reanalyses [*Gibson et al.*, 1997] used for an area of about  $11^\circ \times 11^\circ$  in Norway (covering the proxy site of Nigardsbreen glacier at  $61^\circ 43'N$ ,  $7^\circ 08'E$  to be investigated) and on local observational records for 22 synoptic weather stations within that area. This will in the following be described in more detail.

### **2.4.1 ECMWF Reanalyses (Predictors)**

The ERA project has produced a validated and reasonably consistent global data set of assimilated data for the period 1979-1993 [*Gibson et al.*, 1997]. The objective has been to obtain atmospheric syntheses based on the best available observations and data assimilation systems. In this study, ERA data constitute the potential predictors for the development of the statistical model. We use ERA 24 hour forecasts for precipitation in order to address the spin-up problem and to have a consistent picture of precipitation [*Stendel and Arpe*, 1997]. For all other surface and pressure level variables (Table 1), 6 hourly initialized analyses are taken and daily averaged. We extract pressure level variables on the 1000, 925, 850, 700, 500, 400, and 300 hPa levels.

---

**Table 1.** Large-Scale Predictors From ECMWF Reanalyses

| Predictor Type   | Predictors   |
|--|--|
| Pressure level predictors<br>(1000, 925, 850*,<br>700*, 500*, 400*,<br>300* hPa) | temperature*, dew point temperature*,<br>$u$ wind velocity*, $v$ wind velocity*,<br>vertical velocity*, vorticity*, divergence*,<br>geopotential height*, relative humidity*   |
| Surface predictors   | large-scale precipitation, convective<br>precipitation, mean sea level pressure*,<br>total cloud cover, total column water<br>vapor  |
| Composite predictors†  | geopotential thickness at 925-1000,<br>850-1000, 700-1000, 500-1000,<br>500-850*, 500-700* hPa,<br>seasonal cycle: $\sin(\text{day})^*$ , seasonal<br>cycle: $\cos(\text{day})^*$ , seasonal cycle:<br>$\sin(2 \cdot \text{day})^*$ , seasonal cycle: $\cos(2 \cdot \text{day})^*$ ,<br>large-scale+convective precipitation,<br>square root of total precipitation,<br>vertically integrated liquid water, lapse<br>rate of the lower troposphere (see text),<br>K index [George, 1960] |

\* The model version excluding near-surface predictors (see text) uses exclusively potential predictors on the 850, 700, 500, 400, and 300 hPa levels, mean sea level pressure, geopotential thickness, and the “seasonal cycle” predictors (predictors marked with asterisks).

† See text for definition of composite predictors.

Composite predictors (Table 1) are calculated directly from ERA data. “Geopotential  $a - b$  hPa” means geopotential height on level  $a$  minus geopotential height on level  $b$  (geopotential thickness). The four “seasonal cycle” functions are potential predictors to account for seasonal-specific features while establishing the statistical model between large-scale predictors and local observations. “Seasonal cycle:  $\cos(\text{day})$ ” represents a cosine function with a period of 1 year. It is calculated for each day of the year and has a maximum (+1) at January 1 and a minimum (-1) at July 1. It is the most relevant “seasonal cycle” predictor for the statistical model; for the prediction of local temperature, it may, for example, be used in order to enhance or weaken the seasonal cycle that appears in the ERA large-scale 850 hPa temperature. “Seasonal cycle:  $\sin(\text{day})$ ” is a sine function with a period of 1 year and a maximum at April 1 and a minimum at October 1. “Seasonal cycle:  $\sin(2 \cdot \text{day})$ ” is a sine function with a period of half a year and maxima at February 15 and August 15 and minima at May 15 and November 15. “Seasonal cycle:  $\cos(2 \cdot \text{day})$ ” is a cosine

function with a period of half a year and maxima at January 1 and July 1 and minima at April 1 and October 1. Further composite predictors are the sum of large-scale and convective precipitation in the ERA output (total precipitation), the square root of total precipitation, the vertically integrated liquid water content (total column water minus total column water vapor), the temperature lapse rate of the lower troposphere (linear regression between temperatures on the geopotential heights of the 1000, 925, 850, and 700 hPa levels) and the K index as an atmospheric stability index which involves temperature and dew point temperature at various levels and may be related to precipitation [George, 1960; Karl *et al.*, 1990].

Before applying ERA output to the statistical model, it is interpolated from the original T106 ( $\sim 1.1^\circ \times 1.1^\circ$ ) to T30 ( $\sim 3.8^\circ \times 3.8^\circ$ ) resolution in order to meet the resolution of the ECHAM GCM runs which we intend to use afterwards. For each location of the operational weather stations we compute weighted area means for an area covering roughly 1200 km x 1200 km (corresponding to nine grid points in T30 resolution) as input for the statistical model. Additional experiments with original T106 resolution of ERA output (using 16 grid points to cover the area of investigation) are also analyzed (see section 2.5.6).

#### **2.4.2 Observed Station Data (Predictands)**

The predictands (dependent variables) of the model consist of observational data for 22 operational weather stations (see Figure 2 for locations) in the vicinity of Nigardsbreen glacier, Norway. Most stations (exceptions: 02 Hustad-Nerland, 03 Reimegrend, 08 Tynkrysset, 22 Eidfjord-Bu, 23 Sognefjell Mountain; these stations are not used) cover the period 1979-1993. We interpolate missing values in the 6 hourly weather data before daily averaging. However, data quality is adequate for most stations in that period and only a few data are missing.

Table 2 shows the observed parameters used as input for the statistical model. Composite predictands (Table 2) are logarithm, square root as well as cube and fourth root of observed 24 hour precipitation (prediction of local precipitation may be improved using these predictands),  $u$  wind and  $v$  wind components (calculated from wind direction and wind velocity), and relative humidity (calculated from temperature and dew point temperature).

---

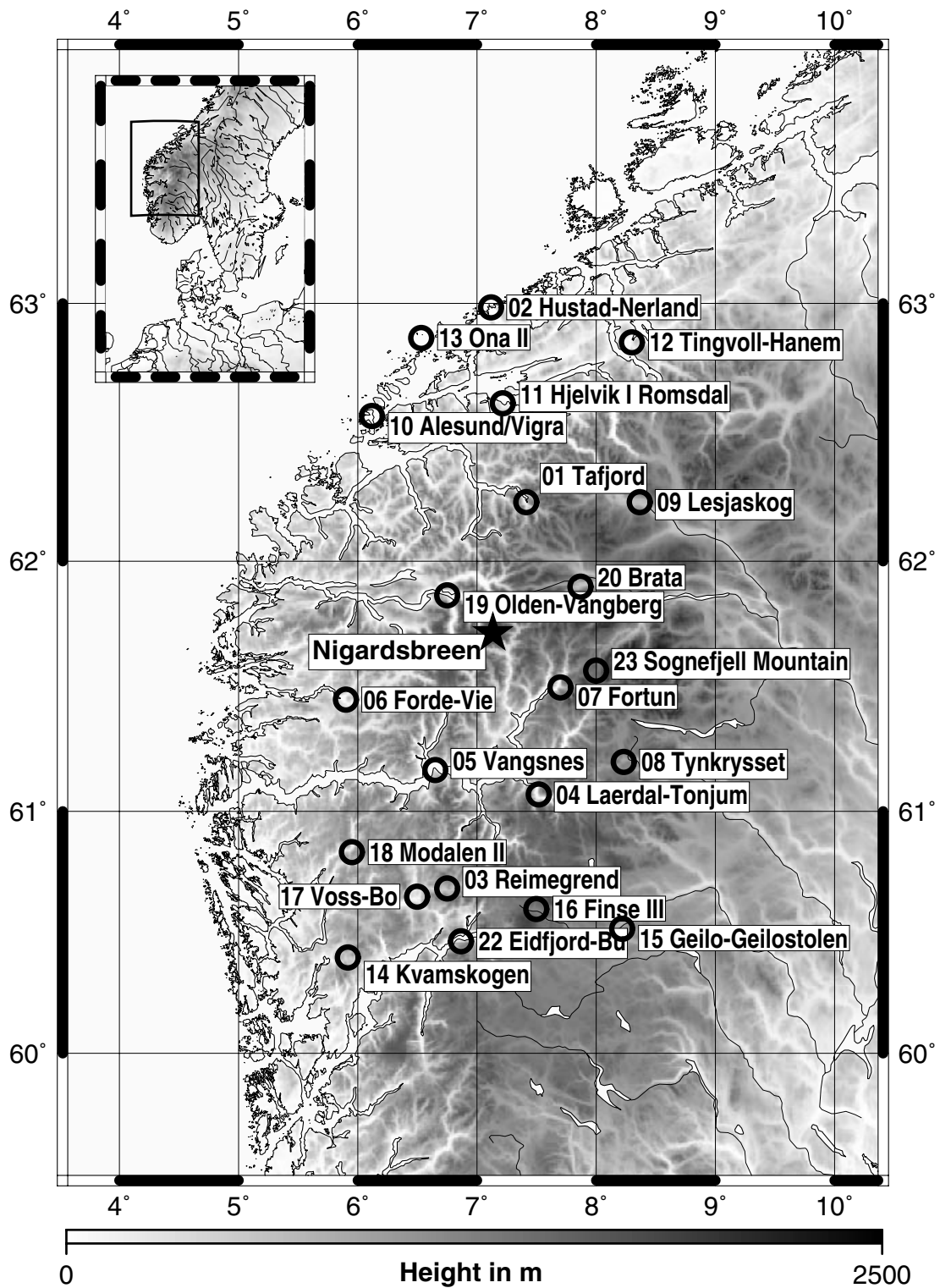


**Figure 2.** Location of operational weather stations used for development of the statistical model. We anticipate being able to provide reliable local outputs for the Nigardsbreen valley glacier (61°43'N, 7°08'E).

**Table 2.** Predictands From Observed Weather Station Data

| Predictand Type                    | Predictands   |
|------------------------------------|---|
| Observed predictands               | pressure reduced, wind direction, wind velocity, temperature, dew point temperature, 24 hour precipitation, total cloud amount    |
| Composite predictands <sup>†</sup> | logarithm, square root, cube, and fourth root of 24 hour precipitation, $u$ wind component, $v$ wind component, relative humidity |

Results only for a selection of these parameters will be presented in this chapter.

<sup>†</sup> See text for definition of composite predictands.

## 2.5 Results of Statistical Modeling

The complete data set that can potentially enter the statistical model consists of daily values of 76 large-scale potential predictors from ECMWF reanalyses and 14 observed local predictands for the period 1979-1993, thus about 5500 daily sets of 90 variables for each of the 22 stations.

### 2.5.1 Role of Near-Surface Predictors

In order to investigate the role of near-surface predictors for the statistical model, we choose two different model versions. In the first one, we allow all predictors (all those in Table 1) to potentially enter the equations. The predictors which are finally selected by the model represent only a small subset of these variables; for local precipitation, for example, usually not more than five large-scale predictors play a significant role and are therefore actually used. In the second model version we use potential predictors above the 850 hPa level only (850, 700, 500, 400, and 300 hPa), additionally mean sea level pressure and the seasonal cycle (noted by asterisks in Table 1). Here, near-surface predictors are excluded in order to be able to get stable results even when applying the model to various GCMs which might differ in the underlying topography and in the representation of surface processes. It is found that the correlation between observed and predicted variables in this model only slightly decreases compared to the first model version, which suggests that predictors above the 850 hPa level are already sufficient for the prediction of the desired local surface

variables. The large-scale variability of the synoptic timescale flow is thus well determined from predictors above the 850 hPa level.

### 2.5.2 General Model Performance

Figures 3a - 3f show an example of statistical model output for the Norwegian station Kvamskogen (60°24'N, 5°55'E, 408 m above sea level). Here, we perform the statistical model on a daily basis with reanalyses at T30 resolution including predictors above the 850 hPa level only (second model version) for the period 1979-1992 (observational data for 1993 was only partly available). The shaded curves show large-scale direct reanalyses for the station without statistical modeling, the solid curves represent statistically simulated results, and the dotted curves show observational data. The correlation coefficient  $r$  between simulated records and observations is shown in the top left corner of each graph.

The station is generally characterized by an exceptionally high amount of observed precipitation (up to 4000 mm/yr) which can naturally not be represented by the direct large-scale reanalysis precipitation (about 1300 mm/yr).

In order to achieve the best fit, the statistical model finally selects three large-scale predictors for the prediction of local precipitation (Table 3). These can be found in the upper right part of Table 3 together with their relative impacts in the final equations. The predictors enter the equations such that (1) negative vertical velocity (upward air movement at 850 hPa, relative impact 60%), (2) positive  $u$ -wind velocity (westerly winds at 700 hPa, relative impact 20%) and (3) positive vorticity (cyclonic movement at 700 hPa, relative impact 20%) on the large scale determine an increase of local precipitation, which at this station is strongly orographically enhanced. Using these three predictors exclusively, the explained variance ( $r^2$ ) between the statistical simulation and the observed record of precipitation is 47.7% for daily data for the complete years 1979-1992 (bottom right part of Table 3).

The explained variance can be further analyzed by investigating the skill of the model for each season individually. The explained variance for daily data in summer (June, July, August (JJA); Table 3, bottom right) is rather low (29.6%) compared to the winter (December, January, February (DJF)) value (59.9%). Also monthly means (57.2% compared to 90.1% in winter) and seasonal means (46.0% compared to 94.0% in winter) remain low. The reason for that might be that the amount of precipitation in summer is smaller (see Figure 4a) and less strongly coupled to atmospheric dynamics than in winter. In summer we believe that convective precipitation has a much higher impact, which weakens the skill of the statistical

---

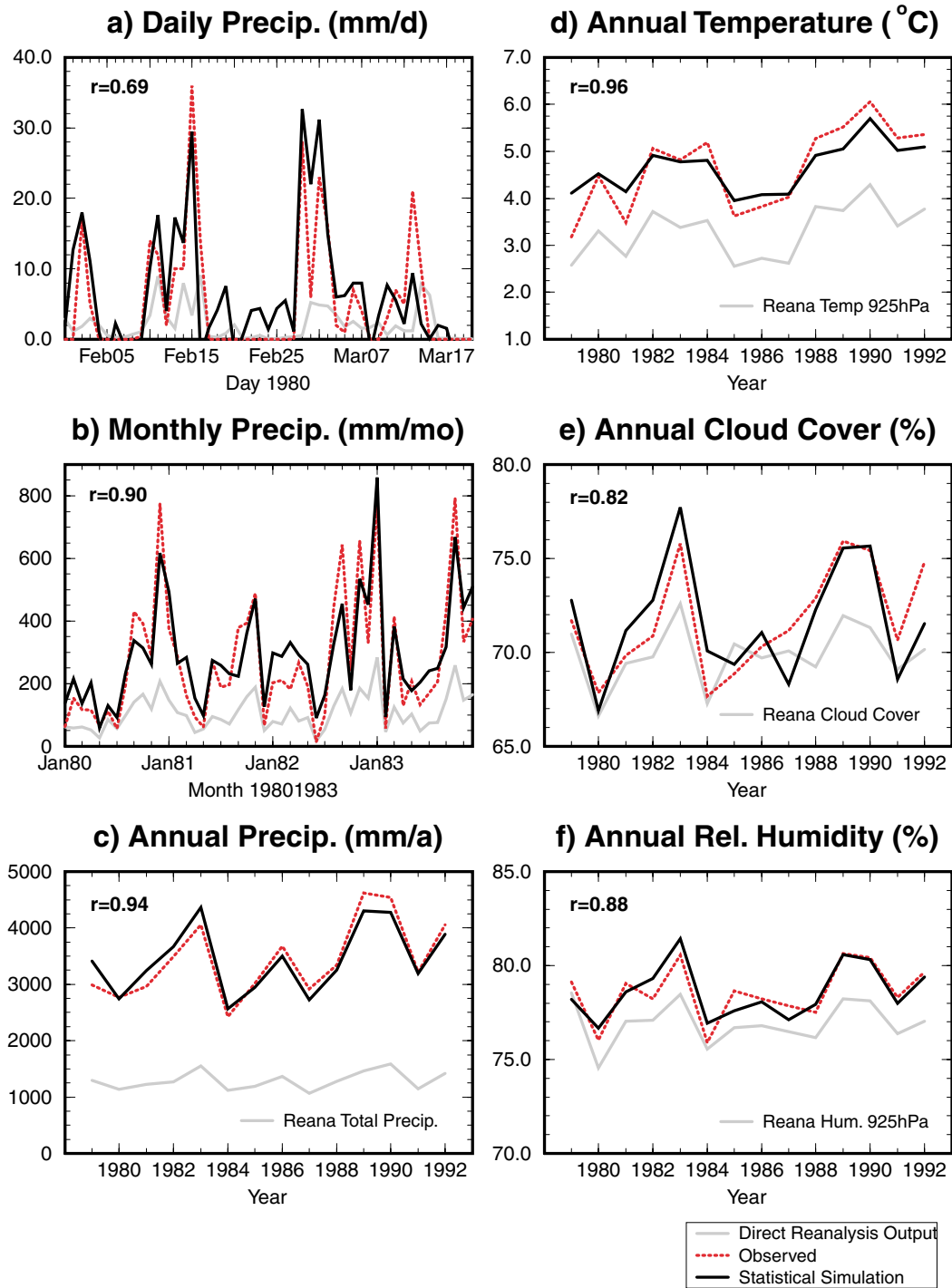


**Figure 3.** Results of the statistical model for station Kvamskogen ( $60^{\circ}24'N$ ,  $5^{\circ}55'E$ , 408 m above sea level, station 14 in Figure 2). Local output is shown for (a) daily precipitation, February 1 to March 19, 1980, (b) monthly precipitation, January 1980 to December 1983, (c-f) annual precipitation, temperature, total cloud cover, and relative humidity, 1979-1992. Solid lines show statistically simulated results, dotted lines represent observed data, and shaded lines are directly interpolated reanalyses without statistical modeling. The correlation coefficient  $r$  between simulations and observations is shown in the top left corner of each graph (see text).

**Table 3.** Predictors Selected by the Statistical Model and Percentage of Observed Variance Explained

| Local Temperature:<br>Predictors and Relative<br>Impact for Complete Years<br>1979-1992 |         |         | Local Precipitation:<br>Predictors and Relative<br>Impact for Complete Years<br>1979-1992 |       |         |        |
|---|---------|---------|---|-------|---------|--------|
| temperature at 850 hPa<br>relative impact 65%   |         |         | vertical velocity at 850 hPa<br>relative impact 60%                                       |       |         |        |
| seasonal cycle: cos(day)<br>relative impact 25%   |         |         | vorticity at 700 hPa<br>relative impact 20%   |       |         |        |
| relative humidity at 850 hPa<br>relative impact 10%                                     |         |         | zonal wind at 700 hPa<br>relative impact 20%  |       |         |        |
| <u>Total Explained Variance for<br/>Local Temperature</u>                               |         |         | <u>Total Explained Variance for<br/>Local Precipitation</u>                               |       |         |        |
|   | Daily   | Monthly | Annual  | Daily | Monthly | Annual |
| Year  | (91.3%) | 85.0%   | 91.9%   | 47.7% | 81.7%   | 88.6%  |
| JJA   | 69.8%   | 79.4%   | 77.5%   | 29.6% | 57.2%   | 46.0%  |
| DJF   | 71.7%   | 93.5%   | 95.7%   | 59.9% | 90.1%   | 94.0%  |

The predictors are shown with their individual relative impact in the final equations for local temperature and local precipitation for station Kvamskogen using daily data for complete years within the period 1979-1992 (see section 2.4.1 for further explanation of the “seasonal cycle” predictor). The bottom part of the table shows the percentage of observed variance explained by the statistical model for the whole year, June, July, and August (JJA) only, and December, January, and February (DJF) only each for original daily data, monthly-averaged output of the statistical model after removing the seasonal cycle, and yearly means of statistical model output (which means seasonally averaged output in the case of JJA and DJF).

model using large-scale predictors as input. Figure 3a shows an example of daily precipitation in February/March 1980 for periods where the model does not produce enough precipitation (e.g., around March 13) and periods where actually nonexistent precipitation is generated (e.g., within the period February 17 to February 27 no precipitation was observed). However, the explained variance for monthly means for the complete year is as high as 81.7% (Figure 3b for 1980-1983); annual means (Figure 3c) even show a remarkable explained variance of 88.6%. This means that monthly and annual mean precipitation is realistically simulated by the statistical model (Figure 3c) on the basis of daily input values. Further experiments using monthly and yearly values (section 2.5.6) indicate that daily values are required to obtain such robust and physically reasonable couplings. Local climatic conditions can be modeled well using daily large-scale predictors. However, the orographic

effect plays an important role and is perhaps the easiest to determine, especially in wintertime with pronounced synoptic flow.

Figures 3d, 3e, and 3f show the model results for annual means of temperature, cloud cover, and relative humidity, respectively. The predictors chosen for local temperature (Table 3, upper left) are large-scale temperature at 850 hPa with the highest relative impact (65%), followed by the seasonal cycle (25%; see section 2.4.1 concerning “seasonal cycle:  $\cos(\text{day})$ ”) and relative humidity at 850 hPa (10%). The explained variance of 91.3% for daily data (Table 3, bottom left) is not representative because it includes the seasonal cycle. However, monthly data can explain 85% of the variance after removing the seasonal cycle, and yearly data can explain as much as 91.9%. The explained variance of annual total cloud cover (67.2%; Figure 3e) is also improved compared to the direct large-scale reanalyses. The same is true for annual relative humidity (Figure 3f) compared to relative humidity at 925 hPa from reanalyses.

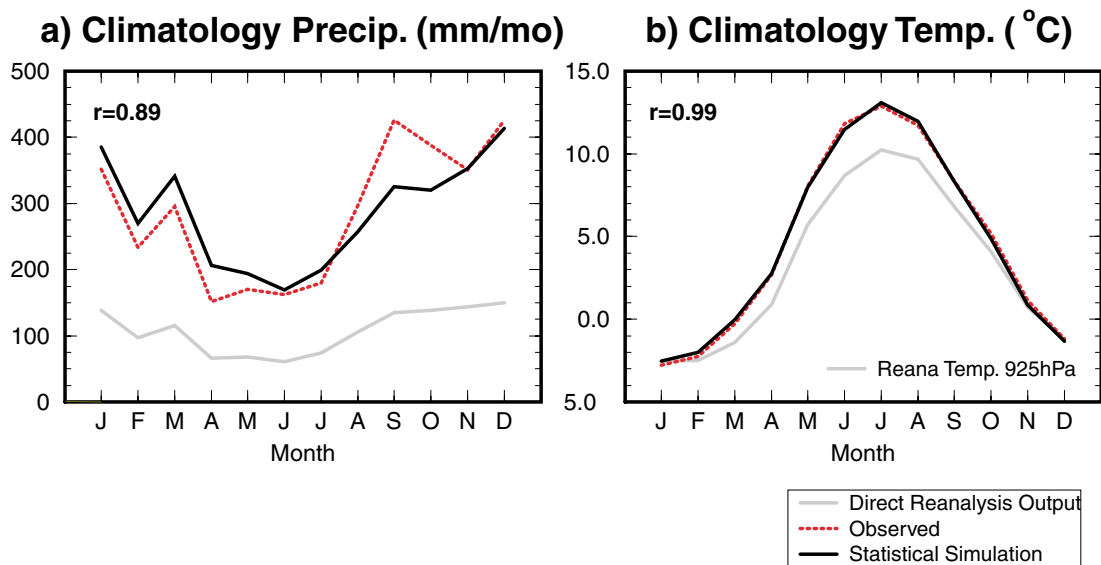


**Figure 4.** Climatology for the period 1979-1992 of (a) precipitation and (b) temperature for observed station data (dotted lines), statistically simulated output (solid lines) and direct reanalysis output (shaded lines) for station Kvamskogen. The correlation coefficient  $r$  between simulations and observations is shown in the top left corner of each graph.

The climatologies of precipitation and temperature for the period 1979-1992 are shown in Figure 4a and 4b, respectively, each for observed station data, statistical simulations, and directly interpolated reanalysis output. Although we do not have a

perfect match between observed data and simulated output for precipitation (Figure 4a), it is clearly visible how the seasonal cycle is enhanced and the climatology is improved compared to direct reanalysis output. This is also true for temperature (Figure 4b). The seasonal cycle of large-scale temperature is modified and matches the observed one nearly perfectly, also demonstrating the qualitative influence of the “seasonal cycle” predictor (see section 2.4.1).

This is just one example out of all stations used in this study. The following section provides information on the skill of the model for other stations within the area of investigation.

### **2.5.3 Spatial Homogeneity of the Statistical Model**

The statistical model may use different optimized predictors with varying relative impacts for the same observed variable at each station due to its local setting. This is demonstrated for 17 stations in the area of Nigardsbreen glacier, Norway. Figure 5 shows the explained variances for observed local temperature (Figure 5a) and observed local precipitation (Figure 5b) for each operational weather station (see Figure 2 for locations; five stations did not cover the ERA time period and are not used, see section 2.4.2). They were calculated using monthly-averaged values after removing the seasonal cycle, and they are split among the large-scale predictors from ECMWF reanalyses chosen by the statistical model. Also shown is the average of explained variance over all stations and its composition.

In general, spatial homogeneity for temperature (Figure 5a) is much higher than for precipitation, as can be expected. The dominant predictors for local temperature are large-scale temperature at 850 hPa, the seasonal cycle (see section 2.4.1 concerning “seasonal cycle:  $\cos(\text{day})$ ”), and relative humidity at 850 hPa with an averaged explained variance of 42.7%, 22.6%, and 8.7%, respectively. Although large-scale temperature has a dominant influence in the equations, its monthly climatology is modified by the “seasonal cycle” predictor as has already been mentioned in section 2.5.2 (Figure 4b). Without including this predictor, the simulation changes qualitatively, and the explained variance decreases significantly. With the daily large-scale temperature predictor alone we would not achieve the maximum skill of the statistical model. On average, 78.6% of observed local temperature could be explained by the statistical model for all stations.

---

## Explained Variance split among Predictors

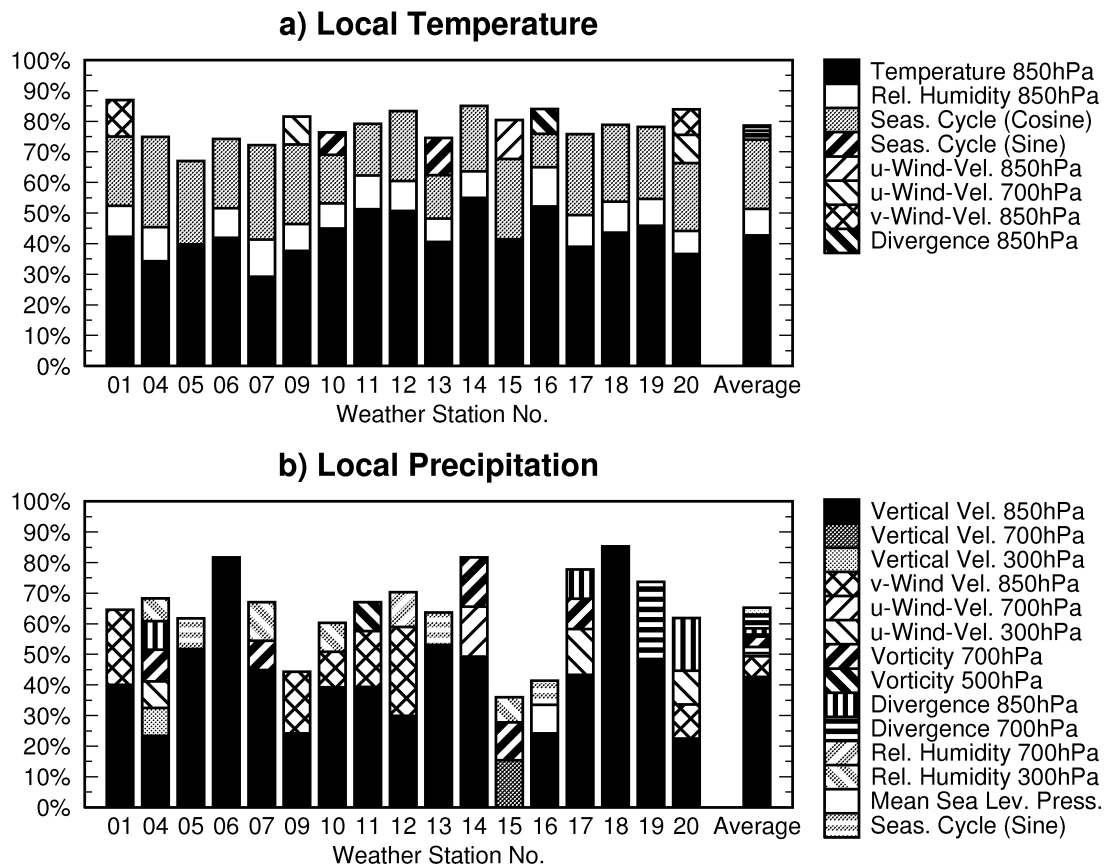


**Figure 5.** Explained variances of the statistical model for (a) observed local temperature and (b) observed local precipitation for each weather station (see Figure 2 for location of stations). The explained variances are split among the large-scale predictors from ECMWF reanalyses chosen by the model.

The explained variance and composition of predictors for local precipitation (Figure 5b) varies significantly for each station. The predictors selected by the statistical model and their impact can be different even for stations that are located close to each other (see, e.g., stations 04 and 05). This is due to the localized variance which is a characteristic of precipitation for stations in a specific local setting. With respect to total explained variance, we may divide the stations into three groups. Stations 18, 14, 06, 17, and 19 belong to the first group with the highest total explained variance (more than 80% on average). These stations are mainly located in the west of the area to be investigated (see Figure 2). The most dominant predictor by far is vertical velocity at 850 hPa, explaining 61.6% of observed variance on average. Remarkably, for stations 18 and 06 it is also the only predictor selected by the statistical model. This demonstrates the strong coupling of local precipitation to atmospheric

dynamics. Further predictors with smaller influence on particular stations are divergence, vorticity, and wind velocity at varying pressure levels. The second group consists of stations 12, 04, 11, 07, 01, 13, 05, 20, and 10 with total explained variances that are close to the average of 65.2% over all stations. These stations are mainly located in the center and in the north of the area. Besides vertical velocity at 850 hPa,  $v$  wind velocity at 850 hPa also plays an important role for some of these stations. For stations 12 and 01, as much as 30% and 24% of variance, respectively, can be explained by this predictor; westerly winds are associated with an increase of precipitation here. For the third group of stations, the total explained variances of only 44%, 41%, and 36% (stations 09, 16, and 15, respectively) are far below the average over all stations. There is no obvious reason for this; either measurement data quality has an influence here, or it is just impossible to find better large-scale predictors for these local settings out of the set of 76 variables from ECMWF reanalyses using the linear regression model.

Besides giving insight into the spatial homogeneity of the statistical model, this section demonstrates the need for the statistical modeling procedure itself. This also becomes clear due to the following experiment: We run the statistical model using additional potential surface predictors including large-scale and convective precipitation from ECMWF reanalyses (model version 1, see section 2.5.1). In this case, the precipitation predictors are either not even selected by the model for the simulation of local precipitation (true for most stations), or the impact of these predictors is extremely small. That means that just by using the direct grid point output of reanalyses (this is, of course, also true for the output of GCM experiments), it is impossible to have a realistic picture of local precipitation. For the simulation of local temperatures, the situation is less extreme, but we also find a considerable improvement compared to the direct grid point output of a model (especially for the seasonal cycle; see section 2.5.2). This is due to the inclusion of additional predictors and the adaptation to the local setting of a station including the orography. For the simulation of a valley glacier, for example, both local temperature (including seasonality) and precipitation are crucial, and the statistical modeling procedure as proposed here is therefore essential.

It should be mentioned that we do not claim that this approach will work equally well in any other part of the world. However, we have carried out further experiments for an area surrounding a valley glacier located in the Swiss Alps (Rhônegletscher; 46°37'N, 8°24'E; see Chapter 4, section 4.2.2) and for an Austrian valley glacier (Hintereisferner; 46°48'N, 10°56'E; not reported in this thesis) with comparably good results and we have planned further experiments for other locations.

---

#### 2.5.4 Model Runs for Specific Seasons of the Year

Is it possible that different predictors may be required for different seasons of the year? The simulation of proxy indicators may require realistic local output with a particular interest in specific seasons (e.g., the growing season of trees or the melting period of glaciers). In order to further investigate the seasonal performance of the statistical model, we carried out experiments allowing daily data for single seasons only as input (Table 4). Compared to the model with full year daily input (Table 3), the composition of predictors and their individual impacts may change. The main results are as follows:

1. With regard to JJA temperatures, if we restrict input data to daily values of JJA (Table 4) then local JJA temperatures are determined by large-scale zonal wind at 850 hPa (relative impact 17%) and vertical velocity at 500 hPa (relative impact 12%), in addition to 850 hPa temperature (relative impact 71%). Here, the daily, monthly, and seasonal explained variance for JJA is 81%, 91.8%, and 89.1%, respectively (bottom part of Table 4). Compared to the seasonal performance with full year input (69.8%, 79.4%, and 77.5%; Table 3, bottom part) the explained variances improve significantly and the predictors have changed.
2. With regard to DJF temperatures, the explained variance for Northern Hemispheric winter (75.8% in Table 4 with daily DJF input data only) is slightly improved compared to the full year input (71.7% in Table 3), whereas monthly and seasonal values remain nearly constant. This means that the large-scale flow patterns in wintertime are already reasonably well determined by the full year input data.

For the prediction of local precipitation, experiments with daily data for specific seasons are also carried out. Although the complete set of potential large-scale predictors (Table 1, predictors marked with asterisks) is offered to the statistical model (as usual), the composition of selected predictors for summer (JJA) precipitation remains the same as for the full year input (Table 3). Also, the total explained variance of 29.7% for daily data remains almost constant (compared to 29.6% in Table 3), demonstrating that even the season-specific statistical model is not able to improve the relations between large-scale variables and local summer precipitation. As mentioned in section 2.5.2, we believe that this is due to the relatively large contribution of convective precipitation in summer, which weakens the skill of the statistical model using large-scale predictors as input. For winter (DJF) precipitation the statistical model again selects vertical velocity at 850 hPa with a relative impact of 66% (compared to 60% for the full year input, Table 3). In contrast to the full year model run, it also selects vorticity at 850 hPa (relative

---

**Table 4.** Predictors Selected and Performance of the Season-Specific Statistical Model for Local Temperature

| Local Temperature:<br>Predictors and Relative<br>Impact for JJA Only<br>1979-1992 |         |        | Local Temperature:<br>Predictors and Relative<br>Impact for DJF Only<br>1979-1992 |         |        |
|---|---------|--------|---|---------|--------|
| temperature at 850 hPa<br>relative impact 71%                                     |         |        | temperature at 850 hPa<br>relative impact 60%                                     |         |        |
| zonal wind at 850hPa<br>relative impact 17%                                       |         |        | relative humidity at 850 hPa<br>relative impact 24%                               |         |        |
| vertical velocity at 500 hPa<br>relative impact 12%                               |         |        | zonal wind at 500 hPa<br>relative impact 16%                                      |         |        |
| Total Explained Variance for<br>Local Temperature, JJA<br>Only                    |         |        | Total Explained Variance for<br>Local Temperature, DJF<br>Only                    |         |        |
| Daily   | Monthly | Annual | Daily   | Monthly | Annual |
| 81.0%   | 91.8%   | 89.1%  | 75.8%   | 94.5%   | 95.6%  |

The model was developed with daily reanalyses and weather station data using JJA values only and DJF values only within the period 1979-1992 (see text and Table 3 for further explanations). The bottom part of the table shows the percentage of observed variance explained by the statistical model for JJA only and DJF only each for original daily data, monthly averaged output of the statistical model after removing the seasonal cycle, and seasonal means of statistical model output.

impact 19%) and temperature at 400 hPa (relative impact 15%). However, in spite of the fact that the predictors are modified to maximize the skill of the model in winter, the total explained variance is not significantly improved; it remains at 60.8% for daily data (compared to 59.9%, Table 3). That means that for our experiments with our set of potential predictors, the quality of simulations for local precipitation is not seasonally dependent as for local temperature. Predictors selected for the full year already seem to be optimized even for the simulation of individual seasons.

We may conclude that for selected observed variables (valid for local temperature but not for local precipitation), the capability to simulate individual seasons can be improved significantly by developing a seasonal-specific statistical model.

### 2.5.5 Model Validation Experiments

In order to address the questions of whether the model works on independent data, and whether it is transferable to other time periods with different climatic conditions, two further experiments are carried out.

In the first experiment we develop the model for the second half of the ECMWF reanalysis time period (1985-1992) only (Figure 6). For the purpose of validation, the statistical relationships obtained are then applied to an independent validation sample, in this case the first half of the reanalysis time period (1979-1984). The annual means of precipitation and temperature for this experiment are shown in Figures 6a and 6b. For temperature (Figure 6b), statistical simulations and observed data are of the same order of magnitude for the developmental and validation sample (also comparable to Figure 3d using the full time period 1979-1992 for development). For precipitation (Figure 6a) the model produces slightly enhanced values in the validation sample. The tendency to produce too much precipitation in this period can already be seen in the experiment using the full time period 1979-1992 for development (Figure 3c) but is enhanced here. However, the model is able to simulate the local variables for this independent validation sample rather realistically, although it is not developed for this time period (i.e., it does not use any local observations in the period 1979-1984 for fitting).

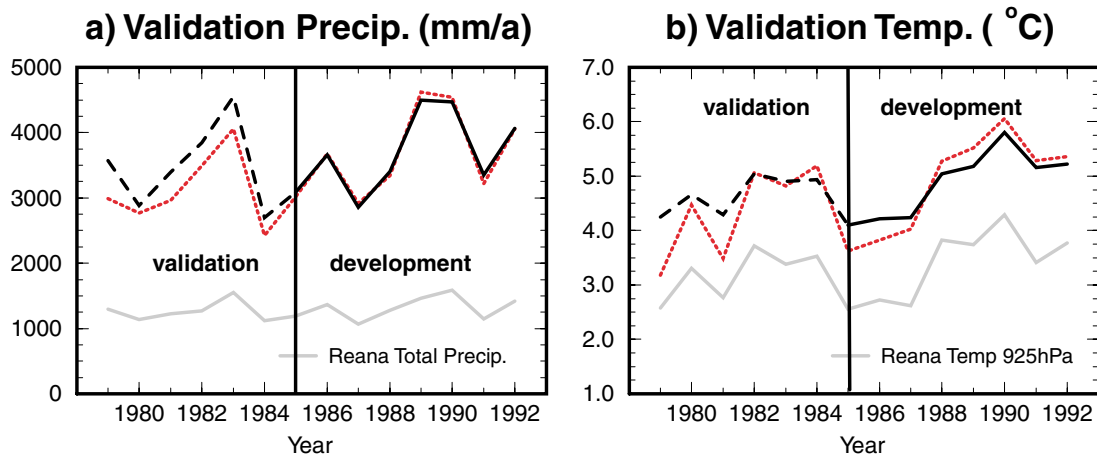


**Figure 6.** Validation experiment for station Kvamskogen (a) for local annual precipitation and (b) for local annual temperature. The model is developed for the 1985-1992 period only (developmental sample). The statistical relationships obtained are then applied to independent reanalyses for 1979-1984 (validation sample). The solid and dashed lines show the statistical model output for the developmental and validation sample, respectively, dotted lines represent observed data, and shaded lines are directly interpolated reanalyses without statistical modeling. See Figures 3c and 3d (using full time period 1979-1992 for development) for comparison.

**Statistical Distribution of Daily Local Temperatures  
Station Kvamskogen, Stat. Modeled ECMWF Re-Analyses 1979–1992**

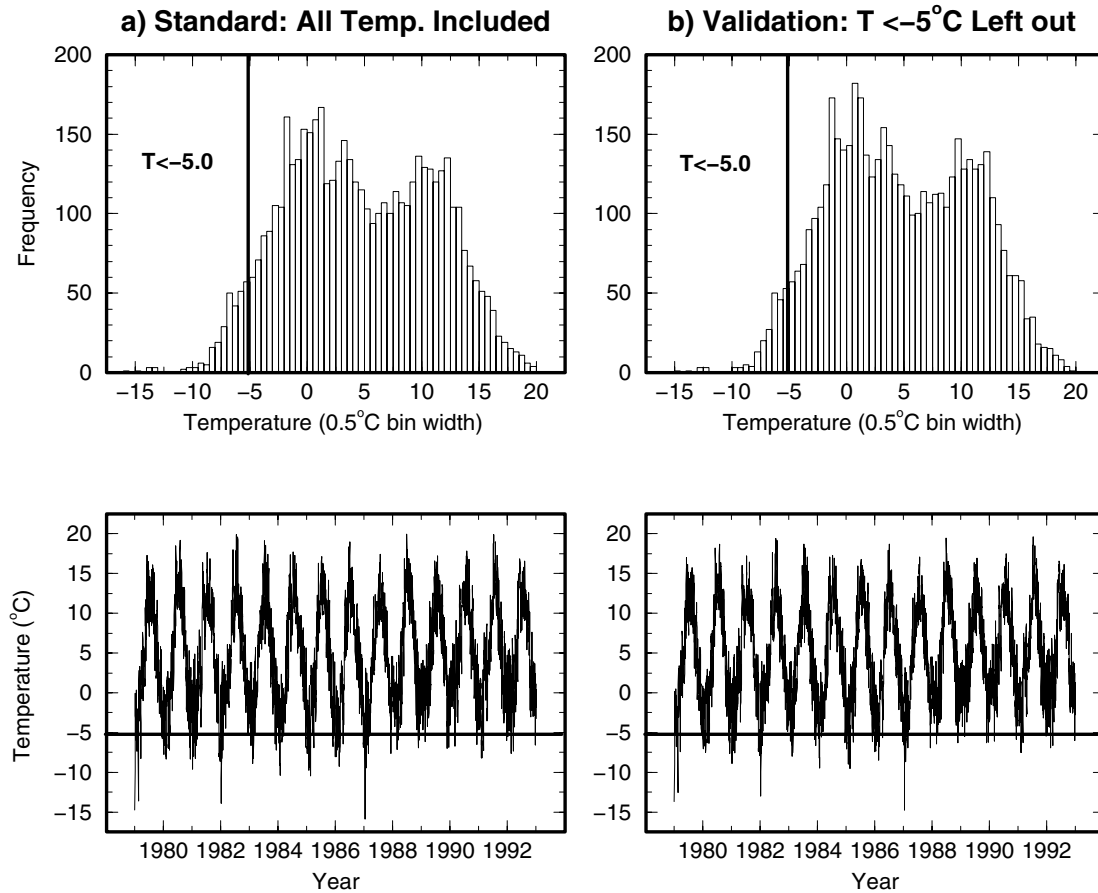


**Figure 7.** Statistical distribution (top graph) of daily local temperatures for station Kvamskogen after statistical modeling for the period 1979–1992 and time series of daily temperatures (bottom graph) for (a) all temperature events included for the development of the model and (b) events with temperatures less than  $-5^{\circ}\text{C}$  excluded from model development. Although the model in Figure 7b is not developed for events  $< -5^{\circ}\text{C}$  it still has realistically simulated them; the differences in distribution between Figures 7a and 7b are reasonably small. This shows that, as long as the extreme events do not correspond to a fundamentally different weather regime, then the statistical model is still able to simulate them.

The second experiment addresses the question of whether the model can produce realistic output for events which differ from events the model is actually developed for. These events may occur under slightly changed climatic conditions (which are not fundamentally different in their large-scale flow properties, see below and section 2.6). If the model is developed using present-day climatic conditions (represented by ECMWF reanalyses), is it then applicable to GCM output for

preindustrial times? The statistical distribution of daily local temperatures for station Kvamskogen after statistical downscaling of ECMWF reanalyses for the period 1979-1992 is shown in Figure 7. The standard experiment (Figure 7a) includes all temperature events occurring for the development of the model. For the validation experiment (Figure 7b), events with temperatures less than  $-5^{\circ}\text{C}$  are excluded prior to model development; afterwards, the statistical relationships are calculated in the same way. Although this model is not developed for these events it has still realistically simulated them, which can be clearly seen in the distribution (Figure 7b, top graph) and the time series (Figure 7b, bottom graph) of temperatures. The differences between the standard and validation experiment (Figure 7a and 7b respectively) are reasonably small. This shows that, as long as the extreme events do not correspond to fundamentally different (and possibly nonlinear) weather regimes, then the statistical model is still able to simulate them. This is to a large extent true for the events of the preindustrial output of the GCM (see section 2.6) which will be applied below. Here, the general coupling between the large-scale flow and local weather parameters deduced from present-day climate is to a great extent maintained.

The two described experiments demonstrate the applicability of the statistical model to independent data sets, and they also show that we may simulate events which have not been visited in the developmental time period as far as the events do not correspond to fundamentally different (and possibly nonlinear) weather regimes.

### **2.5.6 Impact of Spatiotemporal Resolution of Predictors**

Our intention is to produce reliable local monthly or annual mean output from reanalyses and GCMs comparable to corresponding local weather station data. Although we do not aim to produce perfect predictions on a daily basis, it emerges from the experiments that our model requires daily predictor data as input in order to achieve the statistically closest and most robust relationships. Consequently, the output can best be averaged to monthly or annual means after the statistical calculations have been carried out using daily predictor data.

Monthly means as input have also been tested, but the results are less good; the model sometimes attempts to use near-collinear predictors for least squares estimation, which particularly becomes a problem when being applied to independent data. Furthermore, the actual physical relations between large-scale flow and local variables cannot be represented as satisfactorily as when daily data is used as input; a lot of information is averaged out. This is especially important for the simulation of local precipitation; the model has no choice other than to select predictors which

---

represent much less meaningful physical relations to the large-scale flow compared to those when daily data is used.

This emphasizes the role of synoptic timescale variability in the close relations between local weather and large-scale circulation patterns. Averaging the predictors means that this information is partly removed and the correlation therefore weakens.

The impact of spatial resolution of predictors is investigated, producing statistical model output both using large-scale predictors (see section 2.4.1 for definition) from the interpolated T30 data set ( $\sim 3.8^\circ \times 3.8^\circ$ ) and using original reanalyses at T106 resolution ( $\sim 1.1^\circ \times 1.1^\circ$ ) for comparison. Although the interpolated reanalyses would maybe not be completely similar to the output of a conceivable reanalyses project using actual T30 resolution from the beginning, they are suitable for providing information on the impact of model resolution. It is found that summer temperatures (JJA) are most sensitive. For the example given in Table 3, the explained variance of monthly data for JJA (seasonal cycle removed) is increased from 79.4% (T30 resolution) to 84.5% (T106 resolution); annual data improve from 77.5% (T30 resolution) to 83.3% (T106 resolution). The sensitivity for local precipitation is of the same order. Monthly means for JJA increase from 57.2% (Table 3) to 62.1%, annual means from 46.0% to 51.7%. The improvements are not more extreme since even at T106 resolution, the predictors still represent the large-scale flow which is already well represented at T30 resolution for the area to be investigated.

In spite of these improvements, we may conclude that the overall ability to produce satisfactory statistical model output is already given using T30 predictor resolution, which is also the resolution of the ECHAM4 GCM runs which will be used below.

## **2.6 Application to ECHAM4 GCM: Control and Preindustrial Run**

The statistical relationships derived from ECMWF reanalyses and local station data are applied to the output of the ECHAM4 general circulation model coupled to a mixed layer ocean (ECHAM4/MLO) developed at the Max-Planck-Institut für Meteorologie (MPI) and the Deutsches Klimarechenzentrum (DKRZ) in Hamburg [Roeckner *et al.*, 1996; Roeckner, 1997; Roeckner *et al.*, 1999] (see Chapter 4 for application to ECHAM4/OPYC coupled GCM). A general comparison between the present-day climate as simulated by the ECHAM4 GCM and ECMWF analyses can be found in Roeckner *et al.* [1996]. We use a long integration of a control run and a run with constant preindustrial greenhouse gas concentrations for our experiments.

---

The control experiment of the 19-layer ECHAM4/MLO GCM has been performed for 590 years at T30 ( $\sim 3.8^\circ \times 3.8^\circ$ ) resolution. The concentrations of carbon dioxide, methane, and nitrous oxide are fixed at the observed 1990 values [*Intergovernmental Panel on Climate Change (IPCC)*, 1990, Table 2.5]. A 100-year equilibrium run with constant preindustrial greenhouse gas concentrations [*IPCC*, 1995] has also been performed. The global average surface air temperature for the preindustrial run in equilibrium is 1.0°C lower than for the control run.

The daily large-scale output of these models for the area of Nigardsbreen glacier, Norway, is applied to the statistical relationships obtained as described above. As an example, we show the statistically downscaled and yearly-averaged GCM output of surface air temperature deviations for station Ona II (Figure 8). This station is chosen because we are able to compare the variability of simulated data to a long instrumental observed temperature record for the period 1868-1955 which is available from the Global Historical Climatology Network (GHCN) temperature data base [*Peterson and Vose*, 1997]. A long instrumental record of observed precipitation, which could be used for comparison with downscaled precipitation, has however not been available for the area. In Figure 8, we include observed temperature data for station Ona II within the period 1979-1993 obtained from the Swedish Meteorological and Hydrological Institute (SMHI). We have subtracted the mean value of the latter data both from GHCN and SMHI data. The middle plot of Figure 8 shows the observed temperature deviations at station Ona II. The left and right plots of Figure 8 represent statistically downscaled GCM surface air temperature output with constant preindustrial greenhouse gas concentrations and statistically downscaled GCM output for 590 years of the control run, respectively.

In general, we assume that the statistical relationships (established by the linear regression model for present-day climate on a daily basis) between large-scale circulation patterns and local parameters are maintained when applying the statistical model to preindustrial times. In order to support this assumption, we have investigated the differences between the circulation patterns of the preindustrial GCM run and the GCM control run. For the midlatitude regions of interest in this study, we found that the simulated patterns of the predictor fields used for downscaling are similar in both integrations, confirming the validity of the assumption. However, the statistical relations may not be applicable to climates with major general changes in circulation patterns (e.g., simulation for the Last Glacial Maximum), for which the composition and impact of large-scale predictors may differ significantly.

---

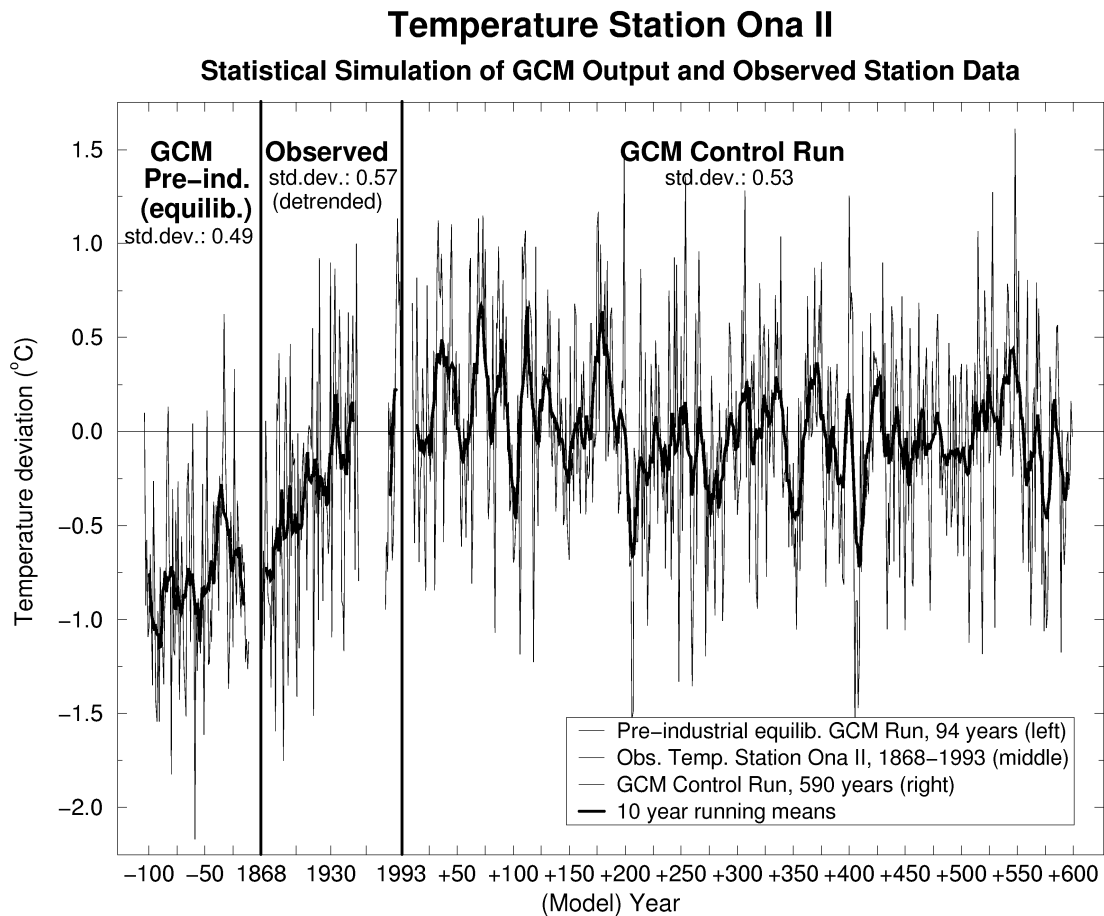


**Figure 8.** Application of the statistical model to GCM output (ECHAM4 T30 L19 Mixed Layer Ocean) for station Ona II. Thin lines are annual mean temperature deviations; thick lines are 10-year running means. The left plot shows statistically downscaled local output from the equilibrium GCM run with constant preindustrial [IPCC, 1995] greenhouse gas concentrations; the right plot represents the 590-year control run of the same model with modern greenhouse gas concentrations. For comparison, observed temperature deviations for Station Ona II are shown in the middle plot.

The first striking feature in Figure 8 is the mean temperature difference of about  $0.8^{\circ}\text{C}$  between the preindustrial GCM run and the control run, which is comparable to the observed temperature increase over the last 125 years for this station. This is due to the large-scale GCM output itself within this region, but it also shows that the statistical model (besides improving the variability of local records) is capable of maintaining mean large-scale temperature changes due to different climatic conditions for this location.

More important for the performance of the statistical model is that the annual variability in GCM output (both control and preindustrial run) closely resembles the observed variability. The standard deviation for the 100-year preindustrial run and

the 590-year control run is 0.49 and 0.53, respectively, compared to 0.57 for the observed (detrended) temperature record. The dynamical GCM output in combination with the statistical modeling procedure therefore appears to be a realistic simulation. However, when comparing a GCM simulation in equilibrium state (constant greenhouse gas concentrations) with observations, it is, of course, possible that the variability is affected by the fact that greenhouse gases are continuously increasing. Experiments with transient coupled GCM runs (ECHAM4/OPYC3) will therefore also be performed in future.

The 10-year running means of the GCM simulations (Figure 8) show a comparable or even slightly higher variability compared to the relatively short observational record of 125 years. Pronounced lower-frequency fluctuations are clearly simulated by the downscaled GCM control experiment.

This section has demonstrated that the statistically modeled dynamical GCM output can realistically simulate both the patterns of observed variability on the annual to decadal scale as well as temperature changes due to different climatic scenarios.

## **2.7 Conclusions**

Local output for temperature, precipitation, and other parameters has been produced by a general circulation model in combination with a statistical downscaling model. Stable and physically reasonable relationships for statistical model development were obtained using large-scale predictors from daily ECMWF reanalyses and local surface observations for the area of Nigardsbreen glacier, Norway. Near-surface predictors (below the 850 hPa level) were excluded in order to be able to get stable results even when applying the model to various GCMs which might differ in the underlying topography and in the representation of surface processes. We found that daily predictor data as input for the statistical model are required in order to achieve statistically the most stable and physically the most reasonable relationships. Satisfactory results of the model were achieved using T30 resolution predictor data.

As an example, the results of statistical downscaling for station Kvamskogen, Norway, have been discussed in detail. This station is characterized by a large amount and high variability in precipitation which can naturally not be represented by the grid-point output of ECMWF reanalyses (or GCM output). Using the downscaling approach, we have been able to explain 82% of the observed monthly local precipitation and 89% of the observed annual precipitation for this station within the time period of the ECMWF reanalyses using large-scale vertical velocity

---

at 850 hPa, vorticity at 700 hPa, and zonal wind at 700 hPa. For local temperature, large-scale temperature at 850 hPa, relative humidity at 850 hPa, and the “seasonal cycle predictor” have been chosen by the statistical model explaining 85% and 92% of observed monthly and annual variance, respectively. For both precipitation and temperature, the monthly climatology for the period of the ECMWF reanalyses could be considerably improved using the downscaling approach.

Investigating the spatial homogeneity of the model for 17 stations in the Nigardsbreen area showed that the composition of predictors and their relative impact (particularly for local precipitation) varies significantly for individual stations due to their local setting. The predominant predictor for local precipitation is vertical velocity at 850 hPa, explaining, on average, more than 41% of variance alone. Other predictors for precipitation, which have an impact on individual stations, are zonal and meridional wind, vorticity, divergence, and relative humidity. For local temperature, spatial homogeneity is much higher than for precipitation, as can be expected. The most important predictor is large-scale temperature at 850 hPa, followed by the “seasonal cycle predictor” and relative humidity at 850 hPa.

Analyzing single seasons individually, it became clear that, particularly for local temperature, it can be useful to develop a specific set of predictors for seasons which can be most relevant for a specific proxy indicator (e.g., for the melting period of glaciers). For station Kvamskogen, for example, the explained variances for both monthly and annual summer (JJA) temperatures could be improved by more than 10% using seasonal-specific statistical relationships.

We validated the model using separate developmental and validation intervals for the reanalyses time period and we carried out a validation experiment with a restricted predictor data set. These experiments demonstrated the applicability of the statistical model to independent data sets, and they also showed that extreme events which have not been visited in the developmental time period can be simulated by the model, as long as they do not correspond to fundamentally different (and possibly nonlinear) weather regimes.

The method has been applied to a multi-century integration of the ECHAM4 / Mixed Layer Ocean GCM with present greenhouse gas concentrations and to an equilibrium run with preindustrial greenhouse gas forcing. The output has been compared to patterns of observed station data in the area of Nigardsbreen glacier for the period 1868-1993. Patterns of observed variability on the annual to decadal scale and temperature changes due to the preindustrial climatic scenario have been realistically simulated for this location.

---

The proposed modeling approach could help to improve a systematic interpretation of paleoclimatic proxy records (obtained, for example, from tree-rings or glaciers) and model-data intercomparisons for past climatic scenarios.

A possible application is the simulation of the response of valley glaciers to specific climatic conditions. This is useful since observed glacier fluctuations represent valuable climatic proxy data extending back over several centuries. In order to simulate glacier variations, the next step is the development of a method to relate glacier mass balance to meteorological data or to downscaled GCM output. This will be the subject of the following chapter.

---

---

**References**

- Barnett, T.P., B. D. Santer, P. D. Jones, R. S. Bradley, and K. R. Briffa, Estimates of low frequency natural variability in near-surface air temperature, *Holocene*, 6, 255-263, 1996.
- Bengtsson, L., The weather forecast, *Pure Appl. Geophys.*, 119, 515-537, 1981.
- Bergeron, T., Richtlinien einer dynamischen Klimatologie, *Meteorol. Z.*, 47, 246-262, 1930. (Engl. transl., Ground plan of a dynamic climatology, *Mon. Weather Rev.*, 59, 219-235, 1931.)
- Bradley, R. S., Are there optimum sites for global paleotemperature reconstruction?, in *Climatic Variations and Forcing Mechanisms of the Last 2000 Years*, edited by P. D. Jones, R. S. Bradley and J. Jouzel, *NATO ASI Ser., Ser. I*, 41, 603-624, 1996.
- Bradley, R. S., and P. D. Jones, "Little Ice Age" summer temperature variations: Their nature and relevance to recent global warming trends, *Holocene*, 3, 367-376, 1993.
- Briffa, K. R., P. D. Jones, T. S. Bartholin, D. Eckstein, F. H. Schweingruber, W. Karlen, P. Zetterberg, and M. Eronen, Fennoscandian summers from AD 500: Temperature changes on short and long timescales, *Clim. Dyn.*, 7, 111-119, 1992.
- Cubasch, U., H. von Storch, J. Waszkewitz, and E. Zorita, Estimates of climate change in southern Europe derived from dynamical climate model output, *Clim. Res.*, 7, 129-149, 1996.
- Dunbar, R. B., G. M. Wellington, M. W. Colgan, and P. W. Glynn, Eastern Pacific sea surface temperature since 1600 A.D., The  $\delta^{18}\text{O}$  record of climate variability in the Galapagos corals, *Paleoceanography*, 9, 291-315, 1994.
- George, J. J. (Ed.), *Weather Forecasting for Aeronautics*, pp. 407-415, Academic, San Diego, Calif., 1960.
- Gibson, J. K., P. Kållberg, S. Uppala, A. Nomura, A. Hernandez, and E. Serrano, ERA Description, *ECMWF Re-Anal. Proj. Rep. Ser., Rep. 1*, Eur. Cent. for Medium-Range Weather Forecasts, Reading, England, 1997.
- Groverman, B. S., and H. E. Landsberg, Reconstruction of Northern Hemisphere temperature: 1579-1880, in *Meteorol. Program Publ., vol. 79-181*, Univ. of Md., College Park, 1979.
- Heyen, H., E. Zorita, and H. von Storch, Statistical downscaling of monthly mean North Atlantic air-pressure to sea level anomalies in the Baltic Sea, *Tellus, Ser. A*, 48, 312-323, 1996.
-

- Intergovernmental Panel on Climate Change (IPCC), *Climate Change, The IPCC Scientific Assessment*, edited by J. T. Houghton et al., Cambridge Univ. Press, New York, 1990.
- IPCC, *Climate Change 1994, Radiative Forcing of Climate Change*, edited by J. T. Houghton et al., p. 80/194, Cambridge Univ. Press, New York, 1995.
- Jones, P. D., and R. S. Bradley, Climatic variations in the longest instrumental records, in *Climate Since A. D. 1500*, edited by R. S. Bradley and P. D. Jones, pp. 246-268, Routledge, New York, 1992.
- Karl, T. R., W.-C. Wang, M. E. Schlesinger, R. W. Knight, and D. Portman, A method of relating general circulation model simulated climate to the observed local climate, I, Seasonal statistics, *J. Climate*, 3, 1053-1079, 1990.
- Kim, J.-W., J.-T. Chang, N. L. Baker, D. S. Wilks, and W. L. Gates, The statistical problem of climate inversion: Determination of the relationship between local and large-scale climate, *Mon. Weather Rev.*, 112, 2069-2077, 1984.
- Landsberg, H. E., B. S. Groveman, and I. M. Hakkarinen, A simple method for approximating the annual temperature of the Northern Hemisphere, *Geophys. Res. Lett.*, 5, 505-506, 1978.
- Manabe, S., and R. J. Stouffer, Low-frequency variability of surface air temperature in a 1000-year integration of a coupled atmosphere-ocean-land surface model, *J. Climate*, 9, 376-393, 1996.
- Mann, M. E., R. S. Bradley, and M. K. Hughes, Global-scale temperature patterns and climate forcing over the past six centuries, *Nature*, 392, 779-787, 1998.
- Mann, M. E., R. S. Bradley, and M. K. Hughes, Northern Hemisphere temperatures during the past millennium: inferences, uncertainties, and limitations, *Geophys. Res. Lett.*, 26, 759-762, 1999.
- Martin E., B. Timbal, and E. Brun, Downscaling of general circulation model outputs - Simulation of the snow climatology of the French Alps and sensitivity to climate change, *Clim. Dyn.*, 13, 45-56, 1996.
- Oerlemans, J., Climate sensitivity of glaciers in southern Norway: Application of an energy-balance model to Nigardsbreen, Helstugubreen and Alftobreen, *J. Glaciol.*, 38, 223-232, 1992.
- Oerlemans, J., Modelling the response of valley glaciers to climatic change, in *Physics and Chemistry of the Atmospheres of the Earth and Other Objects of the Solar System*, edited by C. Boutron, Eur. Res. Course Atmos., vol.2, pp. 91-123, Les Editions de Physique, Les Ulis, France, 1996.
-

- Oerlemans, J., A flow-line model for Nigardsbreen: Projection of future glacier length based on dynamic calibration with the historic record, *Ann. Glaciol.*, 24, 382-389, 1997.
- Paterson, W. S. B. (Ed.), *The Physics of Glaciers*, 3rd ed., Pergamon, New York, 1994.
- Peterson, T. C., and R. S. Vose, An overview of the Global Historical Climatology Network temperature data base, *Bull. Am. Meteorol. Soc.*, 78, 2837-2849, 1997.
- Pfister, C., Monthly temperature and precipitation in central Europe from 1525-1979: Quantifying documentary evidence on weather and its effects, in *Climate Since A. D. 1500*, edited by R. S. Bradley and P. D. Jones, pp. 118-142, Routledge, New York, 1992.
- Reichert, B. K., L. Bengtsson, and O. Åkesson, A statistical-dynamical modeling approach for the simulation of local paleo proxy records using GCM output, *Rep. 274*, Max-Planck-Inst. für Meteorol., Hamburg, Germany, 1998.
- Roeckner, E., L. Arpe, L. Bengtsson, M. Christoph, M. Claussen, L. Dümenil, M. Esch, M. Giorgetta, U. Schlese, and U. Schulzweida, The atmospheric general circulation model ECHAM-4: Model description and simulation of present-day climate, *Rep. 218*, Max-Planck-Inst. für Meteorol., Hamburg, Germany, 1996.
- Roeckner, E., Climate sensitivity experiments with the MPI/ECHAM4 model coupled to a slab ocean (abstract), in *Euroclivar Workshop on Cloud Feedbacks and Climate Change*, edited by C. A. Senior and J. F. B. Mitchell, pp. 20, Hadley Cent. for Clim. Predict. and Res., Bracknell, England, 1997.
- Roeckner, E., L. Bengtsson, J. Feichter, J. Lelieveld and H. Rodhe, Transient climate change simulations with a coupled atmosphere-ocean GCM including the tropospheric sulfur cycle, *J. Climate*, 12, 3004-3032, 1999.
- Stendel, M., and K. Arpe, Evaluation of the Hydrological Cycle in Re-Analysis and Observations, ECMWF Re-Analysis Validation Reports - Part 1, *ECMWF Re-Anal. Proj. Rep. Ser., Rep. 6*, Eur. Cent. for Medium-Range Weather Forecasts, Reading, England, 1997.
- Thompson, L. G., Ice core evidence from Peru and China, in *Climate Since A. D. 1500*, edited by R. S. Bradley, and P. D. Jones, pp. 517-548, Routledge, New York, 1992.
- von Storch, H., and F. W. Zwiers (Eds.), *Statistical Analysis in Climate Research*, Cambridge Univ. Press, New York, 1999.
- von Storch, H., E. Zorita, and U. Cubasch, Downscaling of global climate change estimates to regional scales: An application to Iberian rainfall in wintertime, *J. Climate*, 6, 1161-1171, 1993.
-

Wigley, T. M. L., P. D. Jones, K. R. Briffa, and G. Smith, Obtaining sub-grid-scale information from coarse-resolution general circulation model output, *J. Geophys. Res.*, 95, 1943-1953, 1990.

---

## 3 Relating Glacier Mass Balance to Meteorological Data

---

### ***Relating Glacier Mass Balance to Meteorological Data Using a Seasonal Sensitivity Characteristic (SSC)<sup>2</sup>***

**Abstract.** A method is proposed to quantify the climate sensitivity of the mean specific balance  $B$  of a glacier by a Seasonal Sensitivity Characteristic (SSC). The SSC gives the dependence of  $B$  on monthly anomalies in temperature and precipitation. The SSC is calculated from a mass balance model. Examples for Franz-Josef Glacier (New Zealand), Nigardsbreen (Norway), Hintereisferner (Austria), Peyto Glacier (Canadian Rockies), Abramov Glacier (Kirghizstan) and White Glacier (Canadian Arctic) are discussed. With regard to the climate sensitivity of  $B$  to temperature, the SSCs clearly show that for glaciers in dry climates, the effect of temperature is mainly restricted to summer months. For glaciers in wetter climates, spring and fall temperatures additionally make a significant contribution to the overall sensitivity. The overall sensitivity to precipitation varies considerably between the glaciers, the effect of summer precipitation is also strongly dependant on the altitudinal range of the glaciers.

The SSC is a 2x12 matrix. Multiplying it by monthly perturbations of temperature and precipitation for a particular year yields an estimate of the balance for that year. It is shown that with this technique, mass-balance series can be (re)constructed from long meteorological records or from output of atmospheric models.

### **3.1 Introduction**

Within a global context, glacier fluctuations are of interest primarily for two reasons. Firstly, historic glacier fluctuations contain information on past climatic change that can be extracted with modeling techniques [e.g. *Nye, 1965; Smith and Budd, 1979; Oerlemans, 1997*]. Recently developed glacier modeling techniques make it easier to

---

<sup>2</sup> Oerlemans, J., and B. K. Reichert, *Journal of Glaciology*, 46(152), in press, 2000.

correct for geometric effects and extract a climate record from a glacier length record, for instance. Secondly, there is the generally accepted idea that glacier melt plays a significant role in global sea-level rise [Meier, 1984; Zuo and Oerlemans, 1997; Dyurgerov and Meier, 1997].

Thus for several reasons there is a need to relate glacier mass balance to meteorological data. This data can be long records of instrumental observations, interpolated data from initialization schemes in weather forecast models, or output from GCMs.

Many studies have been carried out in which regression techniques have been used to relate mean observed specific balance and/or equilibrium-line altitude to meteorological quantities [e.g. Lliboutry, 1974; Hoinkes and Steinacker, 1975; Letréguilly 1984; Günther and Widlewski, 1986; Greuell, 1992]. In such studies the number and type of predictors varies between glaciers, depending on what is thought to be suitable for the given climatic setting. In a way, this makes it difficult to compare such studies. In most studies, summer temperature and winter precipitation are assumed or found to be the best predictors, however summer and winter seasons are not defined in a uniform way. Consequently, studies of different glaciers are hard to intercompare. In the near future, output from GCMs will be used more and more to make projections of glacier behaviour around the world (see Chapters 4 and 5 of this thesis). This calls for more structure in the description of the climate - mass balance relation.

We propose to define and use for individual glaciers a Seasonal Sensitivity Characteristic (SSC) that gives the dependence of the mean specific balance to monthly perturbations in temperature and precipitation. The SSC is a  $2 \times 12$  matrix and multiplying it by an appropriate record of 12 monthly temperature values and 12 monthly precipitation values yields an estimate of the mean specific balance. Since instrumental records and GCM output is normally available in the form of monthly mean values, this makes it much easier to reconstruct or project the specific balance. It also facilitates the comparison of the climate sensitivity of individual glaciers. However, even for the longest mass balance records it is not possible to derive monthly sensitivities in a statistical way because the number of unknown quantities (24) would be too large. Therefore, a mass balance model is required to compute the SSC.

In section 3.2, we first define the SSC and show examples for a selection of glaciers in different climatic settings. In section 3.3, we discuss how the SSC can be used to reconstruct the mean specific balance from a series of monthly values of temperature

---

and precipitation. In section 3.4, a comparison is made between a balance record from a full energy balance calculation and from the simpler technique.

### 3.2 The Seasonal Sensitivity Characteristic (SSC)

The mean specific balance  $B$  of a glacier is the specific balance (defined as the annual mass gain or loss of a glacier) over the entire glacier surface. As a unit, we use mwe (meters of water equivalent). For a particular year, the value of the balance with respect to a reference balance  $B_{ref}$  is denoted by  $\Delta B$ :

$$\Delta B = B - B_{ref} \quad (1)$$

The basic idea now is that  $\Delta B$  can be related to monthly mean precipitation ( $P_k$ ) and temperature ( $T_k$ ), we then denote the balance by  $\Delta B_m$  and express it as

$$\Delta B_m = \sum_{k=1}^{12} \left[ C_{T,k} (T_k - T_{ref,k}) + C_{P,k} (P_k / P_{ref,k}) \right] + H \quad (2)$$

where

$$C_{T,k} = \frac{\partial B}{\partial T_k} \quad (3)$$

and

$$C_{P,k} = \frac{\partial B}{\partial (P_k / P_{ref,k})} \quad (4)$$

are monthly sensitivity values associated with the SSC. The index  $k$  refers to the month ( $k = 1, \dots, 12$ ).  $T_{ref,k}$  and  $P_{ref,k}$  are climatological means of monthly values and can be associated with the reference balance (preferably zero).  $C_{T,k}$  has unit mwe  $K^{-1}$ . In the definition of  $C_{P,k}$ , the dependent variable is monthly precipitation divided by the precipitation in the reference case, and  $C_{P,k}$  has the unit mwe.

Equation (2) can be regarded as a linearization of a more general expansion. The term  $H$  represents all nonlinear terms. This includes not only higher-order terms associated with the expansion for a particular month, but also cross-terms in which a perturbation in a certain month several years ago may affect the actual balance through feedbacks in the system (for instance, albedo feedback due to a large positive anomaly in snow accumulation some time ago). The importance of such longer term effects will be discussed in section 3.4.

The SSC consists of the 24 values for  $C_{T,k}$  and  $C_{P,k}$  which can be calculated with a mass balance model. This can potentially be a degree-day model or an energy balance model of any complexity. The only requirement is that the model computes the cumulative balance through the year. Here, we use the model described in *Oerlemans* [1992] (see Chapter 4, section 4.3.1 for description). This model is a mass balance model of intermediate complexity, in which the energy exchange between atmosphere and glacier surface is treated in some detail. However, the thermodynamic processes inside the glacier are not modeled explicitly. The energetics involved in refreezing is dealt with in a schematic way. In *Oerlemans and Fortuin* [1992] this model was applied successfully to 12 glaciers for which good mass balance observations exist. On the basis of some recently performed experimental meteorological work on glaciers [e.g. *Greuell et al.*, 1998] some of the parameterizations have been adjusted (unpublished), but this only has a marginal effect on the basic properties of the model.

The calculation of a SSC proceeds as follows. For a particular glacier, the observed balance profile is simulated as well as possible using the mass balance model [*Oerlemans*, 1992]. The model is then integrated for monthly temperature perturbations (in practice +0.5 K and -0.5 K) and monthly precipitation perturbations (+10% and -10%), and the specific  $C_{T,k}$  and  $C_{P,k}$  values are subsequently determined. The validity and performance of this approach, also for larger perturbations in temperature and precipitation, will be discussed in section 3.4.

SSCs for a selection of glaciers are shown in Figure 1a-f. The sample ranges from a glacier in a very wet climate (Franz-Josef Glacier, annual precipitation  $P_{ann} \sim 6$  m, Figure 1a), through glaciers in a moderately wet climate (e.g. Hintereisferner,  $P_{ann} \sim 1.5$  m, Figure 1c), to glaciers in a very dry climate (White Glacier,  $P_{ann} \sim 0.25$  m, Figure 1f). It should be noted that the mass balance model for Franz-Josef Glacier was calibrated in conjunction with a study using a flow-line model [*Oerlemans*, 1997] since direct mass-balance observations were not available. To facilitate comparison, all SSCs in Figure 1 have been plotted on the same scales.

From this figure it is clear that the sensitivity of  $B$  to temperature and precipitation changes strongly increases with the amount of annual precipitation. This point was discussed by *Oerlemans and Fortuin* [1992] and confirms the long existing idea that glaciers with a large mass-turnover are more sensitive [e.g. *Meier*, 1984]. The reason is that these glaciers naturally extent to lower altitudes with relatively high air temperatures. Therefore, a significant fraction of annual precipitation falls as rain, and this fraction will increase when temperature increases. For glaciers in dry regions, this effect is marginal. Additionally, the enhanced melt rate and the longer melt season have an impact, the contribution of the albedo feedback to the sensitivity

---

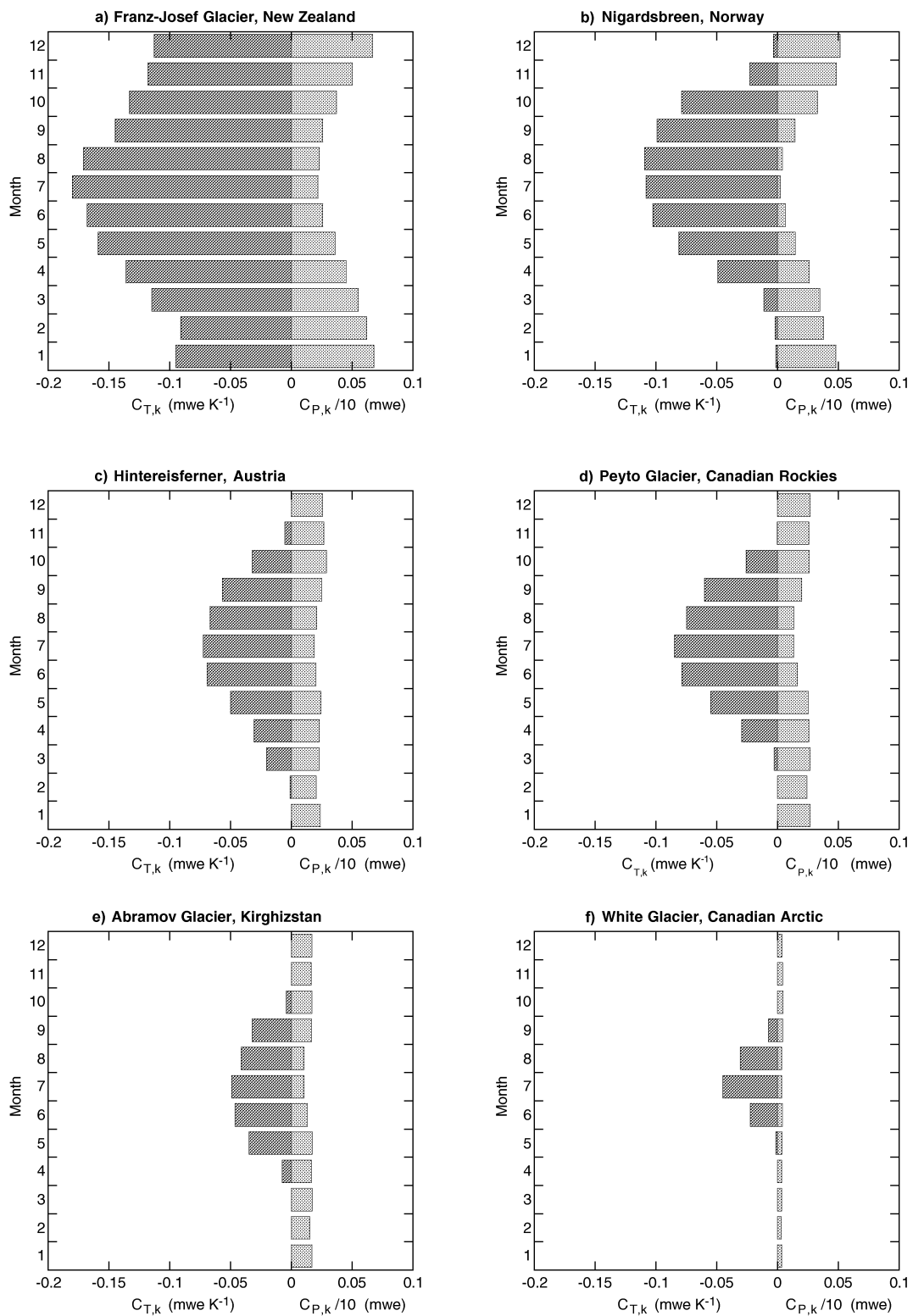


**Figure 1.** Graphic representation of the SSC for a selection of glaciers, as calculated with a mass balance model [mwe is m of water equivalent]. To facilitate comparison, the calendar for Franz-Josef Glacier, which is in the Southern Hemisphere, has been shifted over 6 months.

is also enhanced for higher precipitation rates [*Oerlemans and Fortuin, 1992*].

When looking at the seasonal effects, a number of interesting observations can be made. For Nigardsbreen, winter precipitation is far more important than summer precipitation, as the latter falls as rain over most of the glacier. The maritime character of this glacier is also reflected in the temperature sensitivity. On the lower parts of the glacier, the melt season is long, so May and September make a significant contribution. Franz-Josef Glacier (Southern Hemisphere) is even more maritime (note that the calendar has been shifted by half a year to make the graph comparable to those of the other glaciers). Even a temperature increase in the winter months (Southern Hemisphere) leads to a reduced balance. As mentioned above, this is because of higher melt rates on the tongue and because the fraction of precipitation falling as snow is significantly reduced. On the basis of this result, one would not attempt to seek a correlation between specific balance and summer temperature only.

Hintereisferner and Peyto Glacier are in a moderately wet climate. The accumulation areas of these glaciers cover a larger altitudinal range. As a consequence, an increase in summer precipitation still makes a significant contribution to the annual balance.

Abramov and White Glaciers are both continental glaciers, but from very different latitudes (about 40°N and 79°N, respectively). It appears that for drier glaciers the effect of temperature perturbations is more restricted to the summer. In fact, the temperature sensitivity for White Glacier is determined entirely by the summer months (June, July, August). For this glacier it matters little in what month an increase in precipitation takes place. Virtually all the precipitation falls as snow.

It should again be realized that the seasonal variation of  $C_{p,k}$  also depends on how the precipitation is distributed through the year. A detailed analysis for Hintereisferner, for instance, shows that an equal increase in absolute precipitation through the year has the largest effect in early summer (due to increasing albedo during times of strong solar radiation). However, because the precipitation rate in early summer is lower than the annual mean, this effect does not show up in a sensitivity analysis based on fractional changes in precipitation.

In total, the SSCs of 14 glaciers have been studied. In addition to the ones shown in Figure 1 these are: Engabreen, Alftobreen, Helstugubreen, Devon Ice Cap, Tuyuksy Glacier, Storglaciären, Rhonegletscher and Griesgletscher. Altogether, a large difference between the SSCs is the length of the period for which temperature perturbations affect the annual balance. To quantify this, we introduce a seasonality index  $SI$ , defined as the ratio of the sensitivity in summer to the sensitivity during the entire year:

---

$$SI = \frac{C_{T,6} + C_{T,7} + C_{T,8}}{\sum_{k=1}^{12} C_{T,k}} \quad (5)$$

A high  $SI$  value means that the sensitivity to temperature is mainly restricted to the summer months, low values indicate a longer period for which temperature perturbations affect the annual mass balance. In Figure 2 the  $SI$  values for the 14 glaciers are plotted against annual precipitation. A logarithmic fit is also shown, and the correlation coefficient is fairly large ( $r = 0.955$ ). Interestingly, the correlation coefficient of  $SI$  with the annual temperature range for the 14 glaciers is smaller ( $r = 0.82$ ) but still significant. There is naturally a relationship between the annual temperature range and annual precipitation: wetter climates generally have a smaller temperature range. As a general conclusion we state that the drier the climatic setting of a glacier, the more the sensitivity to temperature change is restricted to the summer months.

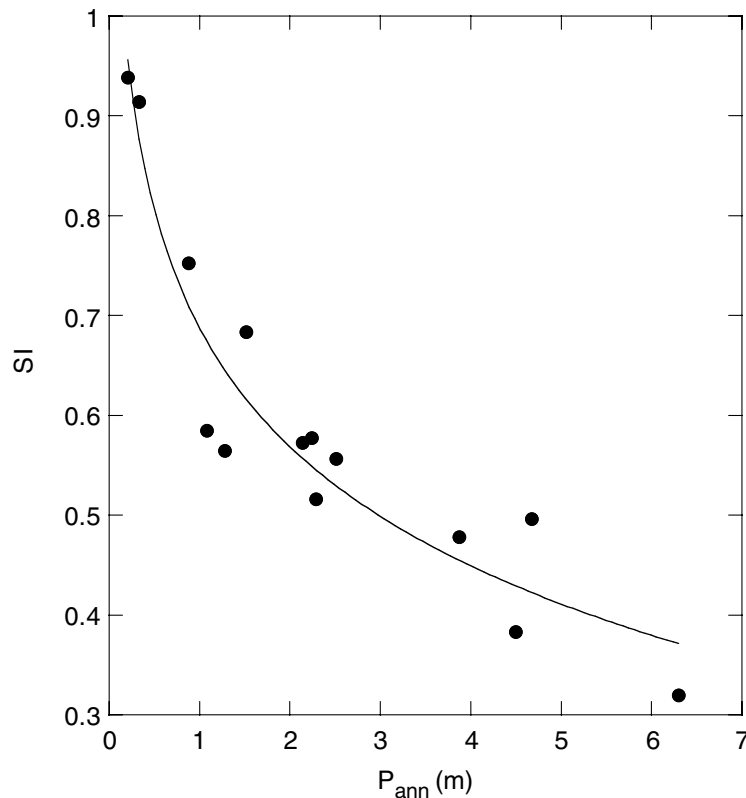


**Figure 2.** The seasonality index ( $SI$ ) plotted against annual precipitation ( $P_{ann}$ ) for a sample of 14 glaciers (Franz-Josef Glacier, Peyto Glacier, Nigardsbreen, Engabreen, Alftobreen, Helstugubreen, Devon Ice Cap, White Glacier, Abramov Glacier, Tuyuksy Glacier, Storglaciären, Hintereisferner, Rhonegletscher and Grieschgletscher).

### 3.3 Application of the SSC to Reconstruct a Mass Balance Series

To illustrate the use of the SSC we have performed some mass balance calculations for Nigardsbreen. A series of annual balance perturbations  $\Delta B(t)$ , where  $t$  is the year, was constructed from meteorological data with Equation (2) omitting the term  $H$ . We refer to this model as the “reduced model” and formulate it as

$$\Delta B(t) = \sum_{k=1}^{12} \left[ SSC_{1,k} (T_{k,t} - T_{ref,k}) + SSC_{2,k} (P_{k,t} / P_{ref,k}) \right] \quad (6)$$

Here the seasonal sensitivity characteristic is written as a  $2 \times 12$  matrix  $SSC_{j,k}$  where the index  $j$  refers to temperature ( $j = 1$ ) or precipitation ( $j = 2$ ) and the index  $k$  to the number of the month. The temperature anomaly of month  $k$  in year  $t$  is denoted by  $T_{k,t}$ , the precipitation anomaly by  $P_{k,t}$ .

Three sets of data were considered:

- (i) A long series from the meteorological observatory at Bergen in western Norway. Precipitation and temperature data are available since 1921, the station is a few hundred kilometers away from Nigardsbreen.
- (ii) Data from three stations around the Jostedalbreen plateau of which Nigardsbreen forms a part. These stations (Vangsnes, Fortun and Olden-Vangberg) are closer to Nigardsbreen, but the series are shorter. Mean values for the three stations were used as input.
- (iii) European Centre for Medium-Range Weather Forecasts (ECMWF) meteorological reanalyses [Gibson *et al.*, 1996], interpolated from grid points (T106 resolution, corresponding roughly to a  $1.1^\circ \times 1.1^\circ$  grid) to the location of Nigardsbreen.

The first results considered are those from the Bergen data (i), presented in Figure 3. In the first calculation (upper panel) only the effect of temperature anomalies was considered ( $SSC_{2,k} = 0$ ); in the second one (second panel) only precipitation anomalies ( $SSC_{1,k} = 0$ ) were used. This reveals the relative importance of fluctuations in temperature and precipitation. Apparently, both quantities are important, although it can be seen that the large positive anomalies are related to large amounts of precipitation (for further analysis of the individual impact of temperature and precipitation see Chapter 4, section 4.6.2). In the lower panel of Figure 3 (total reconstructed balance considering both temperature and precipitation) the measured specific balance for Nigardsbreen for the period 1962-1995 is shown for comparison.

The correlation coefficient between reconstructed and measured balance is  $r = 0.65$  (95% significant for  $r \geq 0.30$ ). One reason why this coefficient is not higher is most likely the large distance between Bergen and Nigardsbreen.

When using data (ii), considering mean values for stations closer to Nigardsbreen, the correlation is higher ( $r = 0.76$ ). An even better result is obtained with data set (iii), the ECMWF reanalyses (Figure 4). For this data set, the correlation coefficient is 0.85 (95% significant for  $r \geq 0.49$ ), but it should be realized that the investigated time period is shorter (1979-1993) since the ECMWF reanalyses did not cover a larger time span at the time of the present analysis.

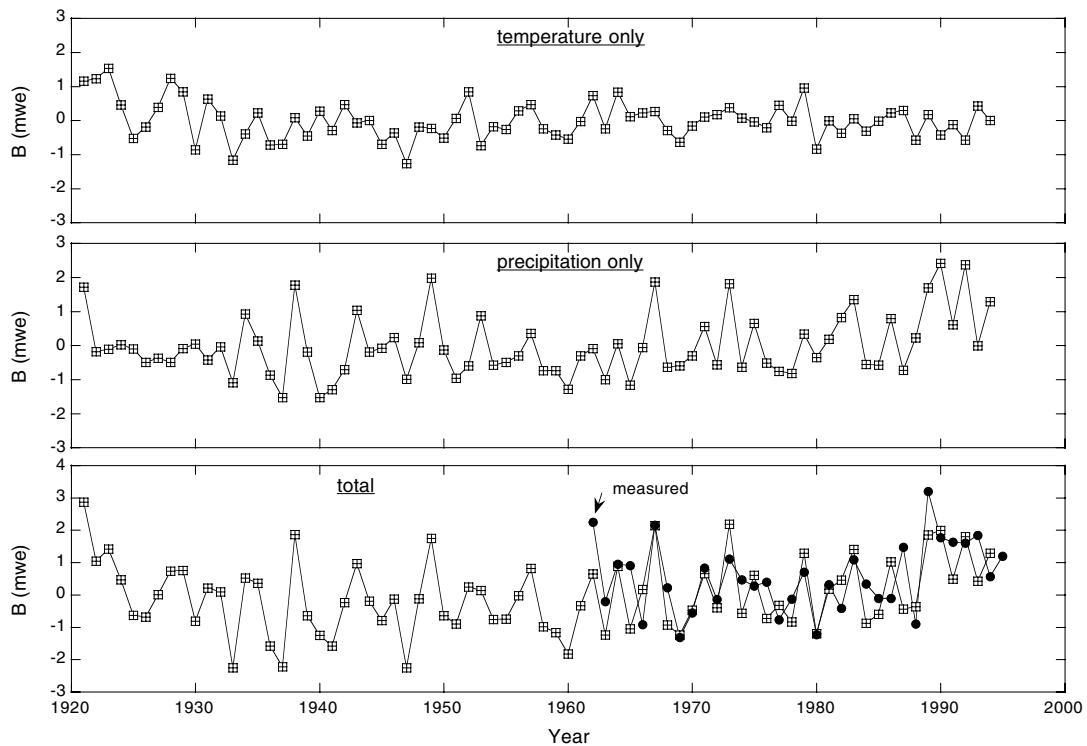


**Figure 3.** Specific balance for Nigardsbreen calculated with the reduced model from monthly perturbations of temperature and precipitation as observed at Bergen, Norway. The calculation is for the present-day geometry. The upper panel shows the effect of temperature anomalies only, the second panel the effect of precipitation anomalies only. In the third panel the total reconstructed balance is compared with mass-balance measurements. Data from Müller [1977], Haeberli [1985], Haeberli and Müller [1988], Haeberli and Hoelzle [1993], Elvehøy and Haakensen [1992], Haakensen [1995].

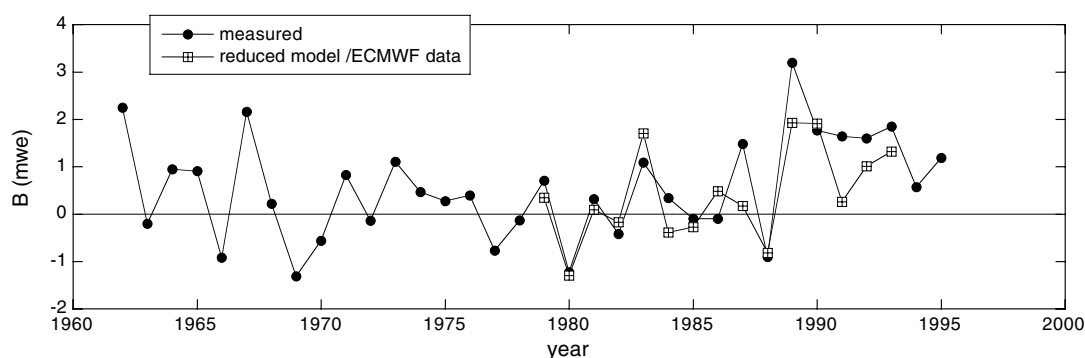


**Figure 4.** A comparison between measured (dots) and reconstructed mean specific balance for Nigardsbreen. The reconstruction with the reduced model is done using ECMWF reanalyses.

### 3.4 Performance of the Reduced Model

As mentioned before, there are two basic assumptions about using Equation (6) for reconstructing glacier mass balance. The first one is that the direct effect of monthly perturbations of temperature and precipitation can be described with a linear expansion. This will only work when the perturbations are sufficiently small. Further analysis showed that in practice errors are acceptable (<10%) if the temperature anomalies do not exceed 2 K and the precipitation anomalies not more than 40%. Of course larger deviations occur every now and then, but, given other uncertainties, it is doubtful if the use of a higher order expansion is worthwhile.

The second assumption involves the mutual interference of monthly perturbations. The effect of a temperature perturbation in June on the annual balance may depend to some extent on a precipitation perturbation in April, for instance.

The best test for the reduced model is to compare it directly with the full mass balance model, run in a time-dependent mode for a longer period of time. We have done this for the Bergen data (data set (i)). The mass-balance model has been started at the beginning of the year 1921 and has run continuously with monthly temperature and precipitation as forcing. In principle, a perturbation in the beginning of the integration will affect the entire further evolution of the balance. Figure 5 shows the result from this run in comparison with the output from the reduced model. The good correspondence between the models is evident. The root mean square difference is 0.22 mwe, the correlation coefficient is 0.97. This shows that the differences between using the SSC and using the full mass balance model to reconstruct a mass balance time series are small.

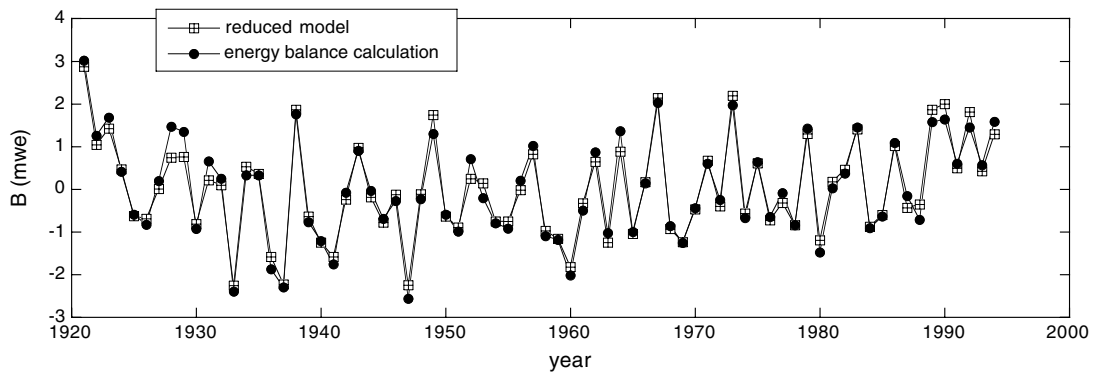


**Figure 5.** Reconstructed specific balance for Nigardsbreen from the reduced model and a full energy-balance calculation. Input data are taken from the meteorological station at Bergen, Norway.

We have repeated the comparison for 100 years of synthetic climate data. This was taken from a control experiment (present-day climate conditions) of a coupled general circulation model (ECHAM4/OPYC [Roeckner *et al.*, 1999]) developed at the Max-Planck-Institut für Meteorologie and the Deutsches Klimarechenzentrum in Hamburg. As can be expected, the result showed a similar high performance of the reduced model in comparison with the full mass balance model, it is therefore not shown. Again, the correlation coefficient was 0.97. A detailed description of experiments using general circulation models, will be given in Chapter 4 (section 4.5).

Another useful comparison is that between the SSC and the annual sensitivity, defined as the change in the mean specific balance for a perturbation in temperature or precipitation that is constant throughout the year. The annual sensitivity can be estimated from the SSC by summing up the individual monthly contributions. The result will not be equal to the outcome of the run of a mass balance model with a constant perturbation through the year. In general, the estimate of the annual sensitivity from the SSC gives slightly smaller values. However, at least for the glaciers considered here, the differences are small (<5%). This is additional evidence for the fact that mutual interference of monthly perturbations is not significant.

### 3.5 Conclusions

The SSC is a well-defined and useful tool to characterize the climatic setting of a glacier. It quantifies the climate sensitivity of the mean specific glacier mass

balance  $B$  to monthly anomalies in temperature and precipitation. It shows in a transparent way the difference in sensitivity between glaciers with large and small mass turnovers, located in regions with high and low annual precipitation. It also elucidates the relative role of changes in temperature and precipitation for mass balance. We have discussed the SSCs for Franz-Josef Glacier (New Zealand), Nigardsbreen (Norway), Hintereisferner (Austria), Peyto Glacier (Canadian Rockies), Abramov Glacier (Kirghizstan) and White Glacier (Canadian Arctic). The accuracy of the calculated SSCs depends on how well the mass balance model is designed and on the quality of the input data. Even though there are significant uncertainties in these, we consider the gross characteristics as shown in Figure 1 to be robust.

We have shown that for glaciers in dry climates, the effect of temperature is mainly restricted to summer months, whereas for glaciers in wetter climates, spring and fall temperatures additionally make a significant contribution. This means that the relative importance of summer temperatures with respect to the entire year generally increases with decreasing annual precipitation. From the investigations in this study, this relationship can be regarded as a robust result.

The SSCs can be used to (re)construct a mass balance time series using meteorological data or general circulation model output. We found the difference between the reduced model and the full energy balance calculation to be small and not relevant in view of other uncertainties.

In the following chapter, the SSCs will be applied to downscaled general circulation models. This will enable us to investigate forcing mechanisms for specific midlatitude glaciers, and also serves as a basis for the simulation of glacier length fluctuations using a dynamic ice flow model (Chapter 5).

---

---

**References**

- Dyurgerov, M. B. and M. F. Meier, Year-to-year fluctuations of global mass balance of small glaciers and their contribution to sea-level changes, *Arct. Alp. Res.*, 29, 392-401, 1997.
- Elvehøy, H. and N. Haakensen (eds.), *Glasiologiske Undersøgelser i Norge 1990 og 1991*, Norges Vassdrags- og Energiverk, Oslo, 103 pp., 1992.
- Gibson, J. K., P. Kållberg, S. Uppala, A. Nomura, A. Hernandez, and E. Serrano, ERA Description, *ECMWF Re-Anal. Proj. Rep. Ser., Rep. 1*, Eur. Cent. for Medium-Range Weather Forecasts, Reading, England, 1997.
- Greuell, W., Hintereisferner, Austria: mass-balance reconstruction and numerical modelling of the historical length variations, *J. Glaciol.*, 38, 233-244, 1992.
- Greuell W. Bohm R. 2m temperatures along melting mid-latitude glaciers and implications for the sensitivity of the mass balance to variations in temperature, *J. Glaciol.*, 44, 9-20, 1998.
- Günther, R. and D. Widlewski, Die Korrelation verschiedener Klimaelemente mit dem Massenhaushalt alpiner und skandinavischer Gletscher, *Z. Gletscherkd. Glazialgeol.*, 22, 125-147, 1986.
- Haakensen, N. (ed.), *Glasiologiske Undersøgelser i Norge 1992 og 1993*, Norges Vassdrags- og Energiverk, Oslo, 139 pp., 1995.
- Haeberli, W., *Fluctuations of Glaciers, 1975-1980 (Vol. IV)*, IASH (ICSU)-UNESCO, 1985.
- Haeberli, W. and M. Hoelzle, *Fluctuations of glaciers 1985-1990 (Vol. VI)*, IASH (ICSU)- UNESCO, 1993.
- Haeberli, W. and P. Müller, *Fluctuations of Glaciers, 1980-1985 (Vol. V)*, IASH (ICSU)- UNESCO, 1988.
- Hoinkes, H. and R. Steinacker, Zur Parametrisierung der Beziehung Klima - Gletscher, *Rivista Italiana di Geofisica e Scienze Affini*, 1, 97-104, 1975.
- Letréguilly, A., *Bilans de masse des glaciers alpin: methods de mesure et repartition spatio-temporelle*, Thesis, LGGE, Grenoble, Publ. 439, 1984.
- Lliboutry, L., Multivariate statistical analysis of glacier annual balance, *J. Glaciol.*, 13, 371-392, 1974.
- Meier, M. F., Contribution of small glaciers to global sea level, *Science*, 226, 1418-1421, 1984.
-

- Müller, F., *Fluctuations of Glaciers, 1970-1975*, (Vol. III), IASH (ICSU)- UNESCO, 1977.
- Nye, J. F., A numerical method of inferring the budget history of a glacier from its advance and retreat, *J. Glaciol.*, 5, 589-607, 1965.
- Oerlemans, J., Climate sensitivity of glaciers in southern Norway: application of an energy-balance model to Nigardsbreen, Hellstugubreen and Alftobreen, *J. Glaciol.*, 38, 223-232, 1992.
- Oerlemans, J., and J. P. F. Fortuin, Sensitivity of glaciers and small ice caps to greenhouse warming, *Science*, 258, 115-117, 1992.
- Oerlemans, J., Climate Sensitivity of Franz-Josef Glacier, New Zealand, as revealed by numerical modelling, *Arctic and Alpine Research*, 29, 233-239, 1997.
- Roeckner, E., L. Bengtsson, J. Feichter, J. Lelieveld and H. Rodhe, Transient climate change simulations with a coupled atmosphere-ocean GCM including the tropospheric sulfur cycle, *J. Climate*, 12, 3004-3032, 1999.
- Smith, I. N. and W. F. Budd, The derivation of past climate change from observed changes of glaciers, in *Proc. of the Symposium on Sea Level, Ice and Climatic Change (Canberra, 1979)*, IAHS Publ, 131, 31-52, 1979.
- Zuo, Z. and J. Oerlemans., Contribution of glacier melt to sea-level rise since AD 1865: a regionally differentiated calculation, *Climate Dyn.*, 13, 835-845, 1997.
-

## 4 Midlatitude Forcing Mechanisms for Glacier Mass Balance

---

### ***Midlatitude Forcing Mechanisms for Glacier Mass Balance Investigated Using General Circulation Models<sup>3</sup>***

**Abstract.** A process-oriented modeling approach is applied in order to simulate glacier mass balance for individual glaciers using statistically downscaled general circulation models (GCMs). Glacier specific Seasonal Sensitivity Characteristics based on a mass balance model of intermediate complexity are used to simulate mass balances of Nigardsbreen (Norway) and Rhonegletscher (Switzerland). Simulations using reanalyses (ECMWF) for the period 1979-1993 are in good agreement with in situ mass balance measurements for Nigardsbreen. The method is applied to multi-century integrations of coupled (ECHAM4/OPYC) and mixed-layer (ECHAM4/MLO) GCMs excluding external forcing. We find a high correlation between decadal variations in the North Atlantic Oscillation (NAO) and mass balance of the glaciers. The dominant factor for this relationship is the strong impact of winter precipitation associated with the NAO. A high NAO phase means enhanced (reduced) winter precipitation for Nigardsbreen (Rhonegletscher), typically leading to a higher (lower) than normal annual mass balance. This mechanism, entirely due to internal variations in the climate system, can explain observed strong positive mass balances for Nigardsbreen and possibly other maritime Norwegian glaciers within the period 1980-1995. It can also partly be responsible for recent strong negative mass balances of Alpine glaciers.

### **4.1 Introduction**

Observed (or reconstructed) glacier fluctuations provide important information on natural (preindustrial) climate variability and are also key elements for the early detection of climate change and possible anthropogenic impacts on climate. They result from changes in the mass and energy balance at the earth's surface and therefore represent valuable climatic proxy data. Due to the typical properties of a

---

<sup>3</sup> Reichert, B. K., Bengtsson, L., and J. Oerlemans, *Journal of Climate*, in prep., 2000.

melting ice or snow surface, glaciers represent highly sensitive climate indicators. The glacierization of the well-documented European Alps, for example, has lost roughly 30 to 40% in surface area and about 50% of its original volume since the middle of the last century, the end of the so-called “Little Ice Age”. Since 1980, a remarkable loss of 10 to 20% of ice volume has been observed [*Haeberli and Beniston, 1998*].

Changes in glacier mass balance (defined as the annual mass gain or loss at the surface) can be viewed as the direct, undelayed reaction of a glacier to climatic variations, whereas variations in glacier length are the indirect, delayed, filtered, and strongly enhanced response. Cumulative glacier mass changes lead to changes in ice thickness which then influence the dynamic redistribution of mass by glacier flow [*Haeberli, 1995*]. Monitoring glacier mass balance is therefore a direct way to reconstruct climatic variations. However, the available mass balance records are relatively short (usually less than 50 years) compared to relatively long records of glacier length (e.g. the record of Untere Grindelwaldgletscher, Switzerland begins in 1534).

General Circulation Models (GCMs) can be used in order to investigate the behavior of glaciers under specific climatic conditions. Natural glacier fluctuations exclusively due to internal variations in the climate system can be simulated. A major advantage of using GCMs is having the opportunity to investigate underlying physical mechanisms responsible for glacier fluctuations inherent to the climate system. If desired, specific external forcings such as, for example, changing greenhouse gas concentrations, can be included.

In this study, we propose a process-oriented modeling approach for the simulation of mass balance of individual glaciers using downscaled GCMs. This approach has two main characteristic features.

Firstly, we simulate the mass balance of *individual* glaciers using a process-based and glacier-specific mass balance model. We apply glacier-specific seasonal sensitivity characteristics calculated from a mass balance model of intermediate complexity. Although several attempts have been made to use one equation to describe a large number of glaciers or even all glaciers on earth [e.g. *Wigley and Raper, 1993*; *Oerlemans, 1989*], the response of individual glaciers to a climatic signal can vary enormously due to their different geometries or their location in different climatic regimes, leading to entirely different energy-balance characteristics. Climate sensitivity may generally vary at least over one order of magnitude for single glaciers, depending to a large extent on precipitation [*Oerlemans and Fortuin, 1992*]. We therefore concentrate on individual glaciers;

---

nevertheless, they will to some extent be representative for glaciers with comparable characteristic features in the same region.

Secondly, we apply a statistical downscaling approach in order to obtain local conditions from GCM output. Glacier volume has been calculated using regional temperature patterns from the direct coarse grid point output of a GCM [Gregory and Oerlemans, 1998] in which the impact of precipitation has not been considered. However, climate sensitivity of glaciers depends on *local* temperature and precipitation. The direct use of coarse GCM grid points (typical resolution, e.g. about  $2.8^\circ \times 2.8^\circ$ ) naturally results in a poor representation of the local climate, especially for precipitation which is highly dependant on local orographic conditions. In this study, both temperature as well as precipitation are therefore downscaled (section 4.2) using daily European Centre for Medium-Range Weather Forecasts (ECMWF) reanalyses [Gibson *et al.*, 1996] and local station data. Downscaled temperature and precipitation are then used as input for the mass balance modeling approach (section 4.3).

For validation of the entire approach including downscaling and mass balance modeling, we simulate glacier mass balance directly using ECMWF reanalyses for comparison with in situ mass balance measurements (section 4.4). This is an important basis for the application of the method to various GCM experiments (section 4.5). The process-oriented modeling approach is particularly interesting since it enables us to investigate forcing mechanisms for glacier mass gain or loss of individual glaciers. As an example, the relationship between the North Atlantic Oscillation (NAO) and the behavior of specific European glaciers will be investigated for Nigardsbreen glacier (Norway) and Rhonegletscher (Switzerland) considering the individual seasonal impact of temperature and precipitation (section 4.6). On the basis of the obtained results, we will furthermore discuss the recent development of observed glacier mass balances, including the observed strong positive mass balances of Nigardsbreen during recent decades (section 4.7).

## **4.2 Statistical Downscaling Approach**

A comparison of three methods of downscaling [Cubasch *et al.*, 1996] shows that direct interpolation of GCM grid points to a local site results in a poor representation of the local climate and that statistical downscaling is an appropriate and inexpensive tool for regions with sufficient observational data to train the model.

---

### 4.2.1 Method

The statistical downscaling approach used in the present study is based on daily operational weather station data in the vicinity of the glacier sites to be investigated and on an extensive set of potential daily large-scale predictors obtained from ECMWF reanalyses. The ECMWF reanalyses consist of a validated and reasonably consistent global data set of assimilated data for the period 1979-1993 [Gibson *et al.*, 1997]. Robust statistical relationships between the large-scale flow obtained from reanalyses and local variables are developed in order to be applied to the output of the European Center/Hamburg (ECHAM) GCM experiments.

A detailed description of the downscaling approach (including model validation, investigation of the role of near-surface predictors, spatial homogeneity of the model, seasonal-specific relationships, the impact of spatiotemporal resolution of predictors, etc.) can be found in Reichert *et al.* [1999]. In the following, we will briefly describe the performance of the statistical model for the areas of interest in this study.

### 4.2.2 Downscaling for Rhonegletscher

Rhonegletscher is a valley glacier located in the Swiss Alps (46°37'N, 8°24'E). Its altitudinal range is 2140 m to 3620 m, the total area covered by the glacier is 17 km<sup>2</sup> [Hoelzle and Haerberli, 1999]. Figure 1 shows the locations of Rhonegletscher and the 24 operational weather stations used for statistical downscaling (stations 13, 14, 04, 18, and 02 are not used since the available records did not cover the complete period of the ECMWF reanalyses).

The explained variances (EV) of the statistical downscaling model with respect to observed local temperature and observed local precipitation have been calculated for individual stations in the area of investigation. For this calculation, we have used monthly-averaged values of the original daily statistical model output after removing the seasonal cycle. The explained variance can be split among the large-scale predictors from ECMWF reanalyses chosen by the statistical model in order to demonstrate their individual impact. Only predictors above the 850 hPa level have been used as potential predictors [Reichert *et al.*, 1999].

For observed local temperature, the explained variance  $r^2$  averaged over all stations is 80.0% (correlation coefficient  $r = 0.90$ ). Dominant large-scale predictors are temperature at 850 hPa (EV: 41.3%), a seasonal cycle predictor (cosine function with a period of one year, extrema at January 1 and July 1; EV: 14.2%; see Reichert *et al.* [1999]), geopotential thickness at 700-850 hPa (EV: 8.0%), and relative humidity at 850 hPa (EV: 5.9%). However, the composition of predictors changes significantly

---

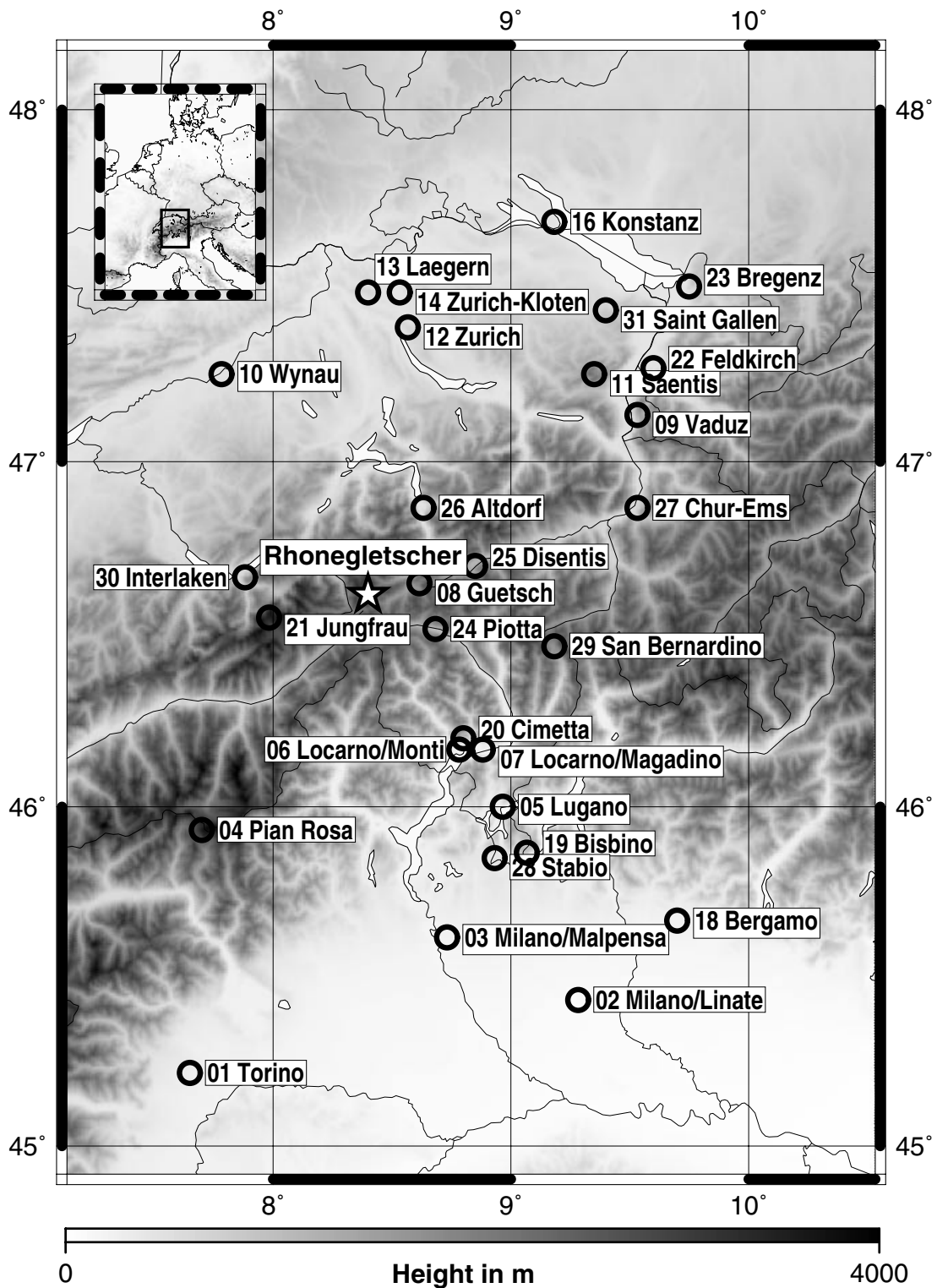


**Figure 1.** Location of Rhonegletscher ( $46^{\circ}37'N$ ,  $8^{\circ}24'E$ ) and operational weather stations used for statistical downscaling. Local temperature and precipitation are simulated from GCM output on the basis of daily large-scale predictors obtained from ECMWF reanalyses and daily station data in the vicinity of the glacier.

between individual stations. Stations 08 Guetsch and 11 Saentis are located at high elevations (2284 m and 2500 m respectively). Here, the only predictor chosen by the model is geopotential thickness at 700-850 hPa, explaining more than 95% of the monthly-averaged local temperature. For station 21 Jungfrau (elevation: 3576 m) the predictors are geopotential thickness at 500-850 hPa and at 400-500 hPa together explaining 94% of the observed values. The predominant predictor for all other stations (elevations below 1700 m) is generally large-scale temperature at 850 hPa.

For observed local precipitation, both the explained variance as well as the spatial homogeneity of predictors are generally lower than for temperature, as can be expected. The characteristic composition of predictors is dependent on the meridional location of the stations within the area of investigation. Stations located more in the south of the Alps (stations 01, 03, 05, 06, 07, 19, 20, and 28) show a more uniform composition of predictors than other stations. The averaged explained variance in the area is 60%, predominant predictors are vorticity at 700 hPa (EV about 15%), zonal wind at 700 hPa (EV: 15-20%), and vertical velocity at 500 hPa (EV: 10-15%). For stations located in the north (stations 09-12, 16, 22, 23, 31) and the central parts of the Alps (stations 08, 21, 24-27, 29, 30), vertical velocity at 850 hPa plays an important role (EV: 15-25% for some stations) in addition to vorticity at 700 hPa (EV: up to 15%). Also meridional wind at 850 hPa (EV: 5-15%) and at 700 hPa (particularly for stations 10, 12, and 16; EV: 10-15%) may have a considerable additional impact, dependant on the local setting of the stations.

Among all stations, station 08 Guetsch (46°39'N, 8°37'E) is the closest station to Rhonegletscher (Figure 1) and also its altitude (2284 m asl) lies within the altitudinal range of the glacier. This station is therefore assumed to best represent the local climate of the glacier site for the simulation of glacier fluctuations. The explained variance for observed local temperature is 97%, while the explained variance with respect to the *month-to-month* variability of local precipitation is below the average over all stations (51%). However, as Figure 2 demonstrates, the simulated climatology of precipitation for the period 1979-1993, which will be most important for the Seasonal Sensitivity Characteristic (SSC) of the glacier (see section 4.3.3), is improved substantially compared to direct ECMWF reanalyses, and is in good agreement with the observed climatology (correlation coefficient  $r = 0.82$ ; 95% significant for  $r \geq 0.57$ ). The statistical model was validated using independent data as described in Reichert *et al.* [1999].

---

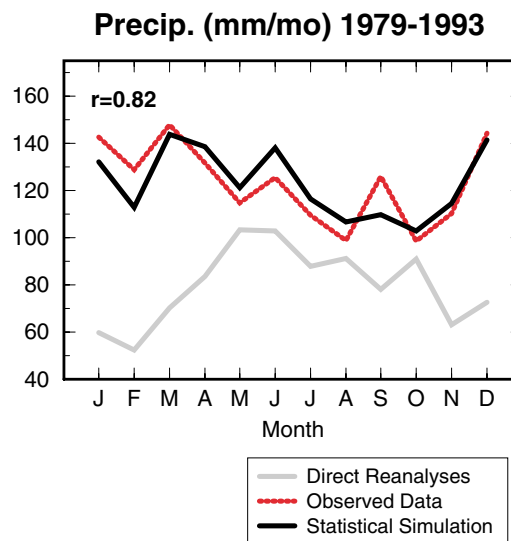


**Figure 2.** Monthly means of precipitation averaged over the period 1979-1993 for station Guetsch (46°39'N, 8°37'E). Observed station data (dotted line), statistically downscaled results (solid line), and interpolated reanalyses without statistical modeling (shaded line) are shown. The simulated climatology is in good agreement with observations (correlation coefficient  $r = 0.82$ ).

### 4.2.3 Downscaling for Nigardsbreen

Nigardsbreen is an outlet glacier of Jostedalbreen, the largest ice cap of the European continent. It is located in Norway (61°43'N, 7°08'E), its elevation ranges from 295 m to 1950 m above sea level. The total area of the glacier is 47 km<sup>2</sup> [Hoelzle and Haeberli, 1999].

The location of stations for Nigardsbreen and the complete application of the downscaling approach used in this study is described in Reichert *et al.* [1999]. The explained variance for local temperature averaged over 17 stations in the vicinity of the glacier (79%) is comparable to the average for Rhonegletscher. The explained variance for local precipitation is however higher (65%) in comparison with Rhonegletscher. This is due to the fact that for the Nigardsbreen area, local precipitation is already rather well determined by large-scale vertical velocity at 850 hPa explaining more than 41% of variance alone. In this area, station Vangsnes (61°10'N, 6°39'E) will be used for the simulation of glacier fluctuations.

### 4.3 Sensitivity of Glacier Mass Balance to Meteorological Data

In this study, the sensitivity of mass balance to meteorological data is represented by glacier specific Seasonal Sensitivity Characteristics (SSC) [Oerlemans and Reichert, 2000; see also Chapter 3] calculated from a mass balance model of intermediate complexity [Oerlemans, 1992]. In the following, we will give a brief summary of this approach.

#### 4.3.1 The Mass Balance Model

The *specific mass balance*  $M$  of a glacier is the resultant of all processes in a year that lead to mass gain or loss at the surface on a unit area, expressed in m water equivalent (mwe).

The *mean specific mass balance*  $B$  over the entire glacier can be expressed as

$$B = \frac{1}{S_T} \sum_i M(h_i) S(h_i)$$

with a discrete elevation-area distribution  $S(h_i)$ , the total glacier area  $S_T$  and the sum taken over all elevation intervals centered around the elevation  $h_i$ .

In principle, the mass balance model integrates the energy-balance equation for the ice/snow surface in time, on a grid covering the entire elevation range:

$$\Psi = (1 - \alpha) G + I_{in} + I_{out} + H_s + H_l$$

Here, the energy balance  $\Psi$  is expressed in terms of the absorbed solar radiation (albedo  $\alpha$ , global radiation  $G$ ), the incoming and outgoing longwave fluxes ( $I_{in}$  and  $I_{out}$ ) and the turbulent fluxes of sensible and latent heat ( $H_s$  and  $H_l$ ). As soon as the energy balance becomes positive, melting occurs at the surface.

The specific mass balance  $M$  can then be written as

$$M = \int_{year} [(1 - f) \min(0; -\Psi L^{-1}) + P^*] dt$$

with  $L$  as the latent heat of melting,  $f$  as the fraction of meltwater that refreezes and does not contribute to mass loss, and  $P^*$  as the accumulation rate at which solid precipitation is added to the surface.

---

The albedo  $\alpha$  represents a major problem due to significant feed-backs and strong variations in space and time depending on the melt and accumulation history itself. The model generates the albedo internally using a simple scheme, so that main features broadly match available data from valley glaciers. A “background albedo profile” is empirically developed so that typical albedo patterns of a valley glacier at the end of the ablation season are matched. This profile, snow depth, and an age-independent snow albedo is then used for the calculation of the glacier albedo.

Refreezing (meltwater does not run off, but penetrates into the snowpack) is considered in the model, specifying the relationship between the fraction of melt energy involved in run-off and the snow/ice temperature.

### 4.3.2 Seasonal Sensitivity Characteristic (SSC)

In order to quantify the climate sensitivity of the mean specific balance  $B$  of a glacier and to apply it to downscaled GCM output, a Seasonal Sensitivity Characteristic (SSC) is used in this study. It represents the dependence of  $B$  on monthly perturbations in temperature and precipitation, and has been calculated from the mass balance model described above [Oerlemans and Reichert, 2000]. Annual deviations  $\Delta B$  of the mean specific balance  $B$  are expressed as

$$\Delta B = \sum_{k=1}^{12} [c_{T,k} (T_k - T_{ref,k}) + c_{P,k} (P_k / P_{ref,k})] + H$$

with the sum taken over all months of the year. Here,  $T_k$  and  $P_k$  represent monthly temperature and precipitation,  $T_{ref,k}$  and  $P_{ref,k}$  are climatological means of monthly values, and  $H$  represents nonlinear terms (which are neglected for glaciers considered in this study [Oerlemans and Reichert, 2000]).

The coefficients

$$c_{T,k} = \frac{\partial B}{\partial T_k} \quad \text{and} \quad c_{P,k} = \frac{\partial B}{\partial (P_k / P_{ref,k})}$$

have been determined by the mass balance model and represent the 24 values of the SSC. They quantify the change in mass balance resulting from a change in monthly temperature (unit of  $c_{T,k}$  is mwe/K) and from a relative change in monthly precipitation (unit of  $c_{P,k}$  is mwe) respectively.

The differences between using SSCs to reconstruct a mass balance series and using the full mass balance model itself have been tested and are found to be small

[Oerlemans and Reichert, 2000], and are therefore not relevant for the purpose of the present study.

### 4.3.3 Sensitivity of Nigardsbreen and Rhonegletscher

The specific SSCs for Nigardsbreen and Rhonegletscher with respect to temperature and precipitation are shown in Figure 3.

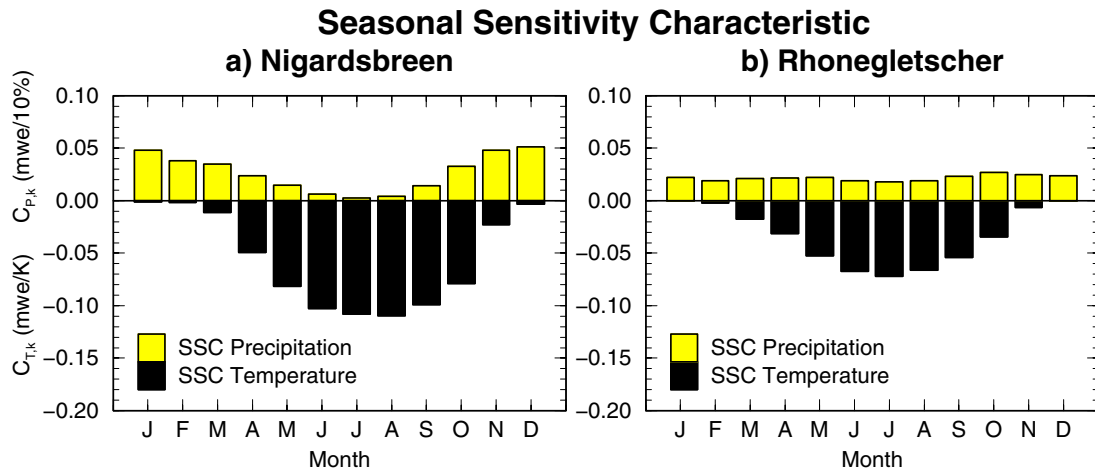


**Figure 3.** Glacier specific Seasonal Sensitivity Characteristic (SSC) for (a) Nigardsbreen and (b) Rhonegletscher. The SSC represents the dependence of glacier mass balance on monthly anomalies in temperature (solid bars) and precipitation (shaded bars). For Nigardsbreen, a 1°C temperature increase in summer (JJA) would, for example, roughly have the same effect (0.1 mwe in mass balance; mwe is m water equivalent) as a 20% decrease of precipitation in winter (DJF).

Nigardsbreen (Figure 3a) can be identified having maritime character. The melt season especially on the lower parts of the glacier is long, the sensitivity  $c_{T,k}$  to changes in temperature remains high from May to October (-0.08 to -0.11 mwe/K). Temperature anomalies during these months therefore lead to a strong response in mass balance. On the other hand, a temperature change in winter (December, January, February (DJF)) has almost no effect since melting hardly occurs. The sensitivity of mass balance to relative changes in precipitation is very low in summer (June, July, August (JJA)) compared to the winter values. The reason is that summer precipitation falls as rain over most parts of the glacier. An increase in precipitation has therefore only a marginal effect compared to the enhancement of mass balance in winter when precipitation mainly falls as snow and can be added to the surface.

The accumulation area of Rhonegletscher (Figure 3b) is located at higher altitudes (2140 m to 3620 m) compared to Nigardsbreen (295 m to 1950 m). As a consequence, also summer precipitation (with a large fraction falling as snow at these altitudes) has a considerable effect on the annual mass balance, the sensitivity is in fact only slightly lower than in winter. With respect to changes in monthly temperature, Rhonegletscher is less sensitive (-0.07 mwe/K in summer) than Nigardsbreen (-0.11 mwe/K in summer).

#### 4.4 Validation of Glacier Mass Balance Using ECMWF Reanalyses

An opportunity to validate the entire process-based modeling approach applied in this study, including the statistical downscaling strategy and the simulation of mass balance using SSCs, is the simulation of glacier mass balance using ECMWF Reanalyses. Simulated mass balance records can be compared to actual in situ measurements of mass balance for the period 1979-1993.

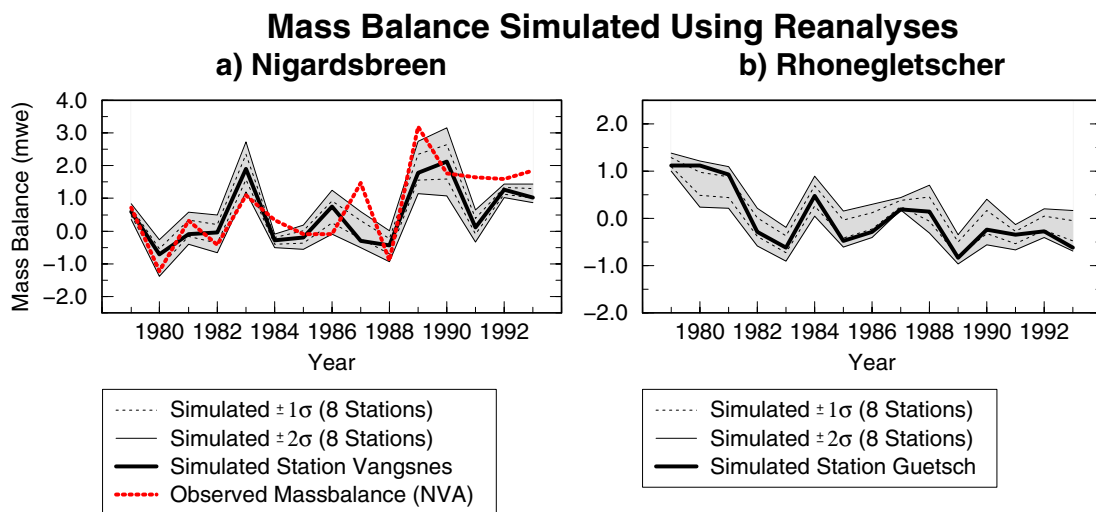


**Figure 4.** Process-based glacier mass balance simulations for (a) Nigardsbreen and (b) Rhonegletscher using ECMWF reanalyses. Observational data of 8 weather stations in the vicinity of each glacier are used for statistical downscaling. The gray shaded area represents the variability due to the choice of the station (mean over all stations  $\pm$  two standard deviations  $\sigma$ ). Heavy solid lines denote simulated mass balances using station Vangsnes (a) and station Guetsch (b). The heavy dotted line shows in situ measurements of mass balance for Nigardsbreen (a).

For Nigardsbreen glacier (Figure 4a), reliable measurements have been carried out by the Norwegian Water Resources and Energy Administration (Norges Vassdrags- og Energiverk, NVE) [*International Association of Scientific Hydrology (IASH)*, 1998, 1999; *Østrem et al.*, 1988]. These in situ measurements (Figure 4a, thick dotted line) are in good agreement with the simulated mass balance using our process-based approach applied to ECMWF reanalyses. We have simulated glacier mass balance using data of 8 operational weather stations in the vicinity of the glacier (stations Laerdal-Tonjum, Vangsnes, Forde-Vie, Fortun, Finse III, Modalen II, Olden-Vangberg, and Brata; see [*Reichert et al.*, 1999] for locations). The gray shaded area in Figure 4a represents the variability of mass balance due to the choice of the station (mean over all stations  $\pm$  two standard deviations  $\sigma$ ). In spite of some years, for which the model produces a significantly lower than observed mass balance (mainly 1987 and 1991), the overall correlation between simulations and measurements is remarkably high. Within the relatively short time period investigated, the correlation coefficient for the mean over all stations is  $r = 0.78$ . The heavy solid line denotes the mass balance simulation for station Vangsnes which will be used for the GCM experiments described in section 4.5 and 4.6.

For Rhonegletscher (Figure 4b), exact measurements of mass balance are not available. However, for the recent variability of mass balance of this glacier, we can infer a standard deviation of about 0.6 m water equivalent (mwe) according to numerous mass balance measurements in the central Alps [*IASH*, 1998]. The standard deviation of the simulated mass balance using station Guetsch (solid line) is 0.62 mwe. Due to the relatively short time period of the ECMWF reanalyses this agreement is not representative, it shows however that the variability of simulations for this glacier is generally comparable to measurements. Station Guetsch will be used for the GCM experiments in section 4.5 and 4.6. We have again applied the approach to 8 stations (stations Guetsch, Piotta, Disentis, Interlaken, San Bernadino, Chur-Ems, and Vaduz; see Figure 1 for locations) in order to get an insight into the spatial homogeneity of mass balance (Figure 4b, gray shaded area). The standard deviation exclusively due to spatial inhomogeneity between all 8 stations, averaged over the entire time period is 0.18 mwe. For Nigardsbreen, we find 0.26 mwe for this quantity. Both values clearly demonstrate the considerable impact on glacier mass balance when using different stations in the vicinity of the glaciers.

The above experiments have enabled the validation of the process-oriented modeling approach applied in this study against observations. This is an important basis for the application to GCM experiments discussed in the following.

---

## **4.5 Simulation of Glacier Mass Balance Using ECHAM4 GCM Integrations**

The GCM integrations used in this study have been performed using a current state-of-the-art climate model, the fourth generation of the European Center/Hamburg general circulation model (ECHAM4) developed at the Max-Planck-Institut für Meteorologie (MPI) and the Deutsches Klimarechenzentrum (DKRZ) in Hamburg [Roeckner *et al.*, 1996]. The origin of the model is the spectral weather prediction model of the ECMWF [Simmons *et al.*, 1989]. The version used in the present study has 19 levels in the vertical extending up to 10 hPa. In order to characterize the role of the deep ocean for the simulation of low frequency climatic variations we use a coupled GCM (ECHAM4/OPYC) for comparison with a mixed-layer GCM (ECHAM4/MLO) without an internal ocean.

### **4.5.1 Coupled GCM Experiment (ECHAM4/OPYC)**

In this model version [Roeckner *et al.*, 1999], ECHAM4 is coupled to the full ocean general circulation model OPYC [Oberhuber, 1993] (see Bacher *et al.* [1998] for coupling strategy) consisting of three sub-models for the interior ocean, for the surface mixed-layer, and for sea ice (dynamic-thermodynamic sea ice model including viscous plastic rheology).

The experiment used is a control integration for present day climatic conditions performed at T42 horizontal resolution (corresponding to a latitude-longitude grid of about  $2.8^\circ \times 2.8^\circ$ ). The concentrations of carbon dioxide, methane, and nitrous oxide are fixed at the observed 1990 values [Intergovernmental Panel on Climate Change (IPCC), 1990, Table 2.5]. After a 100-year spinup, the model has been integrated with constant flux adjustment [Roeckner *et al.*, 1999] for 300 years.

### **4.5.2 Mixed-Layer GCM Experiment (ECHAM4/MLO)**

For this model version [Roeckner, 1997], ECHAM4 is coupled to a mixed-layer ocean model (MLO) including a thermodynamic sea ice model. The mixed layer has a fixed depth of 50 m and is horizontally insulated, an interior ocean is missing. Monthly means of heat are flux corrected using the observed climatological cycle of surface temperatures for the period 1979-1988.

For the multi-century integration used in the present study, the spectral resolution of the atmospheric model has been reduced to T30 (corresponding to a latitude-longitude grid of about  $3.75^\circ \times 3.75^\circ$ ). However, the climatology and many

---

aspects of its variability have been shown to be close to the T42 version of the model [Stendel and Roeckner, 1998] whereas computational costs are significantly reduced. In this study, 590 years of a control integration for present day climatic conditions (defined as for the coupled GCM; section 4.5.1) are used.

### 4.5.3 Mass Balance Simulations

Mass Balance simulations using the above GCM experiments have been performed for Nigardsbreen (Figure 5a) and Rhonegletscher (Figure 5b). Annual values of glacier mass balance (thin lines) and 10 year lowpass filtered values (heavy solid lines) are shown.

Pronounced mass balance fluctuations on time scales of years to decades have been simulated in the experiments. The variability in mass balance is exclusively due to internal variations in the climate system since we use GCM integrations excluding external forcings such as solar irradiation changes, volcanic or anthropogenic effects. In order to compare the variability of the simulated time series, we have computed the standard deviations  $\sigma$  for both the unfiltered and the 10 year lowpass filtered mass balance time series.

For both glaciers, the interannual variability for the mixed-layer GCM experiment (MLO) is higher (significant at 95% confidence level) in comparison with the coupled run (OPYC). For Nigardsbreen, we find  $\sigma_{\text{Nig,MLO}} = 0.69$  mwe (MLO) compared to  $\sigma_{\text{Nig,OPYC}} = 0.61$  mwe (OPYC). For Rhonegletscher, we have  $\sigma_{\text{Rho,MLO}} = 0.91$  mwe compared to  $\sigma_{\text{Rho,OPYC}} = 0.79$  mwe. A further investigation shows that the main reason is the different variability in simulated precipitation in the two model versions (see section 4.6.2 for the impact of precipitation on mass balance). Although the total amount of simulated annual precipitation averaged over the full time period of the experiments is comparable in both models, the standard deviation of precipitation for Nigardsbreen (Rhonegletscher) is by 14% (12%) higher in the mixed-layer GCM relative to the coupled GCM. We assume that this model-specific feature is at least partly related to a different (and in comparison with observations more unrealistic) representation of the pattern of precipitation associated with the NAO in the mixed-layer model.

The standard variations of the 10 year lowpass filtered time series are not significantly different in the two model versions. They read as follows:  $\sigma_{\text{Nig,MLO}} = 0.30$  mwe,  $\sigma_{\text{Nig,OPYC}} = 0.28$  mwe,  $\sigma_{\text{Rho,MLO}} = 0.31$  mwe, and  $\sigma_{\text{Rho,OPYC}} = 0.32$  mwe. This means that decadal scale mass balance variability is actually comparable for the different GCM experiments. However, this is inconsistent with the fact that we would expect a lower variability on time scales of

---

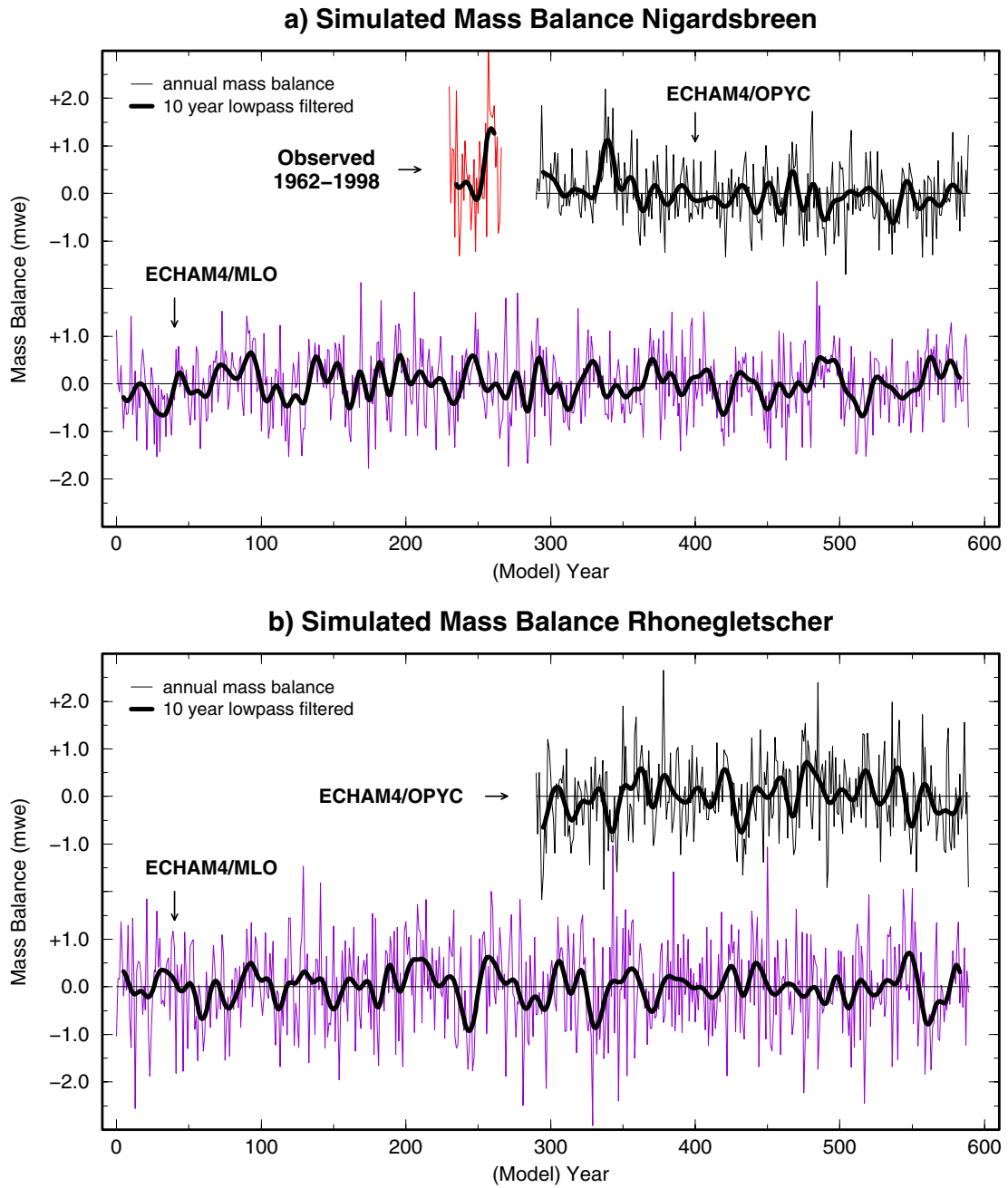


**Figure 5.** Simulation of glacier mass balance exclusively due to internal variations in the climate system using coupled (ECHAM4/OPYC) and mixed-layer (ECHAM4/MLO) GCM experiments. Thin lines represent annual values of mass balance, heavy solid lines denote the smoothed 10 year lowpass filtered versions for (a) Nigardsbreen and (b) Rhonegletscher. The observed mass balance for Nigardsbreen within the period 1962-1998 is shown for comparison (a).

decades in the mixed-layer model due to the lack of an internal ocean. A spectral analysis of simulated averaged northern Hemisphere temperature variations for both models suggests that this should at least be valid for periods longer than 40 years (see section 1.1, Figure 2; also *Bengtsson and Reichert* [2000]). Nevertheless, this cannot be seen in the simulation for the specific midlatitude regions of Nigardsbreen and Rhonegletscher which are strongly influenced by the NAO. One reason is the above mentioned model-specific higher interannual mass balance variability (due to increased variability in precipitation) simulated by the mixed-layer GCM in comparison with the coupled model, which in turn also induces a higher decadal scale variability. If the interannual variability was comparable in both models, we would most likely obtain a relatively lower decadal mass balance variability in the mixed-layer model as could be expected.

For Nigardsbreen, the full record of observations for the period 1962-1998 (Norwegian Water Resources and Energy Administration, see section 4.4) is shown for comparison (Figure 5a). The variability of the observed annual mass balance is slightly higher than in the GCM control experiments. This may have three main reasons: a) although the mass balance model explains a remarkable large part of observed glacier mass balance variations (as the experiments in section 4.4 have shown), some fraction of statistical variance is naturally missing in the simulation, b) the large-scale variability in the GCM experiments serving as basis for statistical downscaling is slightly lower than in ECMWF reanalyses, and c) the continuous increase of greenhouse gas concentrations not considered in the model runs (equilibrium state with constant greenhouse gas concentrations) affects climatic variability (this will be investigated in another study using transient coupled GCM experiments).

However, periods of generally strong positive mass balances, comparable to observed mass balances for Nigardsbreen during the 1980s and the first half of the 1990s (Figure 5a, observed 1962-1998 record; see Figure 13 for larger illustration), do appear in the GCM simulations exclusively due to internal variations in the climate system. A comparable positive mass balance “event” has, for example, been simulated by the coupled ECHAM4/OPYC GCM at around year 50, denoted as year 340 in Figure 5a (particularly evident for the 10 year lowpass filtered time series). It should also be mentioned that in longer coupled GCM integrations, the sampling problem would be reduced and a larger number of simulated “events” of this type could be expected. In the following, we will demonstrate that such “events” can be related to the NAO (section 4.6 and 4.7). A link to the NAO has been proposed in earlier studies [e.g. *Hurrel*, 1995] but can now be investigated in detail, including the responsible mechanisms using multi-century GCM experiments.

---

## 4.6 The Role of the NAO for Glacier Mass Balance

In this section we examine physical mechanisms in the climate system responsible for mass balance variations of the above simulated glaciers. This leads to an investigation of possible relationships with the North Atlantic Oscillation (NAO) as a major source of atmospheric variability. We examine the individual impact of temperature and precipitation on mass balance variations considering individual seasons which may have a distinct impact according to the glacier specific Seasonal Sensitivity Characteristics (SSCs) discussed in section 4.3.

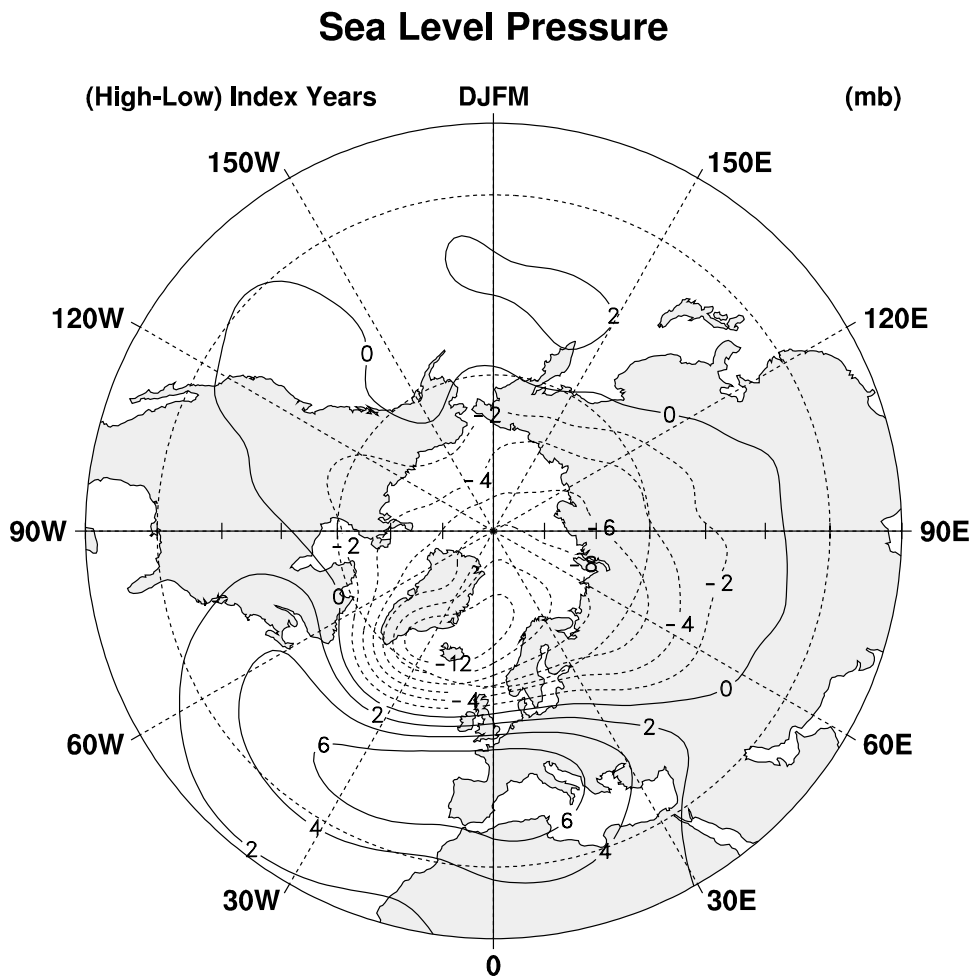
### 4.6.1 NAO Index and Glacier Mass Balance

The North Atlantic Oscillation [*Walker and Bliss, 1932; van Loon and Rogers, 1978; Kushnir and Wallace, 1989; Kushnir, 1994; Hurrell, 1995*] can be associated with variations in the strength of the westerlies over the North Atlantic onto Europe. A positive (negative) phase of the NAO reflects above-normal (below-normal) pressure over the central North Atlantic south of 55°N and below-normal (above-normal) pressure across the high latitudes of the North Atlantic (Figure 6). One center is located near the semipermanent Icelandic low and the other center of opposite sign near the Azores high. The oscillation is present throughout the year in monthly mean data but is most pronounced during winter [*Barnston and Livezey, 1987*].

Several hypothesis have been developed to explain the observed variability in the NAO. The null hypothesis is that the NAO is simply a natural internal mode in the climate system, the ocean turns high frequency stochastic forcing of the atmosphere into low-frequency variability [*Hasselmann, 1976*] which explains the observed redness of the spectrum. Spectral peaks may be due to damped eigenmodes associated with the coupling between ocean and atmosphere [*Latif and Barnett, 1994*]. The memory of the coupled system may be found in the gyral circulation of the ocean [*Grötzner et al., 1998*] and the thermohaline circulation [*Timmermann et al., 1998*].

The NAO has a dominant influence on wintertime temperatures of the Northern Hemisphere (Figure 7). A strong positive phase of the NAO is related to a strong westerly flow over the North Atlantic [*Rogers, 1985*] and can be associated with above-normal temperatures extending from northern Europe across much of Eurasia and below-normal temperatures over the northwest Atlantic [*Hurrell, 1995; Hurrell and van Loon, 1997*].

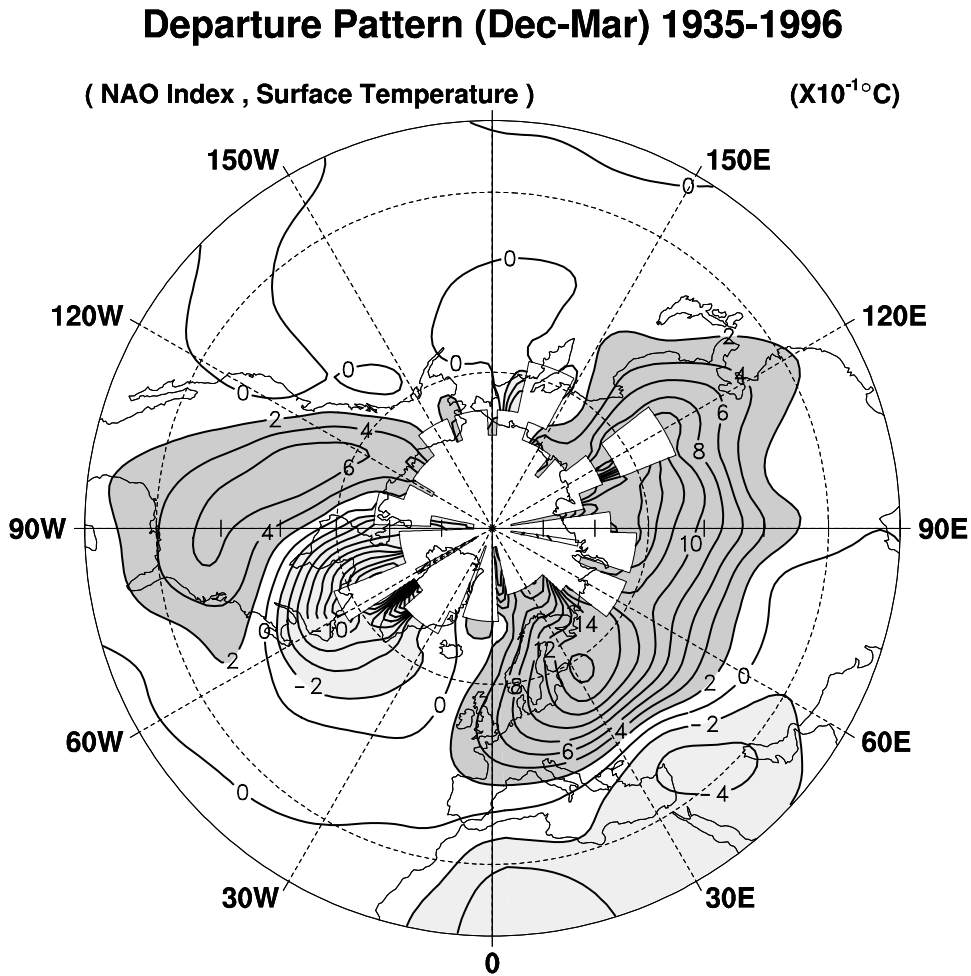
---



**Figure 6.** Observed difference in Sea Level Pressure for high NAO index minus low NAO index winters since 1899. The contour interval is 2 hPa, negative values are dashed. From [Hurrell, 1995].

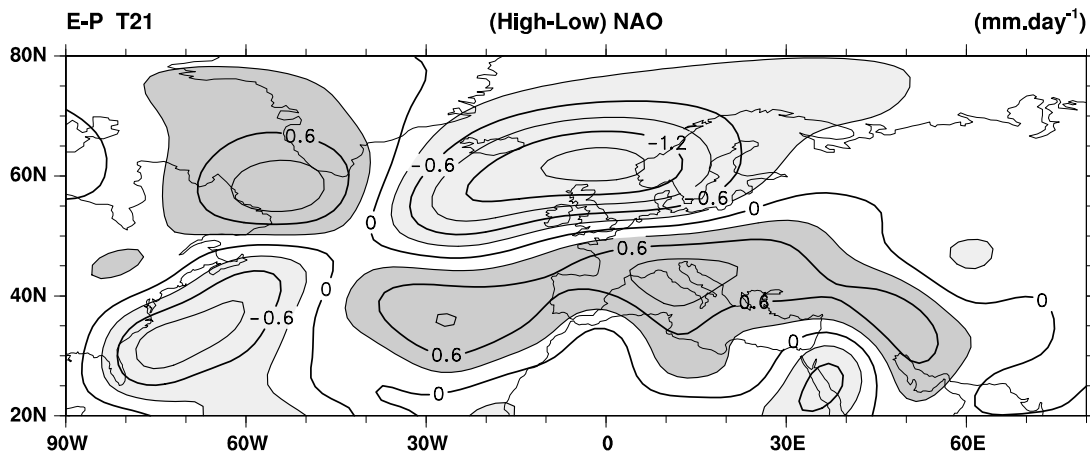
A considerable impact of the NAO on regional winter precipitation has also been observed (Figure 8). High NAO index winters can be related to above-normal precipitation over an area spanning from Iceland to Scandinavia (particularly important for Nigardsbreen glacier investigated in this study) and below-normal precipitation over much of central and southern Europe (important for Rhonegletscher in this study), the northern Mediterranean countries, and west North Africa [van Loon and Rogers, 1978; Hurrell, 1995].

Opposite patterns of temperature and precipitation anomalies are typically observed during pronounced negative phases of the NAO.



**Figure 7.** Observed surface temperature change (unit 0.1°C) associated with a one standard deviation change in the NAO index. Data from *Hurrell and van Loon* [1997] for the winters of 1935-1996 were used. Dark (light) shading indicate positive (negative) changes. From [*Visbeck et al.*, 1998].

The NAO indices of the GCM integrations used in this study are constructed from the differences of normalized pressures in winter (November through March) between area averages located west of Portugal (11°W - 14°W, 40°N - 43°N) and over Iceland (17°W - 20°W, 65°N - 68°N) following the definition of *Hurrell* [1995] (see [*Christoph et al.*, 1999; *Wallace and Gutzler*, 1981]). A positive index value is associated with stronger-than-normal westerlies across the North Atlantic and northwestern Europe, a negative value indicates weaker-than-normal westerlies.



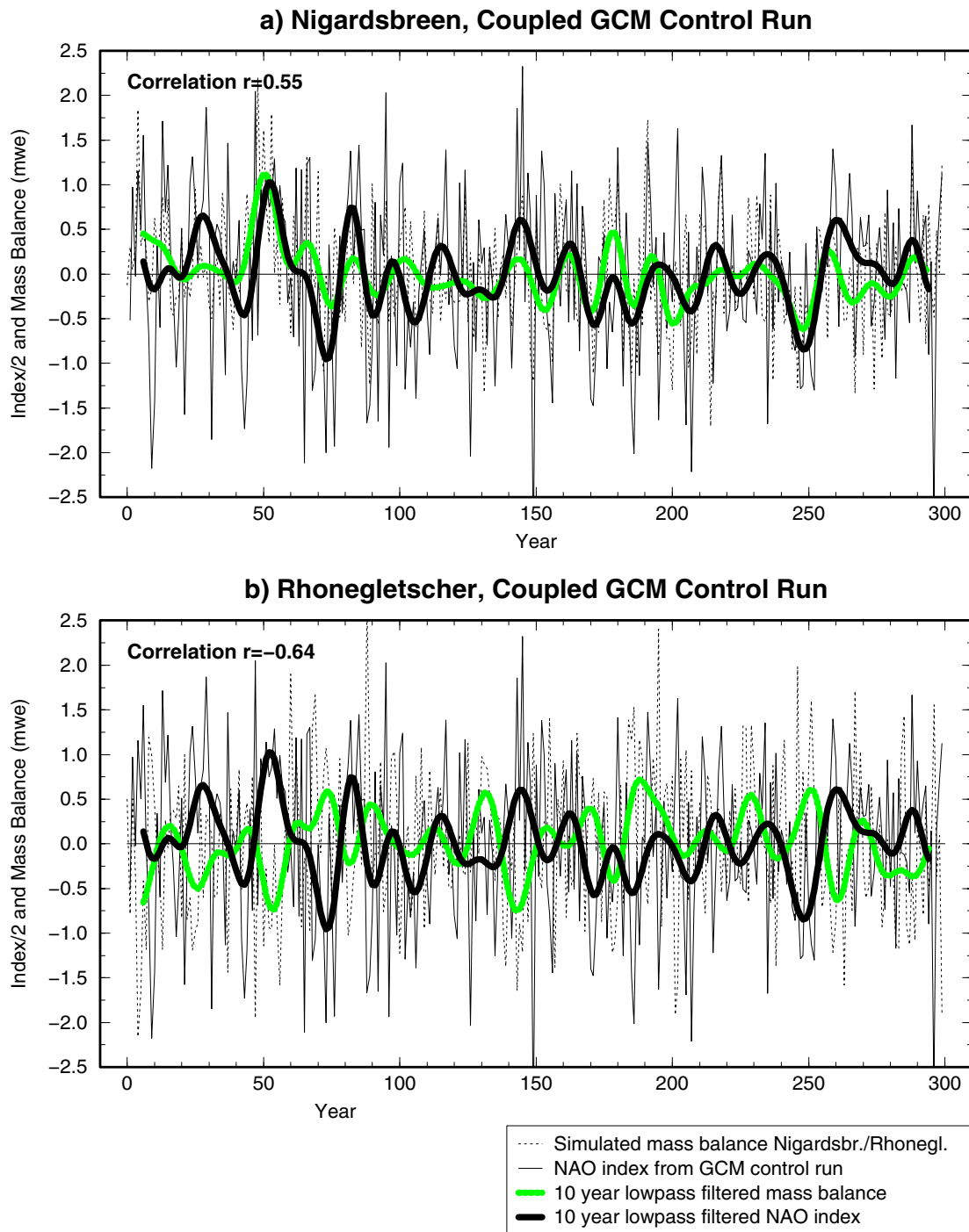
**Figure 8.** Precipitation anomalies associated with the NAO. Evaporation minus precipitation is plotted for high NAO index minus normal or low NAO index winters, computed as a residual of the atmospheric moisture budget using ECMWF global analyses. From [Hurrell, 1995].

Figure 9 shows the unfiltered (solid thin lines) and 10 year lowpass filtered time series (solid heavy lines) of the NAO index for 300 years of the coupled (ECHAM4/OPYC) GCM integration. Glacier mass balance for Nigardsbreen (Figure 9a, dotted line) and Rhonegletscher (Figure 9b, dotted line) as simulated by the experiment (see section 4.5 for description) along with the 10 year lowpass filtered versions (heavy shaded lines) are shown for comparison. For both glaciers, we find a well pronounced correlation between the lowpass filtered NAO index of the model and mass balance. The correlation coefficient for Nigardsbreen is  $r = 0.55$ , for Rhonegletscher we find an anti-correlation of  $r = -0.64$  (both significant at 99% confidence level). This demonstrates the strong link between decadal variations in the North Atlantic Oscillation and decadal variability in glacier mass balance controlled by temperature and precipitation. We will now further investigate the individual role of temperature and precipitation within this relation.

#### 4.6.2 Individual Impact of Temperature and Precipitation on Mass Balance

The individual impact of temperature and precipitation on mass balance of each glacier is illustrated in Figure 10. We have calculated the 10 year lowpass filtered mass balance for Nigardsbreen (Figure 10a) and Rhonegletscher (Figure 10b) as simulated by the coupled GCM using exclusively either precipitation ( $B_P$ , dashed shaded lines) or temperature ( $B_T$ , dashed solid lines). For both glaciers, the mass

## NAO Index and Mass Balance Nigardsbreen/Rhonegletscher



**Figure 9.** NAO index (thin solid line) along with glacier mass balance of (a) Nigardsbreen and (b) Rhonegletscher (thin dotted line) as simulated by the coupled (ECHAM4/OPYC) GCM experiment. The figure illustrates the strong link between the North Atlantic Oscillation and glacier mass balance fluctuations, the correlation coefficients  $r$  for the 10 year lowpass filtered time series (heavy lines) are shown in the top left corner of each graph.

balance variability due to precipitation (standard deviation  $\sigma_{Bp}$ ) is by far higher than the variability due to temperature ( $\sigma_{Bt}$ ). For Nigardsbreen, we find  $\sigma_{Bp} = 0.27$  mwe and  $\sigma_{Bt} = 0.17$  mwe, for Rhonegletscher we have  $\sigma_{Bp} = 0.32$  mwe and  $\sigma_{Bt} = 0.10$  mwe. This means that the individual impact of precipitation on Nigardsbreen glacier mass balance is about 1.6 times higher than the impact of temperature. For Rhonegletscher it is about 3 times higher.

We can furthermore infer that for both glaciers, changes in mass balance due to precipitation are very closely linked to the NAO (Figure 10, solid lines). The correlation coefficient between  $B_p$  and the NAO index is  $r = 0.75$  (Nigardsbreen) and  $r = -0.65$  (Rhonegletscher). On the other hand, mass balance variations due to temperature are not significantly (95% confidence level) correlated with the NAO, we find  $r = -0.20$  (Nigardsbreen) and  $r = -0.17$  (Rhonegletscher). This suggests that for both glaciers, precipitation is by far the dominant factor for the close relationship between glacier mass balance variations and the NAO.

For the mixed-layer GCM experiment (not shown), the standard deviations  $\sigma_{Bt}$  of mass balance due to temperature are comparable to the coupled GCM. The standard deviations  $\sigma_{Bp}$  due to precipitation are slightly higher (e.g. for Rhonegletscher 0.36 mwe relative to 0.32 mwe) due to the model-specific increased variability in simulated precipitation. As mentioned in section 4.5.3, this is connected to the different representation of the pattern of precipitation associated with the NAO in the mixed-layer model.

### 4.6.3 Seasonal Impact on Mass Balance

The actual impact of temperature and precipitation on glacier mass balance for individual months of the year as simulated by the downscaled coupled GCM may now be investigated. For each glacier site, we calculate the standard deviations of the simulated temperature and precipitation variations for a specific month over 300 years of the control experiment. We define the *impact* as the standard deviations multiplied with the corresponding monthly sensitivity values of the glaciers obtained from the Seasonal Sensitivity Characteristics (SSCs) described in section 4.3.3. This means that we account for both the sensitivity of the glaciers as well as the actually simulated local variability of the forcing variables. The resulting mass balance changes presented in Figure 11 can be associated with a one standard deviation change of the forcing variables for individual months.

While the SSCs as illustrated in Figure 3 may at first glance have suggested a rather low overall *sensitivity* of both glaciers to precipitation changes, we find that

## Impact of Temperature and Precipitation on Mass Balance

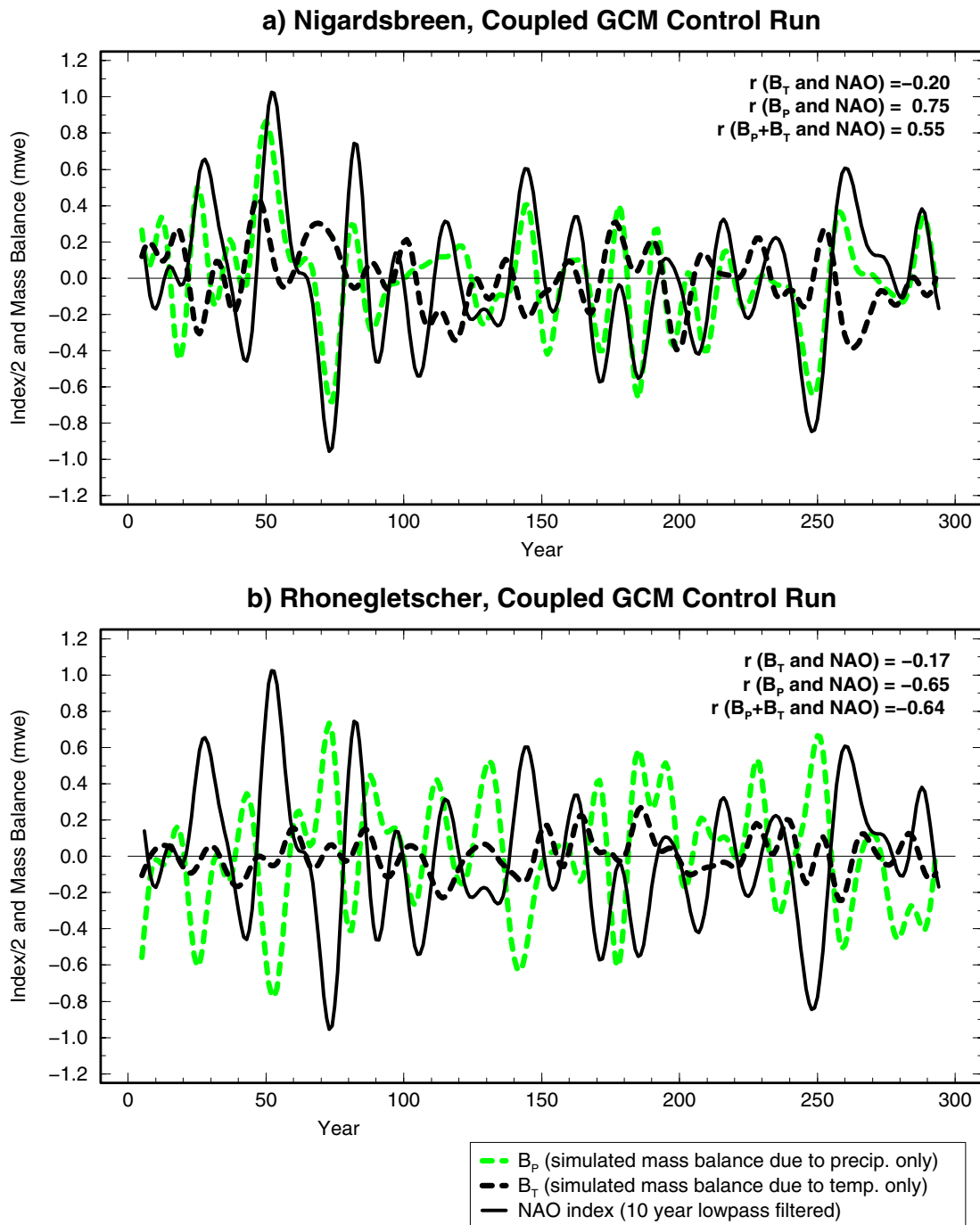


**Figure 10.** Individual impact of temperature and precipitation on glacier mass balance for (a) Nigardsbreen and (b) Rhonegletscher as simulated by the coupled GCM (ECHAM4/OPYC). We present the 10 year lowpass filtered mass balance  $B_P$  simulated using exclusively precipitation (shaded dashed lines), the mass balance  $B_T$  exclusively due to temperature (solid dashed lines), and the NAO index (solid lines). Correlation coefficients between the NAO index on one hand and  $B_P$ ,  $B_T$ , and  $B_P + B_T$  (resulting total mass balance as in Figure 9) respectively on the other hand are shown in the top right corner of each graph.

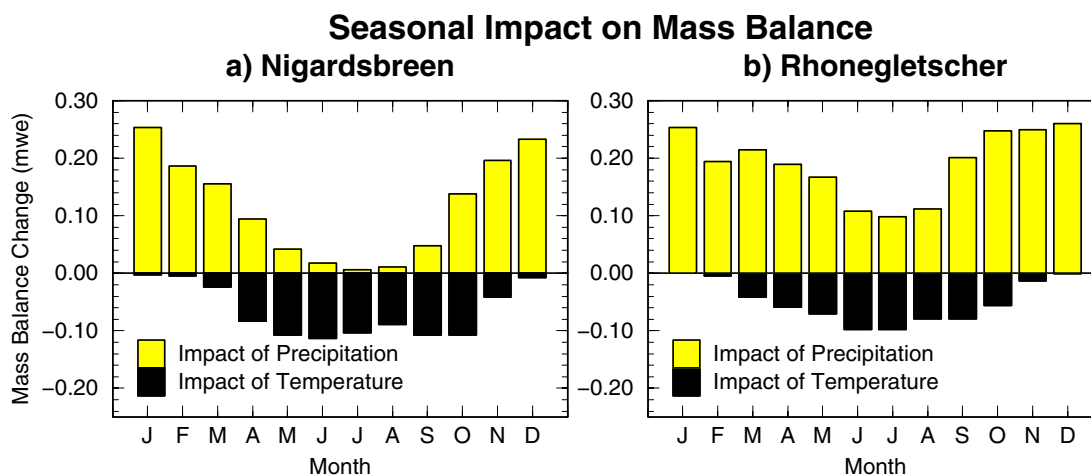


**Figure 11.** Impact (defined as sensitivity  $\times$  GCM-simulated variability) on glacier mass balance associated with a one standard deviation change in temperature and precipitation for individual months of the year for (a) Nigardsbreen and (b) Rhonegletscher. The Seasonal Sensitivity Characteristic (Figure 3) and the standard deviation of temperature and precipitation for a specific month as simulated by the downscaled coupled GCM experiment are considered.

the actual *impact* (sensitivity  $\times$  GCM-simulated standard variation) of precipitation changes on mass balance is in fact relatively high in comparison with temperature (Figure 11a, 11b). The reason is of course the relatively high variability in local precipitation as simulated by the downscaled GCM compared to the variability in temperature. This is in agreement with the statement in section 4.6.2 (Figure 10) where we found that the impact of precipitation on the annual mass balance is much stronger (1.6 times for Nigardsbreen, 3 times for Rhonegletscher) than the impact of temperature.

For both glaciers, the simulated variability of temperature in the 300 years of the GCM integration is generally highest in winter (DJF) which can partly be related to the influence of the NAO as will be discussed below. However, because of the very small temperature sensitivity in winter ( $< 0.01$  mwe/K, Figure 3), the overall *impact* of winter temperature changes is extremely small, in fact negligible (Figure 11). On the other hand, we find that relatively small simulated temperature variations in summer (JJA) have a considerable impact on mass balance since the sensitivity of the glaciers is naturally high during this season (melting occurs, Figure 3).

With respect to precipitation, we find a very strong impact on mass balance of the glaciers in winter (Figure 11). This is naturally a consequence of the glacier's high sensitivity (Figure 3) and the high variability in precipitation for this season (related

to the NAO, see below). For Nigardsbreen, the sensitivity in summer (summer precipitation falls as rain over most parts of the glacier, section 4.3.3) and the variability in precipitation are small, the resulting impact is therefore low. For the higher elevated Rhonegletscher, even smaller summer temperature changes have a noticeable impact since the sensitivity to precipitation is nearly constant throughout the year (Figure 3b).

#### **4.6.4 Seasonal Impact of the NAO**

The seasonal impact on mass balance can now further be investigated by examining extreme events of positive and negative NAO phases in the coupled GCM experiment along with their impact on temperature and precipitation. Figure 12 shows the situation during 10 years of a high phase of the NAO index (mean over model years 48-57, see Figure 9) minus 10 years of the following low phase of the NAO index (mean over model years 69-78). The corresponding anomaly patterns of sea level pressure, surface air temperature, and precipitation are presented for the winter (DJF; Figures 12a-12c) and the summer season (JJA; Figures 12d-12f).

The sea level pressure pattern in winter (Figure 12a) is the typical NAO pattern and is realistically represented by the coupled GCM in comparison with observations (see Figure 6). As mentioned earlier (section 4.6.1) the NAO is not well pronounced during summer which can also clearly be seen in the GCM experiment (Figure 12d).

##### **4.6.4.1 Seasonal impact of precipitation**

Positive anomalies in winter precipitation associated with the NAO (Figure 12c) can be found from Iceland to Scandinavia with a maximum anomaly of about 40 mm/month near the Norwegian coast. The pattern is in good agreement with observations (Figure 8). Negative anomalies occur over western and southern Europe with the largest reductions in precipitation (more than 60 mm/month) near the northwestern coast of the Iberian peninsula. The Alps experience a reduction of about 20 mm in monthly precipitation.

Nigardsbreen glacier (61°43'N, 7°08'E) is located near the maximum anomaly (40 mm/month) in winter precipitation associated with the NAO. As we have seen above, the glacier is most sensitive to winter precipitation anomalies (Figure 11a). This demonstrates that the strong impact of precipitation on mass balance (as shown in Figure 10a and 11a) can to a great extent be explained by the strong influence of the NAO. During summer, both the precipitation anomaly due to the NAO (Figure 12f) as well as the sensitivity of the glacier are low, the effect on mass balance is consequently very small.

---

For the region of Rhonegletscher (46°37'N, 8°24'E), we find a reduction in winter precipitation of about 20 mm/month (Figure 12c) exerting a strong impact on the annual mass balance of the glacier (as shown in Figure 10b and 11b). Although the precipitation sensitivity of Rhonegletscher is roughly constant throughout the year, the summer precipitation anomaly associated with the NAO (Figure 12f) is low and its impact is therefore rather restricted.

#### **4.6.4.2 Seasonal impact of temperature**

Positive anomalies of more than 1°C in surface air winter temperature associated with the NAO (Figure 12b) occur over Scandinavia and other parts of northern Europe extending eastwards across much of Eurasia. Negative anomalies can be found over Greenland and parts of the northwest Atlantic.

For the region of Nigardsbreen, we find a considerable winter temperature anomaly of about 2°C associated with the NAO. However, the sensitivity to winter temperature changes is low (Figure 3a), the impact on the annual glacier mass balance is therefore in fact negligible (Figure 11a). This is also true for Rhonegletscher (Figure 11b) which experiences only a small winter temperature anomaly associated with the NAO (Figure 12b). In summer a rather strong impact of temperatures could be expected due to the relatively high sensitivity of the glaciers during this season. However, the simulated temperature anomalies associated with the NAO are low for both glaciers (Figure 12e), their overall impact on the annual mass balance therefore still remains smaller compared to the impact of precipitation.

In summary, we have seen that for both glaciers, 1) the overall impact of precipitation changes on annual mass balance variations is by far higher than the impact of temperature, and 2) mass balance changes of the glaciers are to a large extent caused by variations in winter precipitation associated with the NAO. A high phase of the NAO means clearly enhanced winter precipitation for the region of Nigardsbreen, typically leading to a higher than normal positive mass balance over the year. For Rhonegletscher, a high NAO phase typically means reduced winter precipitation leading to a lower than normal mass balance. The opposite is valid for a low phase of the NAO.

---

### Simulated Sea Level Pressure, Temperature and Precipitation Anomalies Associated with the NAO (ECHAM4/OPYC)

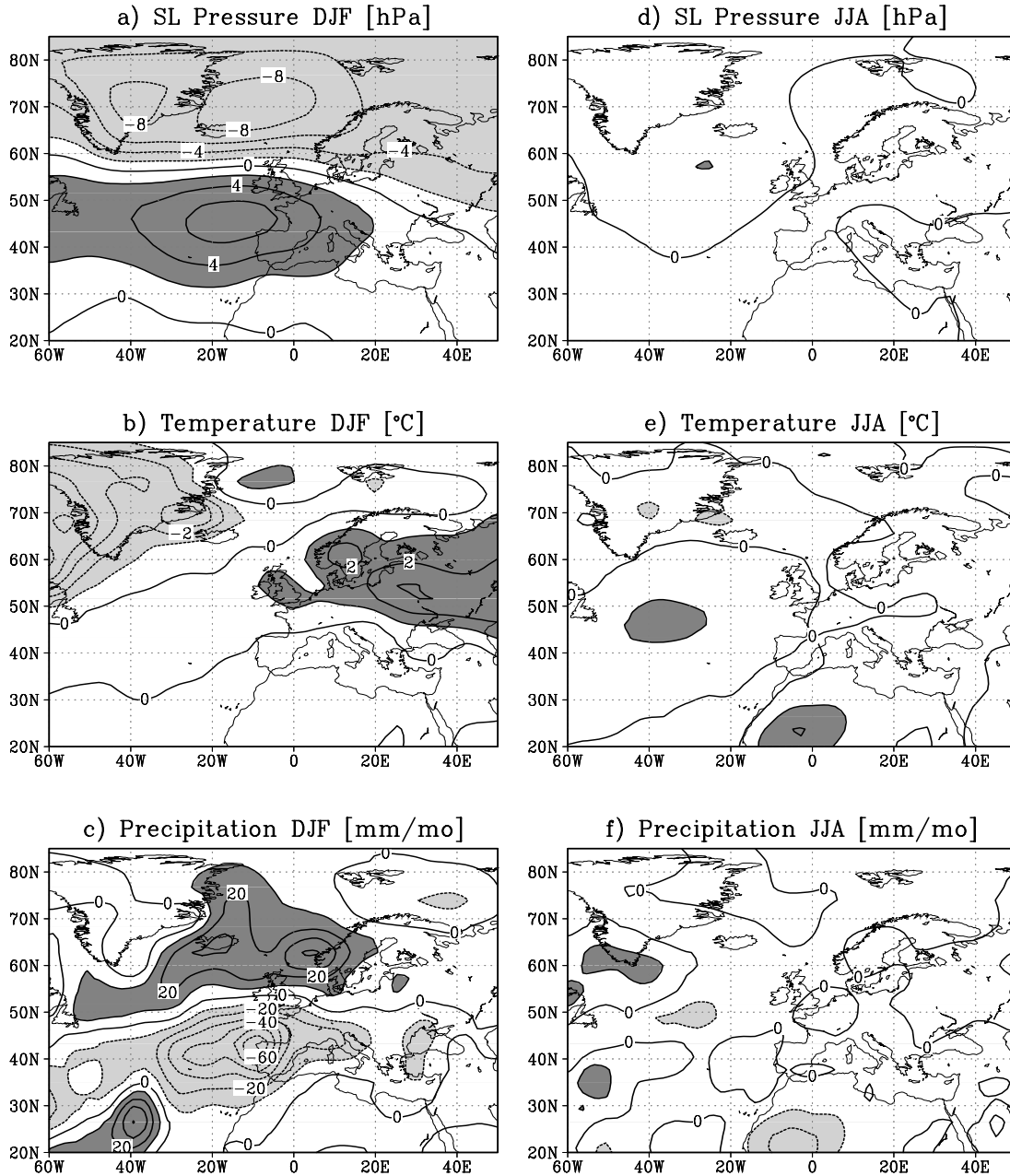


**Figure 12.** Anomalies of sea level pressure (a, d; contour interval 2 hPa), surface air temperature (b, e; contour interval 1°C), and precipitation (c, f; contour interval 10 mm/month) associated with 10 years of a high phase minus 10 years of a low phase of the NAO index as simulated by the coupled GCM. Dark (light) shading indicate positive (negative) anomalies. (a-c) show anomalies for the winter (DJF) season, (d-f) represent summer (JJA) anomalies.

### **4.7 Recently Observed Positive Mass Balances of Norwegian Glaciers**

The net mass balance averaged over available observational data from 32 worldwide glaciers in 10 mountain ranges shows a considerable worldwide glacier mass loss on the order of a few decimeters per year for the period 1980-1997 [IASH, 1999; Haeberli *et al.*, 1999]. In this global context, strong positive mass balances as observed for Nigardsbreen and other maritime glaciers in southwestern Norway over the same time period may appear rather exceptional. With respect to the results obtained above, it is now interesting to discuss these positive mass balances in more detail.

We already mentioned (section 4.5.3) that periods of generally strong positive mass balances, comparable to the observed mass balances for Nigardsbreen within the period 1980-1995 (Figure 13, thin dashed line), appear in the GCM simulations exclusively due to internal climate variations (Figure 5a). We showed that a comparable positive mass balance “event” has, for example, been simulated by the coupled ECHAM4/OPYC GCM at around year 50 (denoted as year 340 in Figure 5a). With respect to the NAO index as presented in Figure 9 it has now become evident that this simulated “event” of positive mass balances can clearly be associated with a strong positive phase of the NAO in the model (Figure 9a, heavy solid line, around year 50).

This is in agreement with observational data illustrated in Figure 13. The observed annual mass balances for Nigardsbreen within the period 1962-1998 (dashed lines) along with the NAO index for the period 1950-1999 (thin solid line) are shown. It is immediately evident that mass balance and NAO index are remarkably well correlated, the correlation coefficient for annual data is  $r = 0.58$  (95% significance level at  $r \geq 0.29$ ) within the period 1962-1998. For the period 1966-1998, the correlation coefficient even increases to  $r = 0.71$  (95% significance level for  $r \geq 0.30$ ). The 10 year lowpass filtered time series (thick lines) indicate that also the decadal trends are comparable for the last three decades.

The investigation of the individual seasonal impact of temperature and precipitation in the GCM experiments (section 4.6.2-4.6.4) showed that this link between mass balance and the NAO is mainly established through winter precipitation variations associated with the NAO exerting a strong impact on the annual mass balance of the glacier.

The GCM experiments and investigation of the forcing factors for glacier mass balance in this study therefore provide evidence for the assumption that generally

---

positive mass balance tendencies as recently observed for Nigardsbreen can be related to enhanced precipitation in winter associated with a positive phase of the NAO. The observed strong positive glacier mass balances within 1980-1995 can thus be seen as a consequence of the corresponding observed persistent positive phase of the NAO within this time period. This mechanism will probably also be valid for other maritime Norwegian glaciers which have also shown strong positive mass balances within this period [IASH, 1999].

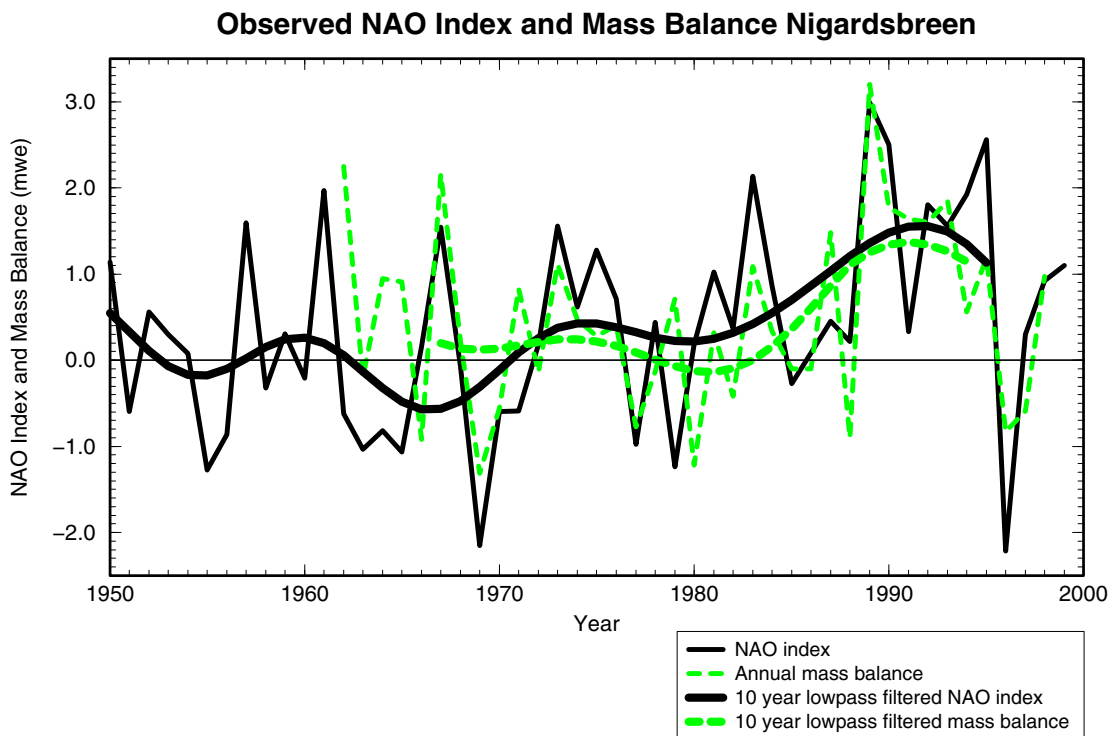


**Figure 13.** Observed NAO Index for the period 1950-1999 (data from *Jones et al.*, 1997; *Osborn et al.*, 1999; solid lines) and observed mass balance for Nigardsbreen 1962-1998 (data from *IASH*, 1998, 1999; dashed lines) along with 10 year lowpass filtered values (heavy lines). The correlation coefficient for annual data is  $r = 0.58$ .

## 4.8 Conclusions

A process-based modeling approach has been applied in order to simulate glacier mass balance records for Nigardsbreen (Norway) and Rhonegletscher (Switzerland) using downscaled GCM experiments.

Statistical downscaling of GCM output is based on the large-scale flow obtained from daily ECMWF reanalyses and local station data in the vicinity of the glaciers. On average, 79% of variance for observed monthly temperatures in the region of Nigardsbreen, and 80% of variance in the region of Rhonegletscher has been explained using reanalyses. For local precipitation, the explained variances are 65% and 51% respectively. The composition of large-scale predictors and their individual impact (especially on precipitation) vary considerably for individual stations within the areas of investigation.

The sensitivity of glacier mass balance to local temperature and precipitation is represented by glacier specific Seasonal Sensitivity Characteristics (SSCs) calculated from a mass balance model of intermediate complexity. The sensitivity of Rhonegletscher to changes in precipitation is almost constant throughout the year whereas for Nigardsbreen, a change in summer precipitation (mainly falling as rain due to the lower elevation) has only a marginal effect. The sensitivity to changes in summer temperatures (when melting occurs) is higher for Nigardsbreen relative to Rhonegletscher. A temperature change in winter has almost no effect on mass balance for both glaciers.

We validate the process-based mass balance modeling approach and the statistical downscaling strategy against observations by simulating glacier mass balance using ECMWF reanalyses. In situ measurements of mass balance for Nigardsbreen are found to be in good agreement with simulations for the period 1979-1993. We find a considerable impact on mass balance when using different stations in the vicinity of the glaciers for downscaling.

Mass balance fluctuations for Nigardsbreen and Rhonegletscher are simulated using multi-century coupled (ECHAM4/OPYC) and mixed-layer (ECHAM4/MLO) GCM integrations excluding external forcings. The experiments show that periods of generally strong positive mass balances, comparable to observed mass balances for Nigardsbreen during the 1980s and the first half of the 1990s do appear in the GCM integrations suggesting that such periods may be explained by internal variations in the climate system. For Nigardsbreen (Rhonegletscher), we find a high correlation (anti-correlation) between decadal variations in the North Atlantic Oscillation and glacier mass balance in the model experiments. The correlation coefficients for the

---

relation between the NAO index and mass balance are  $r = 0.55$  and  $r = -0.64$  for Nigardsbreen and Rhonegletscher respectively.

The actual impact of temperature (precipitation) as simulated by the downscaled GCM experiments on mass balance variations of the glaciers has been defined as the product of glacier sensitivity and one standard deviation of simulated temperature (precipitation) variability for individual months. In the coupled GCM experiment, the overall impact of precipitation changes on glacier mass balance variations is 1.6 times and 3 times higher for Nigardsbreen and Rhonegletscher, respectively, compared to the impact of temperature. Furthermore, precipitation is the dominant factor for the link between mass balance and the NAO. Mass balance changes of the glaciers due to precipitation are to a great extent caused by variations in winter precipitation associated with the NAO. A high phase of the NAO means clearly enhanced winter precipitation for the region of Nigardsbreen, typically leading to a higher than normal positive mass balance over the year. For Rhonegletscher, a high NAO phase typically means reduced winter precipitation leading to a lower than normal mass balance.

This mechanism, established using multi-century coupled GCM experiments, can explain the observed strong positive mass balances for Nigardsbreen and possibly other maritime Norwegian glaciers within the period 1980-1995. It has been shown that observed annual glacier mass balances and the observed NAO index are remarkably well correlated within the period 1962-1998. The experiments in this study provide evidence for the assumption that the generally positive mass balance tendencies recently observed for Nigardsbreen can be related to enhanced precipitation in winter associated with a positive phase of the NAO. The observed strong positive glacier mass balances within 1980-1995 can thus be seen as a consequence of the corresponding observed persistent positive NAO phase.

Glacier mass balances of Alpine glaciers have been strongly negative during the decade 1980-1990. The average mass balance value has been  $-0.65$  mwe [Haeberli *et al.*, 1999] resulting in an estimated loss of 10 to 20% of ice volume since 1980 [Haeberli and Beniston, 1998]. The results of the present study indicate that this loss of mass balance can (at least as has been demonstrated for Rhonegletscher) partly be explained by the strong positive phase of the NAO within this time period. However, it is of course necessary to account for the general positive temperature trend observed in this region, extremely warm temperatures have affected the Alpine region considerably within 1980-1990 [Beniston *et al.*, 1994]. Mass balance changes due to precipitation associated with the NAO are in this region therefore superimposed by changes due to the anomalous warm temperatures which occurred in this period.

---

The mass balance records simulated by the method described in this study will serve as basis for the simulation of glacier length records using a dynamic ice flow model. This will enable us to compare simulated glacier length fluctuations to long observed or reconstructed records of glacier length in order to further investigate natural climate variability as indicated by glaciers.

---

---

**References**

- Bacher, A., J. M. Oberhuber, and E. Roeckner, ENSO dynamics and seasonal cycle in the tropical pacific as simulated by the ECHAM4/OPYC3 coupled general circulation model, *Clim. Dyn.*, 14, 431-450, 1998.
- Barnston, A. G., and R. E. Livezey, Classification, seasonality and persistence of low-frequency circulation patterns, *Mon. Wea. Rev.*, 115, 1083-1126, 1987.
- Bengtsson, L., and B. K. Reichert, Globaler Klimawandel und natürliche Klimavariabilität - Welche Ursachen haben sie? (Global climate change and natural climate variability - What are their reasons?), in *Energie und Umwelt - Wo liegen optimale Lösungen?*, edited by S. Wittig and J. Wolfrum, Union der deutschen Akademien der Wissenschaften und Heidelberger Akademie der Wissenschaften, Springer Verlag, Heidelberg, 2000.
- Christoph, M., U. Ulbrich, J. M. Oberhuber, E. Roeckner, The role of ocean dynamics for low-frequency fluctuations of the NAO in a coupled ocean-atmosphere GCM, *Rep. 285*, Max-Planck-Inst. für Meteorol., Hamburg, Germany, 1999.
- Cubasch, U., H. von Storch, J. Waszkewitz, and E. Zorita, Estimates of climate change in southern Europe derived from dynamical climate model output, *Clim. Res.*, 7, 129-149, 1996.
- Gibson, J. K., P. Kållberg, S. Uppala, A. Nomura, A. Hernandez, and E. Serrano, ERA Description, *ECMWF Re-Anal. Proj. Rep. Ser., Rep. 1*, Eur. Cent. for Medium-Range Weather Forecasts, Reading, England, 1997.
- Gregory, J. M., and J. Oerlemans, Simulated future sea-level rise due to glacier melt based on regionally and seasonally resolved temperature changes, *Nature*, 391, 474-476, 1998.
- Grötzner, A., M. Latif, and T. P. Barnett, A decadal climate cycle in the North Atlantic ocean as simulated by the ECHO coupled GCM, *J. Climate*, 11, 831-847, 1998.
- Haeberli, W., Glacier fluctuations and climate change detection, *Geogr. Fis. Dinam. Quat.*, 18, 191-199, 1995.
- Haeberli, W., and M. Beniston, Climate change and its impacts on glaciers and permafrost in the Alps, *Ambio*, 27, 258-265, 1998.
- Haeberli, W., R. Frauenfelder, M. Hoelzle, and M. Maisch, On rates and acceleration trends of global glacier mass changes, *Geografiska Annaler*, 81A, 585-591, 1999.
- Hasselmann, K., Stochastic Climate Models I: Theory, *Tellus*, 28, 473-485, 1976.
-

- Hoelzle, M., and W. Haeberli, World glacier monitoring service, world glacier inventory, digital data available from the *National Snow and Ice Data Center*, nsidc@kryos.colorado.edu, Univ. of Colorado, Boulder, Colorado, 1999.
- Hurrell, J. W., Decadal trends in the North Atlantic Oscillation: regional temperatures and precipitation, *Science*, 269, 676-679, 1995.
- Hurrell, J. W., and H. van Loon, Decadal variations in climate associated with the North Atlantic Oscillation, in *Climate Change Proc. Int. Workshop on Climate Change at High Elevation Sites*, Wengen, Switzerland, 1997.
- Intergovernmental Panel on Climate Change (IPCC), *Climate Change, The IPCC Scientific Assessment*, edited by J. T. Houghton et al., Cambridge Univ. Press, New York, 1990.
- International Association of Scientific Hydrology (IASH), *Fluctuations of Glaciers, International Commission of Snow and Ice (ICSI), Volumes I-VII*, UNESCO, Paris, 1967, 1973, 1977, 1985, 1988, 1993, 1998.
- International Association of Scientific Hydrology (IASH)/UNEP/UNESCO, *Glacier Mass Balance Bulletin No. 5*, edited by W. Haeberli et al., World Glacier Monitoring Service, University and ETH Zurich, 1999.
- Jones, P. D., T. Jonsson and D. Wheeler, Extension to the North Atlantic Oscillation using early instrumental pressure observations from Gibraltar and South-West Iceland. *Int. J. Climatol.*, 17, 1433-1450, 1997.
- Kushnir, Y., Interdecadal variations in the North Atlantic sea surface temperature and associated atmospheric conditions, *J. Climate*, 7, 141-157, 1994.
- Kushnir, Y., and J. M. Wallace, Low Frequency variability in the northern hemisphere winter: geographical distribution, structure and time-scale dependence, *J. Atmos. Sci.*, 46, 3122-3141, 1989.
- Latif, M., and T. P. Barnett, Causes of decadal climate variability over the North Pacific and North America, *Science*, 266, 634-637, 1994.
- Oberhuber, J. M., Simulation of the Atlantic circulation with a coupled sea ice - mixed layer - isopycnal general circulation model. Part I: Model description, *J. Phys. Oceanogr.*, 22, 808-829, 1993.
- Oerlemans, J., A projection of future sea level, *Clim. Change*, 15, 151-174, 1989.
- Oerlemans, J., Climate sensitivity of glaciers in southern Norway: application of an energy-balance model to Nigardsbreen, Helstugubreen and Alftobreen, *J. Glaciol.*, 38, 223-232, 1992.
-

- Oerlemans, J., and J. P. F. Fortuin, Sensitivity of glaciers and small ice caps to greenhouse warming, *Science*, 258, 115-117, 1992.
- Oerlemans, J., and B. K. Reichert, Relating glacier mass balance to meteorological data using a seasonal sensitivity characteristic (SSC), *J. Glaciol.*, 46, in press, 2000.
- Osborn, T. J., K. R. Briffa, S. F. B. Tett, P. D. Jones and R. M. Trigo, Evaluation of the North Atlantic Oscillation as simulated by a coupled climate model, *Clim. Dyn.*, 15, 685-702, 1999.
- Østrem, G., K. D. Selvig, and K. Tandberg (Eds.), *Atlas over breer i Sør-Norge*, Norges Vassdrags- og Energiverk, Hydrologisk Avdeling, Meddelelse, Norway, 1988.
- Reichert, B. K., L. Bengtsson, and O. Åkesson, A statistical modeling approach for the simulation of local paleoclimatic proxy records using general circulation model output, *J. Geophys. Res.*, 104, 19071-19083, 1999.
- Roeckner, E., L. Arpe, L. Bengtsson, M. Christoph, M. Claussen, L. Dümenil, M. Esch, M. Giorgetta, U. Schlese, and U. Schulzweida, The atmospheric general circulation model ECHAM-4: Model description and simulation of present-day climate, *Rep. 218*, Max-Planck-Inst. für Meteorol., Hamburg, Germany, 1996.
- Roeckner, E., Climate sensitivity experiments with the MPI/ECHAM4 model coupled to a slab ocean (abstract), in *Euroclivar Workshop on Cloud Feedbacks and Climate Change*, edited by C. A. Senior and J. F. B. Mitchell, pp. 20, Hadley Cent. for Clim. Predict. and Res., Bracknell, England, 1997.
- Roeckner, E., L. Bengtsson, J. Feichter, J. Lelieveld and H. Rodhe, Transient climate change simulations with a coupled atmosphere-ocean GCM including the tropospheric sulfur cycle, *J. Climate*, 12, 3004-3032, 1999.
- Rogers, J. C., Atmospheric circulation changes with the warming over the Northern North Atlantic in the 1920s, *J. Clim. Appl. Meteorol.*, 24, 1303-1310, 1985.
- Simmons, A. J., D. M. Burridge, M. Jarraud, C. Girard, and W. Wergen, The ECMWF medium-range prediction models: development of the numerical formulations and the impact of increased resolution, *Meteorol. Atmos. Phys.*, 40, 28-60, 1989.
- Stendel, M., and E. Roeckner, Impacts of horizontal resolution on simulated climate statistics in ECHAM4, *Rep. 253*, Max-Planck-Inst. für Meteorol., Hamburg, Germany, 1998.
- Timmermann, A., M. Latif, R. Voss, and A. Grötzner, North Atlantic interdecadal variability: a coupled air-sea mode, *J. Climate*, 11, 1906-1931, 1998.
-

- van Loon, H., and J. C. Rogers, The seesaw in winter temperatures between Greenland and Northern Europe. Part I, General description, *Mon. Wea. Rev.*, *106*, 296-310, 1978.
- Visbeck, M., D. Stammer, J. Toole, P. Chang, J. Hurrell, Y. Kushnir, J. Marshall, M. McCartney, J. McCreary, P. Rhines, W. Robinson, and C. Wunsch, Atlantic climate variability experiment prospectus, *Proc. Workshop Dallas, February 1998 and Workshop Florence, May 1998*, Lamont-Doherty Earth Observatory of Columbia Univ., New York, 1998.
- Walker, G. T., and E. W. Bliss, World weather V, *Mem. R. Meteorol. Soc.*, *4*, 53-84, 1932.
- Wallace, J. M., and D. S. Gutzler, Teleconnections in the geopotential height field during the northern hemisphere winter, *Mon. Wea. Rev.*, *109*, 784-812, 1981.
- Wigley, T. M. L., and S. C. B. Raper, Future changes in global mean temperature and sea level, in *Climate and sea level change: observations, projections and implications*, edited by R. A. Warrick, E. M. Barrow, and T. M. L. Wigley, pp. 111-133, Cambridge University Press, New York, 1993.
-

## 5 Natural Climate Variability as Indicated by Glaciers and Implications for Climate Change

---

### ***Natural Climate Variability as Indicated by Glaciers and Implications for Climate Change: A Modeling Study<sup>4</sup>***

**Abstract.** Glacier fluctuations exclusively due to internal variations in the climate system are simulated using downscaled integrations of both a coupled (ECHAM4/OPYC) and a mixed-layer (ECHAM4/MLO) general circulation model (GCM). We apply a process-based modeling approach using a mass balance model of intermediate complexity and a dynamic ice flow model considering simple shearing flow and sliding. We simulate 10000 year records of glacier length fluctuations for Nigardsbreen (Norway) and Rhonegletscher (Switzerland) using auto-regressive processes determined by statistically downscaled GCM experiments. Return periods and probabilities of specific glacier length changes using GCM integrations excluding external forcings such as solar irradiation changes, volcanic or anthropogenic effects are analyzed and compared to historical glacier length records. Preindustrial fluctuations of the glaciers as far as observed or reconstructed, including their advance during the “Little Ice Age”, can be explained entirely by internal variability in the climate system as represented by a GCM. However, fluctuations comparable to the present-day retreat of the glaciers do not occur in these GCM experiments and must be due to external forcing.

### **5.1 Introduction**

Quantifying natural climate variability and understanding the underlying physical mechanisms are currently major scientific issues, also with respect to investigating the anthropogenic impact on climate. What are the possible physical processes responsible for preindustrial climatic variations over the last millennium such as the “Medieval Warm Period” or the “Little Ice Age” [Grove, 1988] lasting for decades

---

<sup>4</sup> Reichert, B. K., Bengtsson, L., and J. Oerlemans, *Journal of Geophysical Research*, in prep., 2000.

or centuries? Volcanic activity effects the global climate [*Hansen et al.*, 1992; *Lindzen and Giannitsis*, 1998], but only a series of major eruptions are likely to cool global temperature on decadal or longer time scales. Estimations of variability in solar irradiation [*Lean et al.*, 1995; *Hoyt and Schatten*, 1993] are based on indirect and fragmentary evidence but may explain global temperature changes at a level of a few tenths of a degree [*Cubasch et al.*, 1997]. However, a considerable amount of climatic variability over the last millennium may be explained by internal variability in the climate system. *Hasselmann* [1976] demonstrated that low-frequency variations in a system such as the climate could simply be the integrated response of a linear (or nonlinear) system forced by short-term variations such as those of the macroturbulent atmospheric flow at midlatitudes. The dynamics of a physical system can turn short-term stochastic forcing into low-frequency climate variability. This has been demonstrated using ocean general circulation models [*Mikolajewicz and Maier-Reimer*, 1990] and is also applicable to the dynamic response of glacier systems [*Paterson*, 1994] as investigated in this study. Other possible mechanisms inherent to the climate system are internal ocean variability, ENSO variability and other coupled atmosphere-ocean modes [*Sarachik et al.*, 1996; *Bengtsson*, 1999].

General circulation models (GCMs) [e.g., *Roeckner et al.*, 1996] integrated over a long period of time may considerably contribute to the investigation of the role of forcing factors. As an example, it will be shown in this study that fluctuations of specific glaciers, as far as observed or reconstructed prior to industrialization, can be explained by internal variations in the climate system as represented by the control run output of a coupled GCM. External forcings such as solar irradiation changes, volcanic or anthropogenic effects are excluded in the GCM experiments. In addition, a mixed-layer GCM without an internal ocean will be used for comparison.

Our strategy, outlined in Figure 1, is based on statistically downscaled GCM experiments. We combine a process-based modeling approach for the simulation of glacier mass balance (section 5.2) and glacier length (sections 5.4 and 5.5) for specific valley glaciers. In order to simulate long, statistically significant records of low frequency glacier length fluctuations, we use auto-regressive processes applied to the GCM experiments (section 5.3). Simulated glacier fluctuations for Nigardsbreen (Norway) and Rhonegletscher (Switzerland) are compared to historical records of glacier length (section 5.6). We investigate the probability that preindustrial climatic proxy records of glacier length can be explained by internal fluctuations inherent to the climate and the glacier system. We furthermore examine whether it is likely that the general retreat of the glaciers observed during the 20<sup>th</sup> century, may be explained by internal variations as simulated by a GCM or whether additional external forcing is required.

---

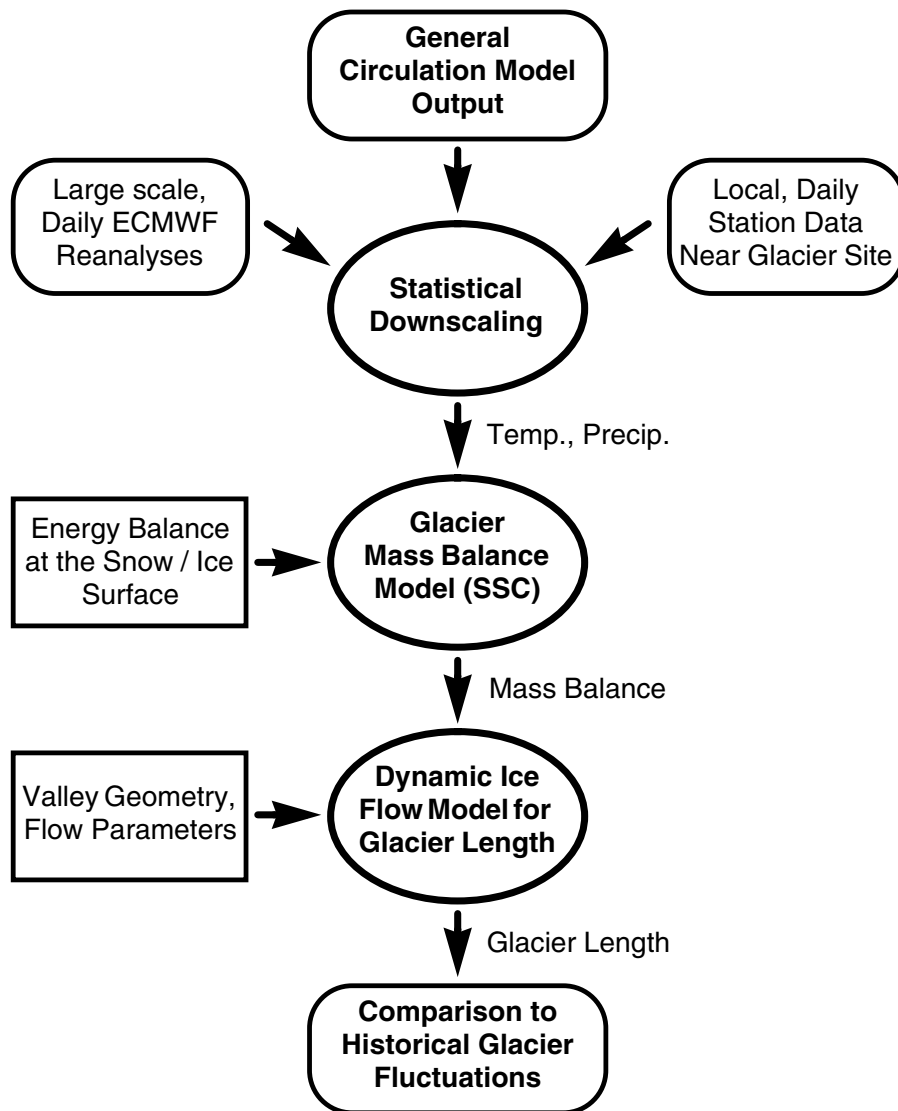


**Figure 1.** General approach for the simulation of glacier fluctuations applied in this study. Statistically downscaled GCM output is used for a glacier specific Seasonal Sensitivity Characteristic (SSC) based on a mass balance model considering the energy balance at the snow / ice surface of the glacier. Glacier length records are simulated using a dynamic ice flow model, and compared to observed or reconstructed historical glacier fluctuations.

## 5.2 Glacier Mass Balance as Simulated Using GCMs

In this study, we use downscaled integrations of the European Center/Hamburg general circulation model ECHAM4 [Roeckner *et al.*, 1996] excluding external forcings such as solar irradiation changes, volcanic or anthropogenic effects. Both an experiment with a coupled version of the model (ECHAM4/OPYC; 300 year control run, T42 resolution; [Roeckner *et al.*, 1999]) and a mixed-layer version without an internal ocean (ECHAM4/MLO; 600 year control run, T30 resolution; [Roeckner, 1997]) are applied. The concentrations of carbon dioxide, methane, and nitrous oxide are fixed at the observed 1990 values.

Statistical downscaling is based on daily reanalyses of the European Centre for Medium-Range Weather Forecasts (ECMWF) [Gibson *et al.*, 1997] and weather station data in the vicinity of the investigated glaciers [Reichert *et al.*, 1999]. A process-based modeling approach using a mass balance model of intermediate complexity and glacier specific seasonal sensitivity characteristics [Oerlemans and Reichert, 2000] has been applied in order to simulate glacier mass balance for Nigardsbreen (Norway; 61°43'N, 7°08'E) and Rhonegletscher (Swiss Alps; 46°37'N, 8°24'E). Mass balance simulations are described in detail in Reichert *et al.* [2000] (Chapter 4 in this thesis).

## 5.3 Auto-regressive Processes for the Simulation of Glacier Mass Balance Records Using GCMs

In order to be able to quantify natural variations in glacier length with high statistical significance, long records of mass balance are required to force a dynamic ice flow model such as that used in this study (section 5.4). Due to the long response times of the investigated glaciers (about 60-70 years, see section 5.4), mass balance time series in the order of thousands of years would be most suitable. However, the output of current coupled GCMs is naturally limited owing to high computational costs. For example, the ECHAM4/OPYC coupled GCM experiment used in this study has been integrated for 300 years, and we use 600 years from the ECHAM4/MLO mixed-layer GCM.

Owing to these limitations, in this study, we apply a method to generate 10000 year records of mass balance from temporally limited GCM integrations using auto-regressive (AR) processes.

---

### 5.3.1 General Method

An auto-regressive process  $X_t$  of the order  $p$ , i.e. an AR( $p$ ) process, is generally defined as

$$X_t = \alpha_0 + \sum_{k=1}^p \alpha_k X_{t-k} + Z_t$$

where  $\alpha_0, \alpha_1, \dots, \alpha_p$  are constants,  $\alpha_p \neq 0$ , and  $Z_t$  is a white noise process. The name “auto-regressive” indicates that the process evolves by regressing past values towards the mean (with a “strength” determined by the auto-regressive parameters  $\alpha_k$ ) and then adding noise [von Storch and Zwiers, 1999].

Our intention is now to fit an AR process of the above type to the mass balance time series simulated from GCM output (section 5.2) and to generate a new mass balance time series of the desired length with similar properties. This is done using the following approach:

1. Calculation of the autocorrelation function of the original time series.
2. Fitting of an AR model to the time series, i.e. estimation of the auto-regressive parameters  $\alpha_k$  (an iterative nonlinear least-squares procedure incorporating backforecasting is used [Box and Jenkins, 1976]).
3. Generation of a new time series with a similar autocorrelation function and standard deviation as the original.

This procedure is applied to the mass balance records for Nigardsbreen and Rhonegletscher using both the coupled and the mixed-layer GCM integrations.

### 5.3.2 AR Processes Applied to Nigardsbreen and Rhonegletscher

The spectra of glacier mass balance as simulated by the GCM experiments are shown in Figure 2. Thin solid lines denote the spectra of equivalent red noise processes and dashed lines represent the 95% confidence levels for accepting the red noise null hypothesis. We generate 10000 year records of mass balance for the two glaciers with comparable frequency contents and similar standard deviations as the original time series. Table 1 shows that the differences between the autocorrelation coefficients of the original and the generated (shown in brackets) mass balance records are very small.

## Simulated Glacier Mass Balance Spectra Downscaled GCM Control Runs Excluding External Forcing

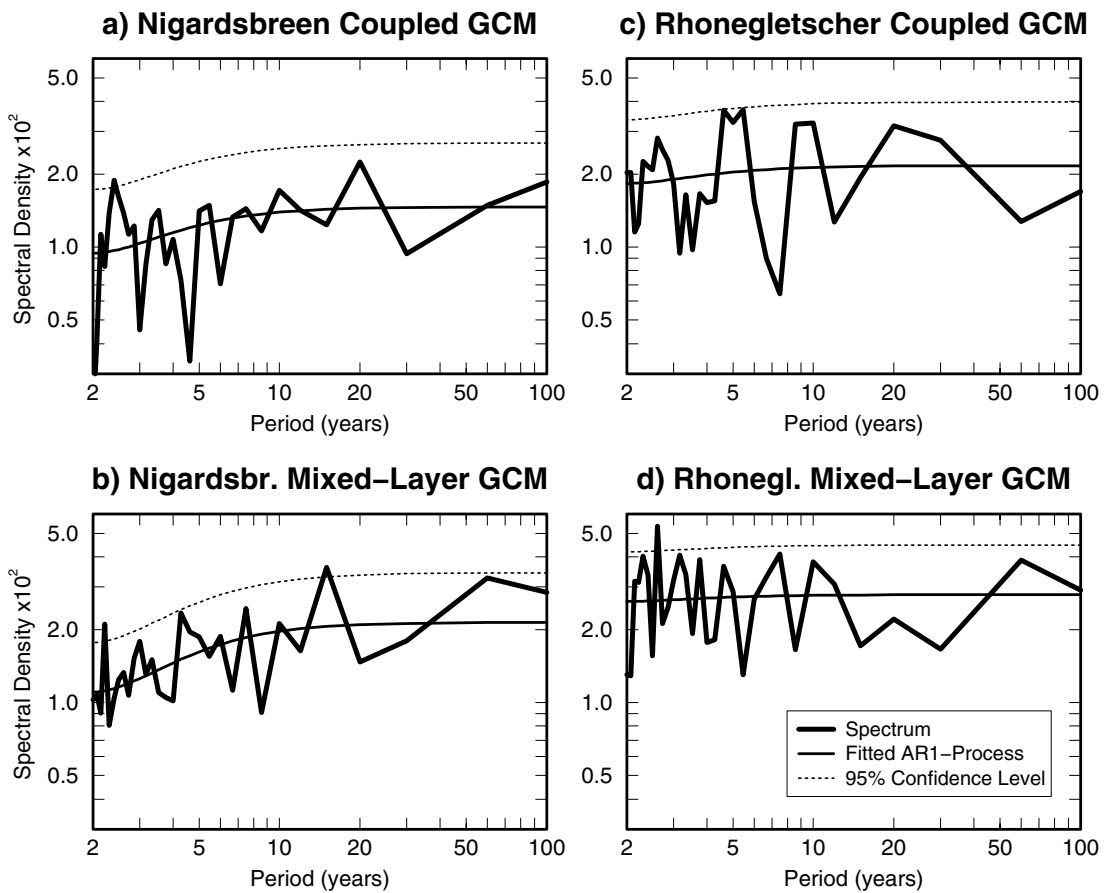


**Figure 2.** Spectra of glacier mass balance records for (a, b) Nigardsbreen and (c, d) Rhonegletscher as simulated by the coupled and the mixed-layer GCM experiments. Thin solid lines denote the spectra of equivalent red noise processes and dashed lines represent the 95% confidence levels for accepting the red noise null hypothesis.

For Nigardsbreen, the mass balance spectrum of the mixed-layer GCM experiment (Figure 2b) essentially shows red noise characteristics. This is also suggested by the autocorrelation coefficients (Table 1), the lag-1 coefficient is 0.16, the lag-2 and lag-3 coefficients (0.05 and 0.03 respectively) are small. For the coupled GCM integration (Figure 2a), the lag-2 and lag-3 coefficients are similar to lag-1 (0.11, Table 1) and play a considerable role in the spectral content of the time series. For the generation of the 10000 year mass balance record, we therefore improve the low frequency spectral content compared to the original time series by choosing an AR(3) instead of an AR(1) process. The corresponding auto-regressive parameters

$\alpha_1$ ,  $\alpha_2$ , and  $\alpha_3$  as estimated by the AR model using the iterative nonlinear least-squares procedure are shown in Table 1. An even higher order AR process is not required, we find that it does not significantly improve the fit of the model any further.

Although the autocorrelation coefficients are generally relatively small (less than 0.2), the strengthening of lower frequencies in the mass balance spectrum compared to a white noise process does have a considerable impact on the variability of glacier length fluctuations as will be demonstrated in section 5.5. A simple white noise process does not represent the mass balance spectrum of Nigardsbreen as simulated by the GCM and would consequently also underestimate low frequency glacier length fluctuations.

For Rhonegletscher, the redness of the spectra for both GCM integrations (Figure 2c, 2d) is much less pronounced than for Nigardsbreen. The spectrum for the mixed-layer GCM, particularly (Figure 2d), is almost white (the lag-1 coefficient is 0.02, Table 1). We can therefore expect a very small impact on low frequency glacier length fluctuations when using the generated time series instead of simply white noise. This will also be demonstrated in section 5.5.

**Table 1.** Autocorrelation Coefficients of Original GCM and of Generated 10000 Year Mass Balance Records (in brackets);  $\alpha_1, \dots, \alpha_3$  are the estimated AR parameters

|                                    | Autocorrelation Coefficients    |   |                                    |
|------------------------------------|---------------------------------|---|------------------------------------|
|                                    | Original, (Generated*)          | AR Parameters $\alpha_1, \dots, \alpha_3$ |                                    |
|                                    | lag-1                           | lag-2                                     | lag-3                              |
| Nigardsbreen,<br>Coupled GCM       | 0.11 (0.12)<br>$\alpha_1=0.091$ | 0.11 (0.12)<br>$\alpha_2=0.089$           | 0.11 (0.11)<br>$\alpha_3=0.092$    |
| Nigardsbreen,<br>Mixed-Layer GCM   | 0.16 (0.17)<br>$\alpha_1=0.160$ | 0.05 (0.06)<br>$\alpha_2=0.024$           | 0.03 (0.02)<br>$\alpha_3=0.014$    |
| Rhonegletscher,<br>Coupled GCM     | 0.04 (0.04)<br>$\alpha_1=0.044$ | 0.00 (0.00)<br>$\alpha_2=-0.004$          | 0.01 (0.00)<br>$\alpha_3=0.010$    |
| Rhonegletscher,<br>Mixed-Layer GCM | 0.02 (0.01)<br>$\alpha_1=0.016$ | -0.04 (-0.05)<br>$\alpha_2=-0.042$        | -0.01 (-0.02)<br>$\alpha_3=-0.013$ |

\*10000 year mass balance records are generated using a third order AR process determined by the parameters  $\alpha_1$ ,  $\alpha_2$ , and  $\alpha_3$  estimated by the AR model.

---

### 5.4 The Ice Flow Model

In order to be able to compare long records of historic glacier fluctuations to modeling studies, a dynamic ice flow model is required. This model calculates the response of glacier geometry (including the position of the glacier front which is usually captured in historic records) to changes in specific mass balance. In the following, a brief description of the ice flow model used in this study [Oerlemans, 1997] is presented.

The prognostic equation of the ice flow model is a continuity equation describing conservation of ice volume:

$$\frac{\partial S}{\partial t} = -\frac{\partial(US)}{\partial x} + \omega B$$

Here,  $x$  is the coordinate along the flowline of the glacier,  $U$  is the vertical mean ice velocity,  $S$  is the area of a cross-section through the glacier perpendicular to the flowline (parameterized by a trapezoidal cross-section),  $B$  is the mass balance, and  $\omega$  is the glacier width at the surface.

Both simple shearing flow and sliding are considered in the model. The vertical mean ice velocity  $U$  is determined by the local “driving stress”  $\tau$  which is proportional to ice thickness  $H$  and surface slope  $\partial h/\partial x$  ( $h$  is surface elevation). After rearrangement of equations [see Oerlemans, 1997] it follows that ice thickness  $H$  is governed by a non-linear diffusion equation which has to be solved by the ice flow model:

$$\frac{\partial H}{\partial t} = \frac{-1}{\omega_0 + \lambda H} \frac{\partial}{\partial x} \left[ D \frac{\partial(b+H)}{\partial x} \right] + B$$

Here,  $H$  is the ice thickness,  $b$  and  $\omega_0$  are the elevation and the width of the bed of the glacier respectively.  $\lambda$  is determined by  $(\omega - \omega_0)/H$ . The diffusivity  $D$  can be expressed as:

$$D = \left( \omega_0 + \frac{\lambda}{2} H \right) \left[ f_d \gamma H^5 \left( \frac{\partial h}{\partial x} \right)^2 + f_s \gamma H^3 \left( \frac{\partial h}{\partial x} \right)^2 \right]$$

with  $h$  as surface elevation,  $f_d$  and  $f_s$  as generalized viscosities referring to deformation and sliding respectively, and  $\gamma$  determined by  $(\rho g)^3$  with ice density  $\rho$  and acceleration due to gravity  $g$ .

---

The equations are solved using standard numerical methods for parabolic equations. Ice thickness, ice velocity, ice volume, and glacier length  $L$  are obtained.

If a climatic state is changed stepwise from a state with equilibrium glacier length  $L_1$  to a state with equilibrium glacier length  $L_2$ , the (*e-folding*) *response time for glacier length*  $t_{rL}$  is defined as the time the glacier needs to reach glacier length  $L_2 - (L_2 - L_1)/e$ . Using the above model, the response time of Nigardsbreen to a stepwise change ( $\delta B = \pm 0.4$  m water equivalent; [Oerlemans, 1997]) in the annual mass balance is 68 years, for Rhonegletscher it is 61 years.

### 5.5 Simulation of Glacier Length Fluctuations Using GCMs

We apply the dynamic ice flow model for Nigardsbreen and Rhonegletscher to the generated 10000 year mass balance records using AR processes from the coupled and mixed-layer GCMs (Figure 3). The simulated glacier length records are exclusively due to internal variations in the climate and glacier system since external forcings have been excluded in the GCM integrations (section 5.2). We have simulated three individual 10000 year glacier length records for each glacier and each GCM experiment in order to investigate

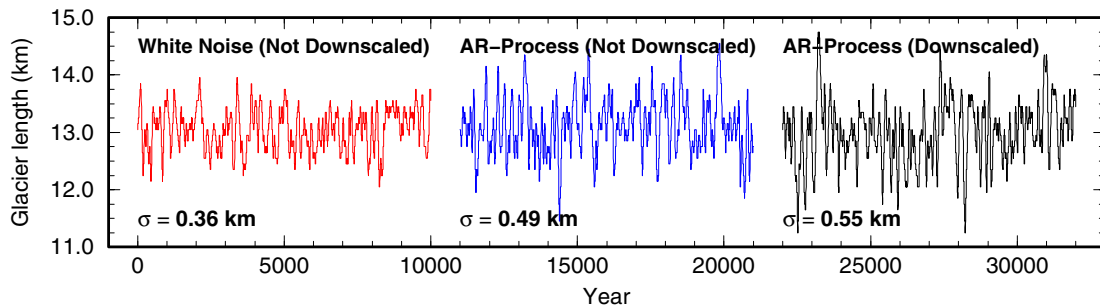
- a) the impact of using the AR-process determined by GCM output instead of simply using white noise, and
- b) the influence of using the statistically downscaled GCM integrations instead of simply interpolating GCM grid point output to the location of the glaciers.

The results are presented in Figure 3. The first glacier length record in each experiment (marked as “White Noise (Not Downscaled)” in the left part of each graph in Figure 3a-3d) is simulated by simply using gaussian white noise as mass balance forcing, with a standard deviation obtained from directly interpolated GCM grid point output without statistical downscaling. This means that the record represents glacier fluctuations that could be expected if neither the spectral content of GCM output nor downscaling played any role. The second record in each experiment (marked as “AR-Process (Not Downscaled)”); Figure 3) demonstrates the impact of using a third order AR-process accounting for the spectral content of the GCM integrations. The standard deviations of the mass balance forcing records are similar to the first record, statistical downscaling is not applied. The third record (“AR-Process (Downscaled)”); Figure 3) additionally considers the impact of statistical downscaling and we therefore consider it as the most realistic representation of glacier fluctuations simulated in this study.

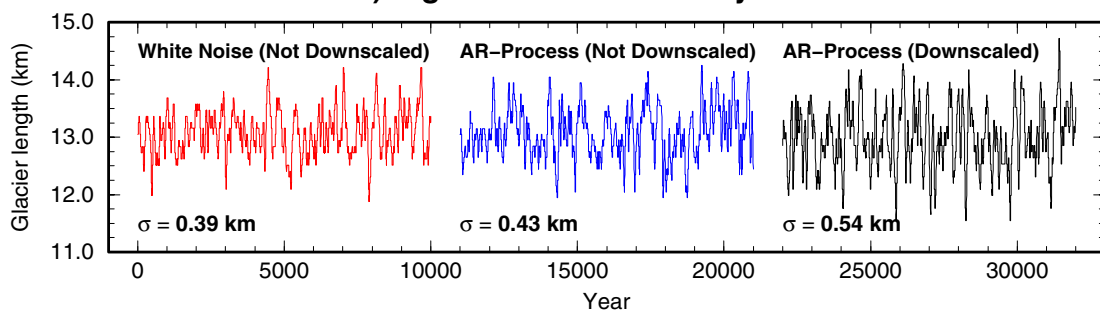
---

### Simulation of Glacier Length Using GCM Output

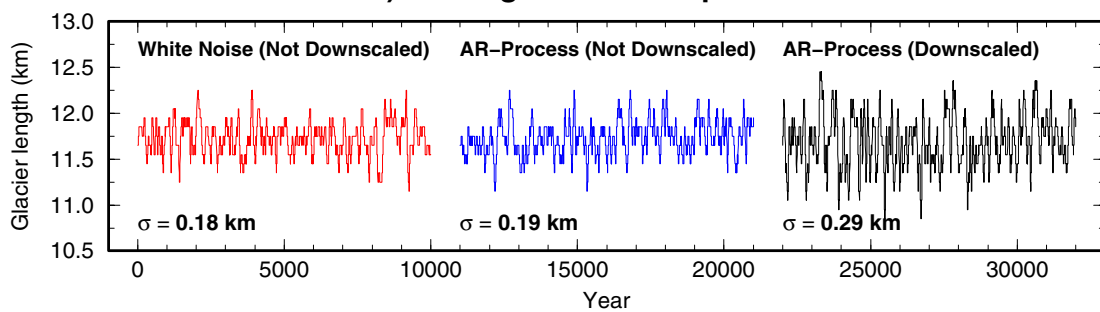
#### a) Nigardsbreen Coupled GCM



#### b) Nigardsbreen Mixed-Layer GCM



#### c) Rhonegletscher Coupled GCM



#### d) Rhonegletscher Mixed-Layer GCM

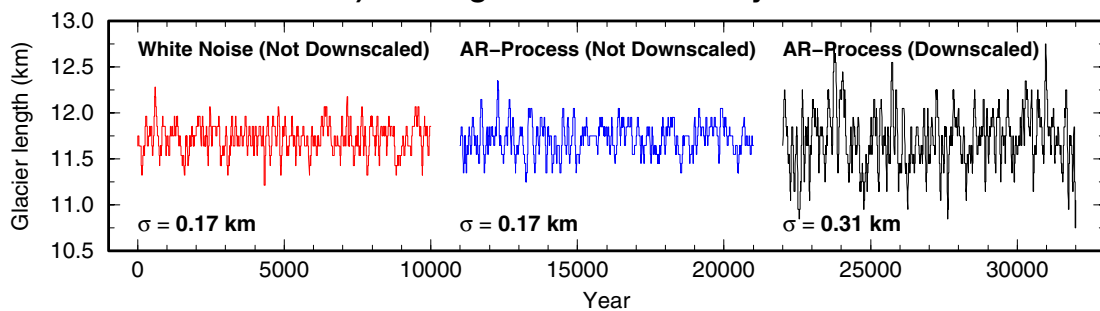


**Figure 3.** 10000 year records of simulated glacier length fluctuations for (a, b) Nigardsbreen and (c, d) Rhonegletscher. The figure demonstrates the individual impact of both statistical downscaling and using AR-processes determined by GCM output instead of simply using white noise with the same variance. Standard deviations  $\sigma$  of glacier length are shown below each record.

The standard deviations  $\sigma$  of glacier length fluctuations for each experiment are shown below each record. For Nigardsbreen, using a third order AR-process determined from the coupled GCM experiment instead of a white noise process (Figure 3a) increases the variability in glacier fluctuations by 36% (standard deviations increase from 0.36 km to 0.49 km). This emphasizes the high impact of the AR-process (see Table 1 for AR parameters) for the generation of low-frequency glacier fluctuations. Statistical downscaling additionally increases the variability by another 12% (from 0.49 km to 0.55 km). For the mixed-layer GCM (Figure 3b), the variability in glacier fluctuations using the AR-process including downscaling is similar to the coupled GCM (0.54 km), the individual impact of the AR-process is however smaller (10%). This is due to the fact that, in contrast to the coupled GCM experiment, the lag-2 and lag-3 autocorrelation coefficients are reasonably small (section 5.3, Table 1), and they consequently hardly contribute to low frequency fluctuations.

As could be expected from the almost white mass balance spectra of Rhonegletscher (Figures 2c and 2d), the influence of the AR-process for glacier length of this glacier is marginal (Figures 3c and 3d). However, due to the local setting of this glacier, the impact of downscaling is high, glacier length variability is increased by about 50% (from 0.19 km to 0.29 km; Figure 3c) for the coupled GCM. The impact is even higher for the mixed-layer GCM (from 0.17 km to 0.31 km; Figure 3d). This shows the substantial influence of statistical downscaling in this region of the Alps. With respect to local observational data, the direct coarse grid point output of a GCM would have underestimated the local climatic variability responsible for glacier fluctuations of Rhonegletscher.

## **5.6 Comparison with Observed Glacier Fluctuations and Statistical Analysis**

Simulated glacier fluctuations will now be compared to observed historical glacier length records for Nigardsbreen and Rhonegletscher. This will enable us to investigate whether preindustrial glacier fluctuations on one hand and the present-day retreat of the glaciers on the other hand can be explained by internal variations in the climate system as simulated by a GCM.

### **5.6.1 Historical Records of Glacier Length Fluctuations**

Observed or reconstructed glacier length variations for the two glaciers are shown in Figure 4. Various historic documents, terminal moraines, photogrammetric methods,

---

and distance measurements have been combined to obtain this record [Hoelzle and Haeberli, 1999].

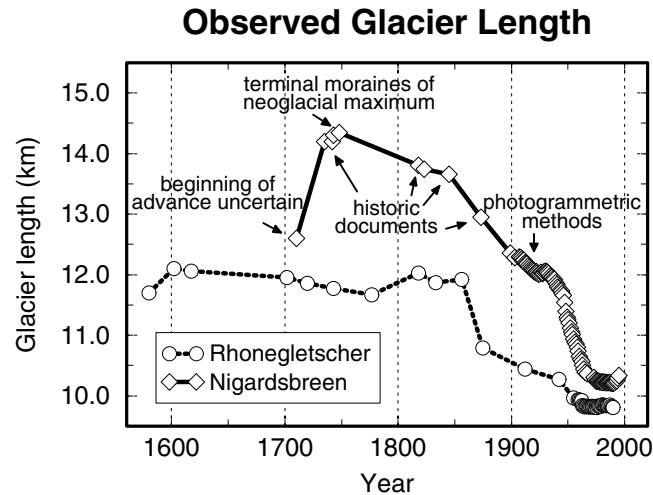


**Figure 4.** Observed (or reconstructed) length variations of Nigardsbreen (solid line; diamonds are data points) and Rhonegletscher (dotted line; circles are data points). Data from Hoelzle and Haeberli [1999].

During the first half of the 18<sup>th</sup> century, Nigardsbreen advanced rapidly (the time of the beginning of the advance is uncertain) and reached a neoglacial maximum in 1748. Since then, a steady retreat has been observed until about 1990 which thereafter came to an end (Figure 4). The retreat of the glacier until 1900 will in the following be noted as “Little Ice Age to 1900 retreat” and can be found to be about 2 km for Nigardsbreen. The retreat until 1990 will be called “Little Ice Age to present-day retreat” and is about 4 km.

Rhonegletscher advanced at the beginning of the records until 1602, followed by a period in which the length of the glacier remained within a range of 11.6-12.1 km until 1860. This time then marks the beginning of a rapid retreat. The “Little Ice Age to 1900 retreat” of the glacier, considering its maximum in 1602, is roughly 1.5 km, the “Little Ice Age to present-day retreat” is about 2.3 km.

### 5.6.2 Statistical Analysis of Simulated Glacier Fluctuations

Figure 5 shows the first 2000 years of the simulated 10000 year glacier length records along with the observations for Nigardsbreen (Figure 5a) and Rhonegletscher (Figure 5b). We concentrate on the results from the coupled GCM experiment using AR-processes including downscaling (Figure 3a, 3c) since we consider them to be

the most realistic simulation of glacier fluctuations in this study. The simulated records show substantial changes in glacier length lasting for decades or even several centuries. It is nevertheless evident that the “Little Ice Age to present-day retreat” of the glaciers exceeds the amplitude of any simulated glacier fluctuation in the records. In the following, this will be analyzed in more detail.

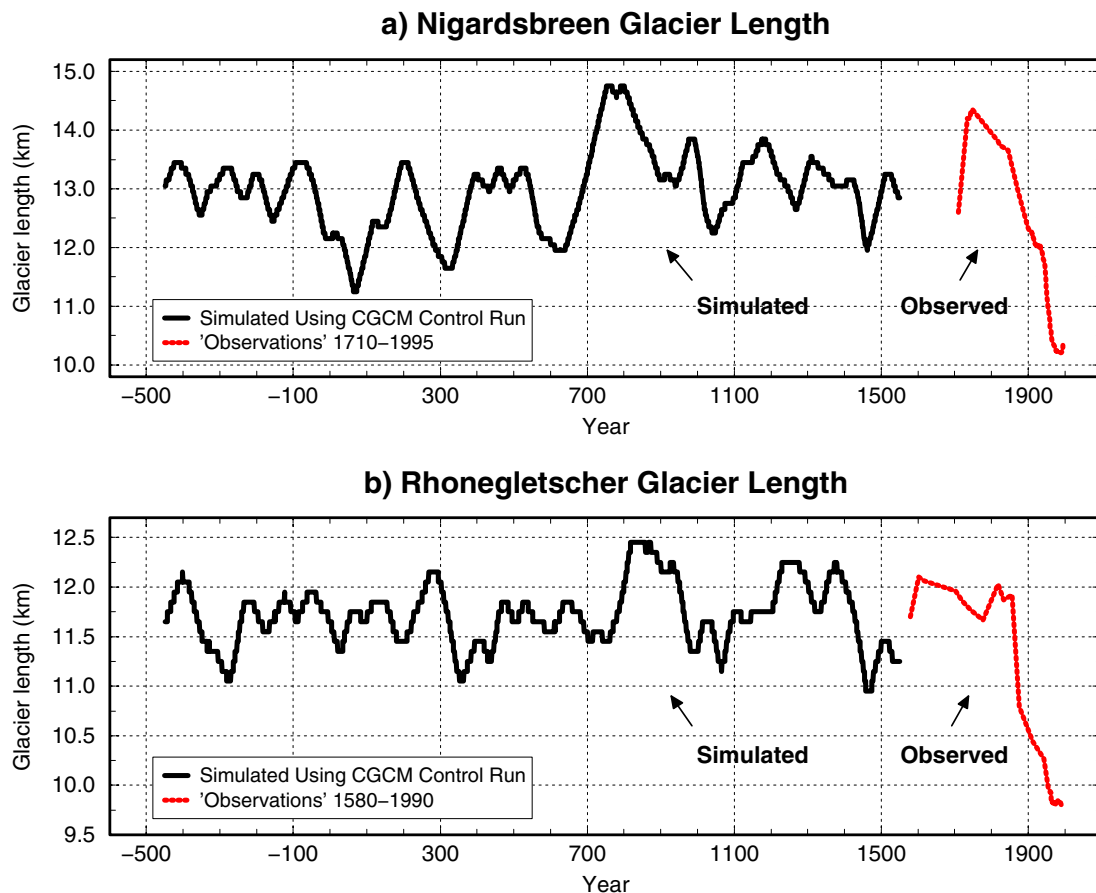


**Figure 5.** Observed and simulated glacier fluctuations for (a) Nigardsbreen and (b) Rhonegletscher. The first 2000 years of simulated glacier length fluctuations exclusively due to internal variations in the climate system are shown (solid lines) using AR-processes from downscaled coupled GCM output.

Figure 6 shows the distribution of glacier fluctuations for the complete 10000 year records. Glacier length changes are calculated as the difference between a local extreme value and the following extreme value, and the number of these “events” is plotted for a bin width of 0.2 km.

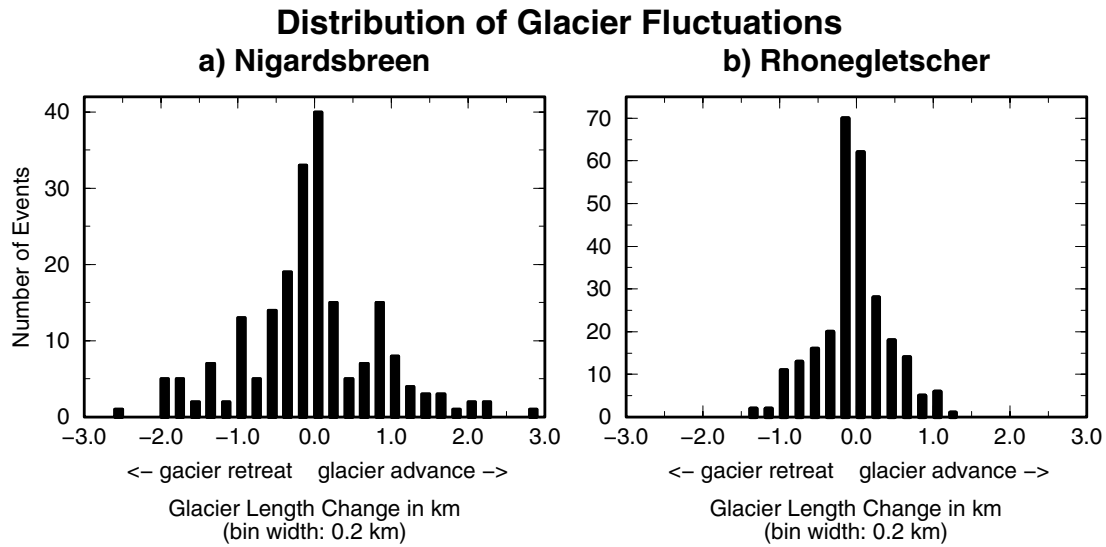


**Figure 6.** Histogram of simulated glacier fluctuations using downscaled coupled GCM integrations. The number of ‘events’ represents specific changes in glacier length in the 10000 year records and is plotted for a bin width of 0.2 km. Negative (positive) values indicate glacier retreat (advance).

The distribution is essentially symmetric with respect to negative and positive glacier length changes, retreat and advance are equally frequent. The maximum change in glacier length over the complete simulated 10000 year records is an advance of 2.8 km for Nigardsbreen lasting for about 200 years (see Figure 5a; around year 700). For Rhonegletscher, the maximum change is a retreat of 1.3 km lasting for more than 100 years (see Figure 5b; around year 1400). Figure 7 shows the corresponding recurrence relationships, the cumulative number of events  $N$  is plotted against glacier length changes  $\Delta L$ , regardless of whether the glacier retreats or advances. The relationships can be well approximated by exponential regression, the recurrence relationships may then be expressed as

$$\begin{aligned} \log N &= -1.95 \Delta L + 5.67 && \text{(Nigardsbreen) and} \\ \log N &= -3.48 \Delta L + 5.78 && \text{(Rhonegletscher).} \end{aligned}$$

The largest simulated glacier length fluctuations ( $\Delta L > 2.5$  km for Nigardsbreen and  $\Delta L > 1.1$  km for Rhonegletscher; Figure 7) fit less well with the regression compared to smaller fluctuations. This can be expected since they occur only a few times within the 10000 year records leading to a sampling problem.

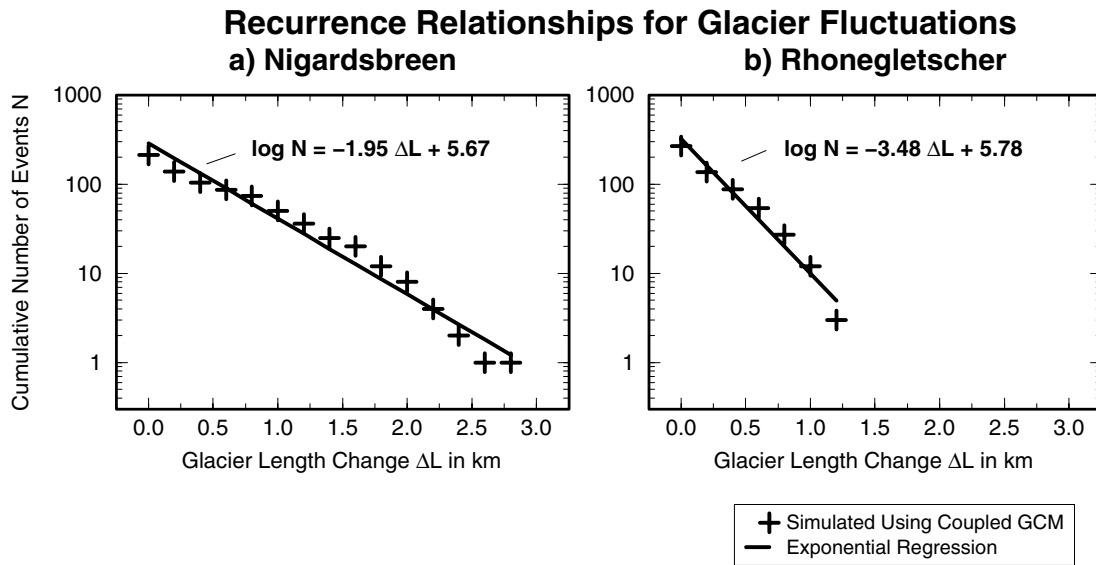


**Figure 7.** Recurrence relationships showing the cumulative number of glacier fluctuation ‘events’  $N$  for a minimum glacier length change  $\Delta L$ . The relationships are approximated by exponential regression.

### 5.6.3 Return Periods of Specific Glacier Length Changes

On the basis of the above established recurrence relationships, we determine return periods  $\alpha$  for the occurrence of specific glacier fluctuations due to internal climate variations as simulated using the coupled GCM integrations (Table 2):

$$\alpha(\Delta L) = \frac{T_{sim}}{N(\Delta L)} = \frac{T_{sim}}{e^{b \cdot \Delta L + a}} = (T_{sim} e^{-a}) \cdot e^{-b \cdot \Delta L}$$

Here,  $T_{sim}$  is the simulated time period (10000 years in our experiments),  $a$  and  $b$  are the glacier specific regression parameters in the recurrence relationships (Nigardsbreen:  $a = 5.67$ ,  $b = -1.95$ ; Rhonegletscher:  $a = 5.78$ ,  $b = -3.48$ ; see above).

Table 2 shows that glacier fluctuations of at least 1 km can roughly be expected to occur every 250 years for Nigardsbreen and every 1000 years for Rhonegletscher. The observed ‘‘Little Ice Age to 1900 retreat’’ of 2 km for Nigardsbreen can be expected with a return period of about 1700 years exclusively due to internal climate fluctuations. For extreme glacier length fluctuations of 3 km we find return period of about 12000 years. For Rhonegletscher, the ‘‘Little Ice Age to 1900’’ retreat of 1.5 km is expected to occur every 5700 years. An extreme change of 2 km length has not been simulated for this glacier in the 10000 year record. However, we can expect

it to occur in a longer integration with a return period of about 33000 years. Figure 8 is a graphical representation of return periods.

**Table 2.** Return Periods of Specific Glacier Length Fluctuations

| Length Change          | Nigardsbreen (years) | Rhonegletscher (years) |
|------------------------|----------------------|------------------------|
| $\Delta L \geq 0.5$ km | 92                   | 176                    |
| $\Delta L \geq 1.0$ km | 243                  | 1004                   |
| $\Delta L \geq 1.5$ km | 644                  | 5732                   |
| $\Delta L \geq 2.0$ km | 1710                 | 32732                  |
| $\Delta L \geq 2.5$ km | 4537                 | (186921)               |
| $\Delta L \geq 3.0$ km | 12039                | (1067440)              |

Return periods in brackets are theoretical estimates only, extending the recurrence relationships considerably beyond glacier fluctuations that actually occurred in the simulated 10000 year records.

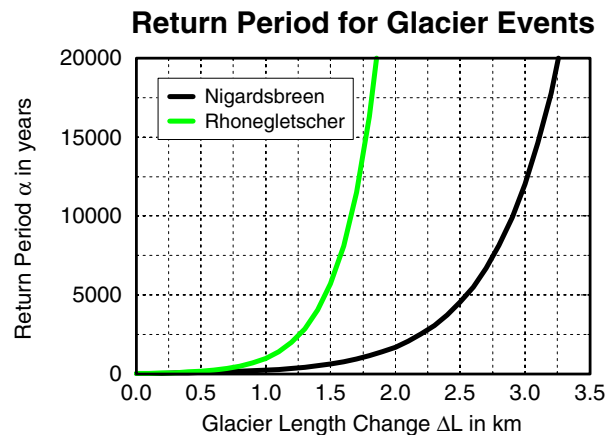


**Figure 8.** Graphical illustration of return period  $\alpha$  in years for glacier ‘events’ representing glacier length changes  $\geq \Delta L$  for Nigardsbreen (solid line) and Rhonegletscher (shaded line).

#### 5.6.4 Probability of Simulating Observed Preindustrial Glacier Length Changes and Present-day Glacier Retreat

We now calculate probabilities for specific glacier fluctuations within a given time interval assuming that their occurrence generally follows a Poisson-process (events occur independently at random instants of time and at a constant mean rate per time

interval [Priestley, 1981]). This approach also accounts for the fact that extreme glacier length changes which might not have been simulated in the 10000 year record, still have a certain (although small) statistical probability of occurrence, and they might occur in a much longer simulated record. The probability  $P$  for the occurrence of a glacier length change  $\Delta L$  (represented by its return period  $\alpha$ ) within a time interval  $T$  can be expressed as

$$P(T, \alpha) = 1 - e^{-T/\alpha}$$

Substituting return period  $\alpha$  with the definition in section 5.6.3, we may write

$$P(T, \Delta L) = 1 - \exp\left(-\frac{T}{T_{sim}} \cdot e^{b \cdot \Delta L + a}\right)$$

$T_{sim}$  is the length of simulated records,  $a$  and  $b$  are the regression parameters obtained from the recurrence relationships. The  $P(T, \Delta L)$  relations for both Nigardsbreen and Rhonegletscher are illustrated in Figure 9. We show probabilities of occurrence  $P$  for glacier fluctuations  $\Delta L$  within investigated time periods of  $T = 100$ ,  $T = 500$ ,  $T = 2000$ , and  $T = 10000$  years.

For Nigardsbreen (Figure 9a), the probability that observed preindustrial glacier length changes of 2 km (“Little Ice Age to 1900 retreat”, see Figure 4) occur within a time period of  $T = 10000$  years exclusively due to internal climate variations is  $P = 99.7\%$  (Figure 9a, solid line). This is naturally a consequence of the fact that these glacier fluctuations actually frequently occur in the simulated record (see Figure 6). On the other hand, the observed “Little Ice Age to present-day retreat” of 4 km (see Figure 4) has not been simulated, the probability of occurrence is correspondingly small ( $P = 11.1\%$ ). When looking at a time period of  $T = 2000$  years only (Figure 9a, shaded line), the probability of occurrence for preindustrial glacier fluctuations is still 69%, whereas the probability for the present-day retreat drops to 2.3%.

For Rhonegletscher (Figure 9b), the probability of preindustrial glacier length changes within a 10000 year interval (solid line) is 80.4%, for the present-day retreat it is 9.9%. This means that the situation here is generally comparable to Nigardsbreen, preindustrial fluctuations are likely to occur in the simulated records whereas the present-day retreat can hardly be explained by internal climate variations. A time period of  $T = 2000$  years (Figure 9b, shaded line) is however too short to draw firm conclusions, the probabilities are 30.2% and 2.2% respectively.

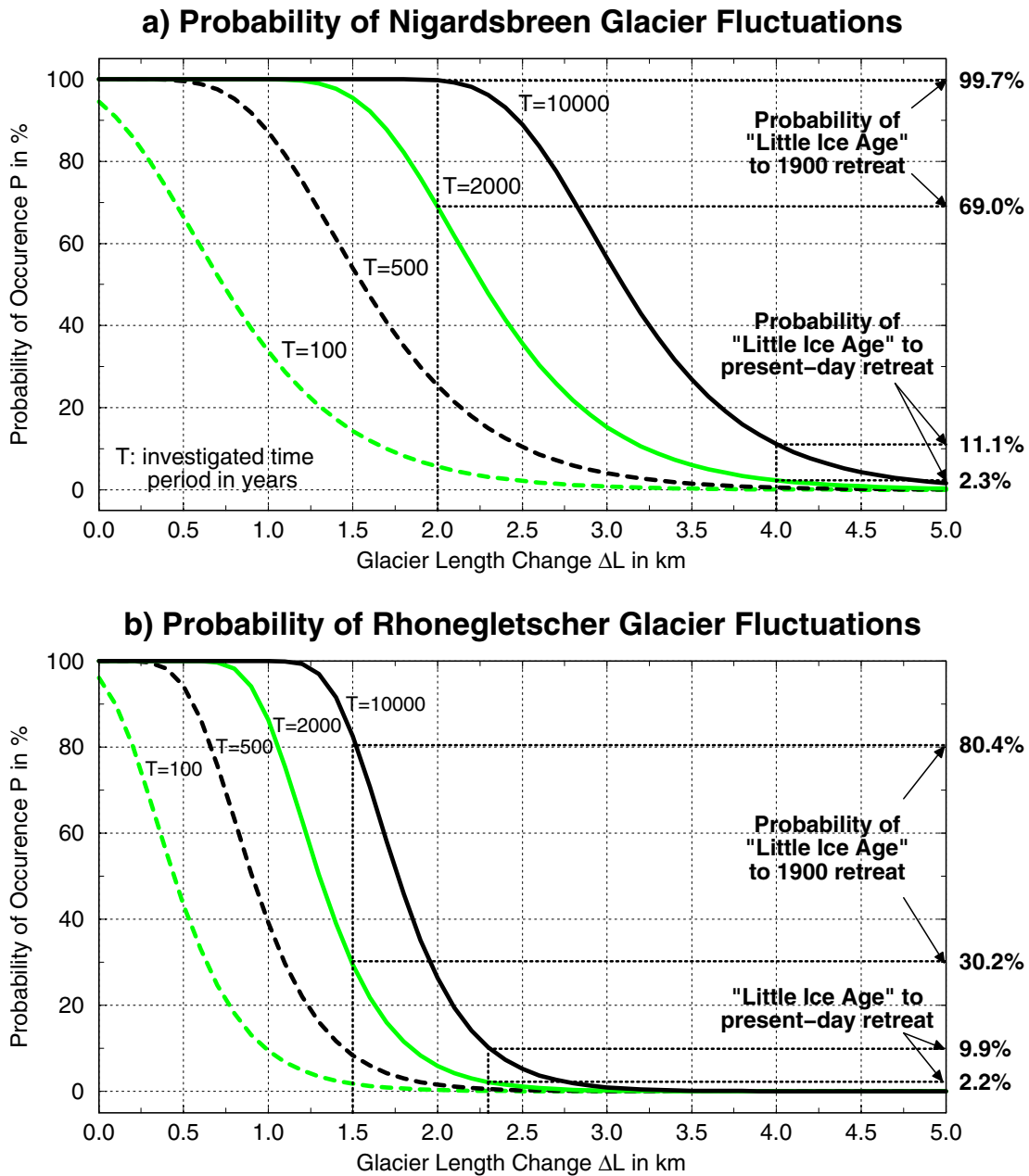


**Figure 9.** Probabilities  $P$  for the occurrence of simulated glacier length changes  $\Delta L$  within a time period of investigation  $T$ , exclusively due to internal climate variations as simulated using the coupled GCM. For Nigardsbreen (a), the probability that observed preindustrial glacier length changes of 2 km ("Little Ice Age to 1900 retreat") occur within a time period of 10000 years is 99.7%, whereas the present-day retreat is unlikely to be explained by internal variability ( $P = 11.1\%$ ). For Rhonegletscher (b), the probabilities are 80.4% and 9.9% respectively.

In this section, we demonstrated that preindustrial fluctuations of the glaciers as far as observed or reconstructed can be explained by internal variations in the climate system as simulated using coupled GCM output. It is however very unlikely that the present-day glacier retreat is entirely due to internal climate variability.

## 5.7 Conclusions

In this study, we have applied a process-based modeling approach for the simulation of glacier fluctuations exclusively due to internal variations in the climate system using GCM experiments. We have simulated 10000 year records of glacier length fluctuations using auto-regressive processes determined by downscaled coupled and mixed-layer GCM output. We have used a mass balance model of intermediate complexity and a dynamic ice flow model for Nigardsbreen (Norway) and Rhonegletscher (Swiss Alps).

For both glaciers, it has been found that local downscaling has a considerable impact on glacier fluctuations, the variability in glacier length is substantially increased compared to simply using direct GCM grid point output. For Nigardsbreen, we have found a high impact when using auto-regressive processes determined by GCM integrations instead of white noise mass balance forcing. The variability of simulated glacier fluctuations using the mixed-layer GCM is comparable to that of the coupled GCM.

Simulated glacier fluctuations have been statistically analyzed in order to compare them to observed historical glacier length records. Relationships between simulated glacier length changes and their frequency of occurrence have been approximated by exponential regression. On the basis of the established recurrence relationships, return periods of specific glacier fluctuation events have been determined. The observed retreat of Nigardsbreen of about 2 km since its “Little Ice Age maximum” until 1900, can be expected to occur with a return period of 1700 years exclusively due to internal climate fluctuations as simulated by the coupled GCM experiment. For Rhonegletscher, the observed “Little Ice Age to 1900 retreat” of about 1.5 km can be expected with a return period of about 5700 years due to internal variability.

Probabilities for specific glacier fluctuations within a given time interval have been calculated, assuming that their occurrence follows a Poisson-process. Probabilities that “preindustrial” glacier fluctuations as the “Little Ice Age to 1900 retreat” occur within a time period of 10000 years are 99.7% for Nigardsbreen and 80.4% for Rhonegletscher. On the other hand, the observed “Little Ice Age to present-day

---

retreat” of the glaciers (4 km for Nigardsbreen and 2.3 km for Rhonegletscher) has not been simulated in the experiments and is therefore very unlikely to be explained by internal variations in the climate system. The probabilities of occurrence for these events are 11.1% and 9.9% respectively.

We conclude that preindustrial glacier fluctuations as far as observed or reconstructed can be explained by internal variations in the climate system as simulated using GCM experiments. It is however very unlikely that the present-day glacier retreat is entirely due to internal climate variability. The results imply that this retreat is due to external forcing, greenhouse gas forcing is a potential candidate which will have to be investigated in additional future experiments.

---

---

**References**

- Bengtsson, L., Uncertainties of global climate prediction, *Proc. of the Symposium on Global Biogeochemical Cycles in the Climate System, September 22-27, 1998*, Max-Planck-Inst. für Biogeochem., Jena, Germany, in press, 1999.
- Box, G. E. P., and G. M. Jenkins (Eds.), *Time series analysis: forecasting and control*, Holden-Day, San Francisco, 1976.
- Cubasch, U. R., R. Voss, G. C. Hegerl, J. Waszkewitz, and T. J. Crowley, Simulation of the influence of solar radiation variations on the global climate with an ocean-atmosphere general circulation model, *Clim. Dyn.*, *13*, 757-767, 1997.
- Gibson, J. K., P. Kållberg, S. Uppala, A. Nomura, A. Hernandez, and E. Serrano, ERA Description, *ECMWF Re-Anal. Proj. Rep. Ser., Rep. 1*, Eur. Cent. for Medium-Range Weather Forecasts, Reading, England, 1997.
- Grove, J. M. (Ed.), *The Little Ice Age*, Methuen, London, 1988.
- Hansen, J., I. Fung, R. Ruedy, and M. Sato, Potential climate impact of Mount Pinatubo eruption, *Geophys. Res. Lett.*, *19*, 215-218, 1992.
- Hasselmann, K., Stochastic Climate Models I: Theory, *Tellus*, *28*, 473-485, 1976.
- Hoelzle, M., and W. Haeberli, World glacier monitoring service, world glacier inventory, digital data available from the *National Snow and Ice Data Center*, nsidc@kryos.colorado.edu, Univ. of Colorado, Boulder, Colorado, 1999.
- Hoyt, D. V., and K. H. Schatten, A discussion of plausible solar irradiance variations 1700-1992, *J. Geophys. Res.*, *98*, 18895-18906, 1993.
- Lean, J., J. Beer, and R. S. Bradley, Reconstruction of solar irradiance since 1610: Implications for climate change, *Geophys. Res. Letters*, *22*, 3195-3198, 1995.
- Lindzen, R. S., and C. Giannitsis, On the climatic implications of volcanic cooling, *J. Geophys. Res.*, *103*, 5929-5941, 1998.
- Mikolajewicz, U. and E. Maier-Reimer, Internal secular variability in an ocean general circulation model, *Clim. Dyn.*, *4*, 145-156, 1990.
- Oerlemans, J., A flow-line model for Nigardsbreen: Projection of future glacier length based on dynamic calibration with the historic record, *Ann. Glaciol.*, *24*, 382-389, 1997.
- Oerlemans, J., and B. K. Reichert, Relating glacier mass balance to meteorological data using a seasonal sensitivity characteristic (SSC), *J. Glaciol.*, *46(152)*, in press, 2000.
-

- Paterson, W. S. B. (Ed.), *The Physics of Glaciers*, 3rd ed., Pergamon, New York, 1994.
- Priestley, M. B. (Ed.), *Spectral Analysis and Time Series*, Academic Press, San Diego, 1981.
- Reichert, B. K., L. Bengtsson, and O. Åkesson, A statistical modeling approach for the simulation of local paleoclimatic proxy records using general circulation model output, *J. Geophys. Res.*, *104*, 19071-19083, 1999.
- Reichert, B. K., L. Bengtsson, and J. Oerlemans, Midlatitude forcing mechanisms for glacier mass balance investigated using general circulation models, *Rep.*, Max-Planck-Inst. für Meteorol., Hamburg, Germany, 2000.
- Roeckner, E., L. Arpe, L. Bengtsson, M. Christoph, M. Claussen, L. Dümenil, M. Esch, M. Giorgetta, U. Schlese, and U. Schulzweida, The atmospheric general circulation model ECHAM-4: Model description and simulation of present-day climate, *Rep. 218*, Max-Planck-Inst. für Meteorol., Hamburg, Germany, 1996.
- Roeckner, E., Climate sensitivity experiments with the MPI/ECHAM4 model coupled to a slab ocean (abstract), in *Euroclivar Workshop on Cloud Feedbacks and Climate Change*, edited by C. A. Senior and J. F. B. Mitchell, pp. 20, Hadley Cent. for Clim. Predict. and Res., Bracknell, England, 1997.
- Roeckner, E., L. Bengtsson, J. Feichter, J. Lelieveld and H. Rodhe, Transient climate change simulations with a coupled atmosphere-ocean GCM including the tropospheric sulfur cycle, *J. Climate*, *12*, 3004-3032, 1999.
- Sarachik, E. S., M. Winton, and F. L. Yin, Mechanisms for decadal-to-centennial climate variability, in *Decadal climate variability*, eds. D. L. T. Anderson and J. Willebrand, *NATO ASI series, vol. 44*, Springer, Berlin, 1996.
- von Storch, H., and F. W. Zwiers (Eds.), *Statistical Analysis in Climate Research*, Cambridge Univ. Press, New York, 1999.
-

## 6 Conclusions and Perspectives

---

### 6.1 Conclusions

The aim of this thesis has been the investigation of a major source of natural climate variability as recorded in paleoclimatic proxy data: internal variations in the climate system. Their dominant impact recorded in preindustrial climatic proxy records has been demonstrated for glacier systems, using downscaled GCM integrations and a process-based modeling approach for the simulation of glacier fluctuations exclusively due to internal climate variability. Preindustrial fluctuations of the investigated glaciers can be explained by internal variations in the climate system, whereas the present-day glacier retreat must be due to external forcing.

In addition to the detailed conclusions provided at the end of each chapter, the results of this study are in the following summarized in order to answer the questions raised in the introduction (section 1.3):

- 1) *Can a statistical downscaling model be established which is appropriate for the simulation of local paleoclimatic proxy records using GCM integrations? In other words, can local output from a GCM be provided which can be used to force a process-based model for a specific proxy indicator? If so, which large-scale predictors from a GCM are most appropriate?*

A model-consistent and stable statistical downscaling approach for GCM output has been developed (Chapter 2) based on large-scale predictors obtained from daily ECMWF reanalyses and daily operational weather station data in the vicinity of the proxy site to be investigated. The method produced a good simulation of local temperature and precipitation for observed weather station data in Norway (section 2.5) and the Alps (section 4.2). Predominant large-scale predictors for the simulation of local temperature are large-scale temperature at 850 hPa, relative humidity at 850 hPa, and a predictor adapting the seasonal cycle of GCM output. For local precipitation, the composition of predictors is less homogeneous within the regions of investigation, however, vertical velocity at

850 hPa, wind velocity, and vorticity at various pressure levels generally have an important impact. The method has successfully been applied to ECHAM4 GCM experiments.

- 2) *Can fluctuations of specific valley glaciers (which represent proxy indicators for low frequency climate variations over several centuries) be simulated using downscaled GCM integrations? How can individual glacier mass balance be related to meteorological data or to downscaled GCM output?*

A method to relate glacier mass balance to meteorological data or to GCM output has been developed in Chapter 3. Climate sensitivities of specific valley glaciers have been quantified by Seasonal Sensitivity Characteristics (SSCs) based on a mass balance model of intermediate complexity. The SSCs represent the dependence of mass balance on monthly anomalies in temperature and precipitation. The sensitivity of Rhonegletscher (Swiss Alps) to changes in precipitation has been found to be almost constant throughout the year whereas for Nigardsbreen glacier (Norway), a change in summer precipitation (mainly falling as rain due to the lower elevation) has only a marginal effect. The sensitivity to changes in summer temperatures (when melting occurs) is higher for Nigardsbreen in comparison with Rhonegletscher, whereas a temperature change in winter has almost no effect on mass balance for both glaciers. It has been shown that simulations using ECMWF reanalyses for the period 1979-1993 are in good agreement with in situ mass balance measurements for Nigardsbreen. The downscaling methodology described above has been used in order to simulate mass balance fluctuations for Nigardsbreen and Rhonegletscher using multi-century coupled (ECHAM4/OPYC) and mixed-layer (ECHAM4/MLO) GCM experiments (Chapter 4).

- 3) *A process-based modeling approach for the simulation of glacier fluctuations, as developed in this study, allows the investigation of underlying forcing mechanisms in the climate system. What are the specific forcing mechanisms driving glacier mass balance changes of Nigardsbreen and Rhonegletscher? Are they connected to fluctuations in the North Atlantic Oscillation (NAO)? What is the individual impact of temperature and precipitation on glacier mass balance?*

For both glaciers, a high correlation between decadal variations in the North Atlantic Oscillation (NAO) and glacier mass balance has been found in the experiments (Chapter 4). The dominant factor for this relationship is the strong impact of winter precipitation associated with the NAO. In the coupled GCM experiment, the overall impact of precipitation changes on glacier mass balance

---

of Nigardsbreen (Rhongletscher) is 1.6 times (3 times) higher than the impact of temperature. A high phase of the NAO means enhanced winter precipitation for the region of Nigardsbreen, typically leading to a higher than normal positive mass balance over the year. For Rhongletscher, a high NAO phase typically means reduced winter precipitation leading to a lower than normal mass balance. This mechanism, entirely due to internal variations in the climate system, can also explain observed strong positive mass balances for Nigardsbreen and possibly other maritime Norwegian glaciers within the period 1980-1995, as a consequence of the corresponding high NAO phase within this period.

- 4) *Can the response of glacier geometry (including glacier length which is captured in historic records) be simulated for changes in specific mass balance, considering the dynamic ice flow of the glaciers? If so, can glacier length fluctuations be quantified which are exclusively due to internal variations in the climate system as simulated by a GCM?*

A dynamic ice flow model considering shearing flow and sliding has successfully been applied in order to simulate glacier fluctuations due to internal climate variations (Chapter 5) using the GCM integrations and SSCs as described above. 10000 year records of glacier length fluctuations using auto-regressive processes determined by the GCM experiments have been generated. The considerable impact of downscaling on the simulation of glacier fluctuations in comparison with simply using the direct coarse grid points of a GCM has been demonstrated. Return periods and probabilities for the occurrence of specific glacier length changes, simulated excluding external forcings such as solar irradiation changes, volcanic or anthropogenic effects have been calculated and compared to historical glacier length records.

- 5) *What are the forcing mechanisms responsible for preindustrial fluctuations of the glaciers as far as observed or reconstructed, including their advance during the “Little Ice Age”? Can these fluctuations be explained entirely by internal climate variability?*

On the basis of the experiments carried out in this study, we conclude that preindustrial fluctuations of the glaciers as far as observed or reconstructed, including their advance during the “Little Ice Age”, can be explained entirely by internal variations in the climate system as represented by a GCM. External forcing is not required. The calculated probabilities that these glacier fluctuations occur within a time period of 10000 years are 99.7% for Nigardsbreen and 80.4% for Rhongletscher.

---

- 6) *Is it likely that the observed present-day glacier retreat is entirely due to internal climate variability or is any external forcing required, such as, for example, greenhouse gas forcing?*

Fluctuations comparable to the observed present-day retreat of the glaciers (4 km for Nigardsbreen and 2.3 km for Rhonegletscher since the “Little Ice Age”) have not occurred in the experiments carried out in this study. This retreat is therefore very unlikely to be explained by internal variations in the climate system. The calculated probabilities of occurrence for such events are 11.1% (Nigardsbreen) and 9.9% (Rhonegletscher) within a time period of 10000 years. The results imply that the present-day retreat must be due to external forcing. Greenhouse gas forcing due to anthropogenic activities is a potential candidate, which has been investigated in additional experiments using transient GCM integrations (see below for perspectives).

The results of this thesis have demonstrated that a process-based approach for the simulation of paleoclimatic proxy records using GCMs is a valuable tool for the investigation of the mechanisms of preindustrial climate variability. This approach has enabled the interpretation of climate variability as indicated by glaciers and is also applicable to other paleoclimatic proxy indicators.

## **6.2 Perspectives**

Further experiments using transient integrations of the ECHAM4/OPYC coupled GCM with continuously increasing concentrations of greenhouse gases and sulfate aerosols [Roeckner *et al.*, 1999] have been carried out. The concentrations of the well-mixed greenhouse gases are prescribed for the past (AD 1860-1990) and projected into the future according to IPCC scenario IS92a [IPCC, 1992]. Glacier mass balance changes have been simulated using the process-based modeling approach developed in this thesis. Initial results indicate generally negative mass balance trends for the investigated glaciers during recent decades (relative to a control experiment with unchanged external forcing). These negative trends appear to be stronger for Alpine glaciers compared to the Norwegian glacier Nigardsbreen. Glacier lengths have also been simulated for Nigardsbreen. They suggest that increasing greenhouse gas concentrations as represented in the GCM experiments are a possible explanation for the observed present-day glacier retreat. However, it needs to be stressed that the simulated time period (AD 1860-2050 for integrations including sulfate aerosols and AD 1860-2100 for the longest integration with greenhouse gas forcing only) is relatively short with respect to the response time of

---

the glacier (about 70 years; see section 5.4) and that internal variations are naturally superimposed on the simulated glacier records. A more detailed analysis of the experiments will be carried out in near future.

Another possible application of the approach developed in this thesis is the simulation of tropical glaciers at high elevation sites, such as Lewis glacier in East Africa [Kruss, 1983] or Qori Kalis in the tropical Andes of Peru [Brecher and Thompson, 1993; Thompson *et al.*, 1986]. Such glaciers represent particularly sensitive climatic indicators, and observations have documented a drastic retreat during recent decades which has accelerated with time [e.g. Hastenrath and Greischar, 1997; Hastenrath and Kruss, 1992]. In this context, an investigation of such glaciers using GCM integrations is certainly particularly interesting.

A further challenging application of the general modeling approach as developed in this thesis is the simulation of dendrochronological proxy data using GCM integrations. This is useful since tree-ring chronologies represent climate archives of the past covering large parts of the earth. Analogous to the investigation of glaciers in this thesis, the intention is then to determine to what extent preindustrial variability recorded in tree-ring records can be explained by internal climate variations as represented by GCMs. This can be addressed by simulating “synthetic” tree-ring records using GCM integrations for comparison with actual in situ tree-ring proxy data. The approach involves downscaling of GCM output as described in this thesis combined with a process-based tree-ring model considering local biological and environmental processes controlling the growth of trees at specific sites [Vaganov *et al.*, 1990; Fritts and Shashkin, 1995]. This model uses meteorological data to calculate seasonal tree-ring growth and cell production. Tree-ring chronologies generated using this model have been demonstrated to be very similar to those collected and measured at specific sites, e.g. in the forest-tundra zone of the Siberian subarctic [Vaganov *et al.*, 1999]. The simulation of tree-rings using GCMs therefore appears to be very promising.

---

## References

- Brecher, H. H., and L. G. Thompson, Measurement of the retreat of Qori Kalis in the tropical Andes of Peru by terrestrial photogrammetry, *Photogramm. Eng. Remote Sens.*, 59, 1017-1022, 1993.
- Fritts, H. C., and A. V. Shashkin, in *Tree rings as indicators of ecosystem health*, edited by T. E. Lewis, 17-58, CRC Press, New York, 1995.
- Hastenrath, S., and L. Greischar, Glacier recession on Kilimanjaro, East Africa 1912-1989, *J. Glaciol.*, 43, 455-459, 1997.
- Hastenrath, S., and P. D. Kruss, The dramatic retreat of Mount Kenya's glaciers between 1963 and 1987, greenhouse forcing, *Ann. Glaciol.*, 16, 127-133, 1992.
- IPCC, *Climate Change 1992: The Supplementary Report to the IPCC Scientific Assessment*, edited by J. T. Houghton, B. A. Callendar, and S. K. Varney, Cambridge Univ. Press, New York, 1992.
- Kruss, P. D., Climate change in East Africa: numerical modeling from the 100 years of terminus record of Lewis Glacier, Mount Kenya, *Z. Gletscherk. Glazialgeol.*, 19, 43-60, 1983.
- Roeckner, E., L. Bengtsson, J. Feichter, J. Lelieveld and H. Rodhe, Transient climate change simulations with a coupled atmosphere-ocean GCM including the tropospheric sulfur cycle, *J. Climate*, 12, 3004-3032, 1999.
- Thompson, L. G., E. Mosley-Thompson, W. Dansgaard, and P. M. Grootes, The "Little Ice Age" as recorded in the stratigraphy of the tropical Quelccaya ice cap, *Science*, 234, 361-364, 1986.
- Vaganov, E. A., I. V. Sviderskaya, and E. N. Kondratyeva, Climatic conditions and tree ring structure: simulation model of trachidogram (in Russian), *Lesovedenie*, 2, 37-45, 1990.
- Vaganov, E. A., Hughes, M. K., Kirilyanov, A. V., Schweingruber, F. H., and P. P. Silkin, Influence of snowfall and melt timing on tree growth in subarctic Eurasia, *Nature*, 400, 149-151, 1999.
-

## **Acknowledgements**

I greatly appreciated the opportunity to work within the pleasant and productive atmosphere of the Climate Modelling Department at the Max-Planck-Institut für Meteorologie in Hamburg.

In particular, I would like to express my gratitude to my supervisor, Prof. Lennart Bengtsson, for making this thesis possible and for his continuous support and expert advice. His open-minded attitude and refreshing enthusiasm in the discussion of scientific subjects has been particularly motivating and stimulating.

I am very grateful to Prof. Hartmut Graßl for his strong interest in my work and for examining this dissertation.

I wish to thank Prof. Hans Oerlemans, Utrecht University, for his valuable scientific support. His profound knowledge of glacier systems, along with detailed and critical discussions we had in Hamburg and Utrecht, represented an important basis for the course of this dissertation. Main results of this work would not have been possible without his expertise.

I would like to thank Ove Åkesson, Swedish Meteorological and Hydrological Institute, for providing me with weather station data, knowledge, and practical help on statistical modeling, particularly at the beginning of my thesis.

I thank Dr. Julie Jones and Dr. Adrian Tompkins, for carefully reviewing the manuscript. Their suggestions and critical comments have greatly helped to improve both grammar and spelling as well as the scientific content of this thesis.

I wish to thank all colleagues at the Max-Planck-Institut who supported me during my PhD in several aspects, in particular:

Dr. Erich Roeckner whose expertise in the ECHAM4 model gave valuable input to this work, Dr. Dietmar Dommenges and Dr. Anselm Grötzner for their help with topics concerning spectral analysis, Dr. Marco Giorgetta, Dr. Martin Stendel, Dr. Bernadette Walter, Dr. Bennert Machenhauer, and Prof. Larry Gates, who contributed with numerous comments and fruitful discussions, Norbert Noreiks for help on graphic representation, Reinhard Budich and the staff from the German Climate Computing Centre (DKRZ) for their tireless computational assistance.

---

Prof. Hans von Storch is thanked for his advice concerning several statistical issues within this work, in particular with regard to the application of auto-regressive processes.

The European Centre for Medium-Range Weather Forecasts (ECMWF) provided meteorological reanalyses, the Swedish Meteorological and Hydrological Institute (SMHI) contributed operational weather station data, and the National Oceanic and Atmospheric Administration (NOAA) made Global Historical Climatology Network (GHCN) data available. Glacier mass balance data and glacier length data was obtained from the World Glacier Monitoring Service (WGMS). ECHAM model simulations were performed at the DKRZ in Hamburg.

Most of all, I thank Serena for her love and encouragement and my parents for their lifelong support and confidence in me.

---

- EXAMENSARBEIT Nr. 46**  
Mai 1997  
**Simulationen zur Bildung und Entwicklung von stratosphärischem Aerosol unter besonderer Berücksichtigung der Pinatuboepisode**  
Claudia Timmreck
- EXAMENSARBEIT Nr. 47**  
Mai 1997  
**Assimilation von  $\delta^{13}\text{C}$ -Daten aus marinen Sedimentbohrkernen in das LSG zur Rekonstruktion der Ozeanzirkulation während des letzten glazialen Maximums**  
Arne M.E. Winguth
- EXAMENSARBEIT Nr. 48**  
Juni 1997  
**Simulation der  $^{18}\text{O}/^{16}\text{O}$ -Zusammensetzung von atmosphärischem Sauerstoff**  
Ulrike Seibt
- EXAMENSARBEIT Nr. 49**  
November 1997  
**Satellitengestützte Fernerkundung und Modellierung des globalen  $\text{CO}_2$ -Austauschs der Landvegetation: Eine Synthese**  
Wolfgang Knorr
- EXAMENSARBEIT Nr. 50**  
Dezember 1997  
**Zeitscheibenexperimente mit dem atmosphärischen Zirkulationsmodell T42-ECHAM3 für eine verdoppelte und verdreifachte  $\text{CO}_2$ -Konzentration unter besonderer Beachtung der Änderungen der nordhemisphärischen troposphärischen Dynamik**  
Jan Perlwitz
- EXAMENSARBEIT Nr. 51**  
Januar 1998  
**Globale natürliche Aerosolfelder interaktiv berechnet mit dem Aerosolteilchenmodul APMO im Klimamodell ECHAM**  
Elke Keup-Thiel
- EXAMENSARBEIT Nr. 52**  
Januar 1998  
**Entwicklung einer Parameterisierung des lateralen Abflusses für Landflächen auf der globalen Skala**  
Stefan Hagemann
- EXAMENSARBEIT Nr. 53**  
Juni 1998  
**Simulation der Dynamik eines Multikomponentensystems am Beispiel vulkanischer Eruptionswolken**  
Michael Herzog
- EXAMENSARBEIT Nr. 54**  
Juni 1998  
**Wurzeln und Klima: Bestimmung ihrer Bedeutung durch Modellsimulationen**  
(Roots and Climate: Assessing their Role with Model Simulations)  
Axel Kleidon
- EXAMENSARBEIT NR. 55**  
Juli 1998  
**On Predictability Limits of ENSO**  
A Study Performed with a Simplified Model of the Tropical Pacific Ocean-Atmosphere System  
Christian Eckert
- EXAMENSARBEIT Nr. 56**  
Juli 1998  
**Use of ocean wave spectra retrieved from ERS-1 SAR wave mode data for global wave modelling**  
Patrick Heimbach
- EXAMENSARBEIT Nr. 57**  
Juli 1998  
**On the Role of the Land Surface Representation and the Numerical Coupling to the Atmosphere for the Simulated Climate of the Global ECHAM4 Model**  
Jan-Peter Schulz
- EXAMENSARBEIT Nr. 58**  
August 1998  
**Messungen zur Wolkenmikrophysik in arktischen Kaltluftausbrüchen**  
Rüdiger Timm

|  |  |
|--|--|
| <b>EXAMENSARBEIT Nr. 59</b><br>August 1998   | <b>Variability on decadal scales in Pacific sea surface temperatures and atmosphere ocean interaction in the coupled general circulation model ECHAM4/OPYC3</b><br>Andreas Bacher      |
| <b>EXAMENSARBEIT Nr. 60</b><br>August 1998   | <b>Development of a Process-Based Model to Derive Methane Emissions from Natural Wetlands for Climate Studies</b><br>Bernadette Walter   |
| <b>EXAMENSARBEIT Nr. 61</b><br>Dezember 1998 | <b>On the benefit of the adjoint technique for inversion of the atmospheric transport employing carbon dioxide as an example of a passive tracer</b><br>Thomas Kaminski                |
| <b>EXAMENSARBEIT Nr. 62</b><br>Januar 1999   | <b>Modellierung der Chemie der globalen Strato- und Troposphäre mit einem drei-dimensionalen Zirkulationsmodell</b><br>Benedikt Steil  |
| <b>EXAMENSARBEIT Nr. 63</b><br>Januar 1999   | <b>Ocean-atmosphere interactions on decadal timescales</b><br>Stephan Venzke   |
| <b>EXAMENSARBEIT Nr. 64</b><br>März 1999     | <b>Modes of Variability as Simulated by a Global Climate Model</b><br>Axel Timmermann  |
| <b>EXAMENSARBEIT Nr. 65</b><br>Juli 1999     | <b>Numerical Simulation of Scavenging Processes in Explosive Volcanic Eruption Clouds</b><br>Christiane Textor   |
| <b>EXAMENSARBEIT Nr. 66</b><br>Juli 1999     | <b>Grobstruktursimulation - eine Methode zur Berechnung turbulenter atmosphärischer Strömungen</b><br>Andreas Chlond   |
| <b>EXAMENSARBEIT Nr. 67</b><br>Dezember 1999 | <b>Satellitengestützte Abschätzung der Einflüsse von kühler Haut und Schaumbedeckung des Ozeans auf den globalen CO<sub>2</sub>-Fluß zwischen Ozean und Atmosphäre</b><br>Stefan Ewald |
| <b>EXAMENSARBEIT Nr. 68</b><br>Februar 2000  | <b>Die direkte Strahlungswirkung von Aerosolteilchen auf ein Klimamodell</b><br>Anke Maria Allner  |
| <b>EXAMENSARBEIT Nr. 69</b><br>Februar 2000  | <b>Räumliche und zeitliche Variabilität von Wasserisotopen im polaren Niederschlag</b><br>(Spatial and Temporal Variability of Water Isotopes in Polar Precipitation)<br>Martin Werner |
| <b>EXAMENSARBEIT Nr. 70</b><br>März 2000     | <b>Bestimmung des turbulenten Impulsflusses mit Hilfe von Doppler- und Interferometriemessungen eines Radar-RASS-Systems</b><br>Lutz Hirsch  |
| <b>EXAMENSARBEIT Nr. 71</b><br>Mai 2000      | <b>Entwicklung und Test eines massenerhaltenden semi-Lagrangischen Transportverfahrens auf einer Kugel</b><br>Markus Peter Olk   |
| <b>EXAMENSARBEIT Nr. 72</b><br>Mai 2000      | <b>Quantification of Natural Climate Variability in Paleoclimatic Proxy Data Using General Circulation Models: Application to Glacier Systems</b><br>Bernhard K. Reichert              |



